uOttawa

L'Université canadienne
Canada's university

FACULTÉ DES ÉTUDES SUPÉRIEURES ET POSTOCTORALES

uOttawa

L'Université canadienne
Canada's university

FACULTY OF GRADUATE AND POSDOCTORAL STUDIES

Wesley Van Whychen
AUTEUR DE LA THÈSE / AUTHOR OF THESIS

M.Sc. (Geography)
GRADE / DEGREE

Faculty of Arts – Department of Geography
FACULTÉ, ÉCOLE, DÉPARTEMENT / FACULTY, SCHOOL, DEPARTMENT

Spatial and Temporal Variations in Ice Motion, Belcher Glacier, Devon Island, Nunavut, Canada

TITRE DE LA THÈSE / TITLE OF THESIS

Luke Copland
DIRECTEUR (DIRECTRICE) DE LA THÈSE / THESIS SUPERVISOR

CO-DIRECTEUR (CO-DIRECTRICE) DE LA THÈSE / THESIS CO-SUPERVISOR

Mike Sawada

Laurence Gray

Gary W. Slater
Le Doyen de la Faculté des études supérieures et postdoctorales / Dean of the Faculty of Graduate and Postdoctoral Studies

Spatial and Temporal Variations in Ice Motion, Belcher Glacier, Devon Island, Nunavut, Canada

Wesley Van Wychen

Thesis submitted to the
Faculty of Graduate and Postdoctoral Studies
in partial fulfillment of the requirements
for the MSc Degree in Physical Geography

Department of Geography
Faculty of Arts
University of Ottawa

Supervisor:
Dr. Luke Copland (University of Ottawa)

Thesis Committee
Dr. Laurence Gray (Canada Centre for Remote Sensing)
Dr. Mike Sawada (University of Ottawa)

Your file Votre référence
ISBN: 978-0-494-69027-7
Our file Notre référence
ISBN: 978-0-494-69027-7

ABSTRACT:

This study presents surface ice motion patterns across Devon Ice Cap, with a particular focus on the Belcher Glacier drainage basin. Between summer 2007 and summer 2009, continuous differential GPS (dGPS) measurements were made to determine the motion at points along the centerline of the Belcher Glacier with ~cm accuracy. In summer 2008, marker stakes were set out on all accessible tributaries in the Belcher basin, with each stake being surveyed with dGPS several times throughout the season. Using synthetic aperture radar (SAR) speckle tracking techniques new velocity maps were produced of seasonal changes in ice motion for the Belcher Glacier. These were validated against the field dGPS results. Ground penetrating radar (GPR) was used to determine the ice depths of each tributary basin in the Belcher Glacier study region. These ice depths are combined with velocities derived from the speckle tracking results to create flux gates which allow for estimates of total ice discharge for the Belcher basin. These volume estimates can be used to improve mass loss estimates for future modeling of Devon Ice Cap.

The velocity results are compared to the work of Burgess et al (2005), who provided flow dynamics and mass loss from the Devon Ice Cap and Belcher Glacier systems using interferometry and speckle tracking of ERS 1/2 data from the mid-1990s and Radarsat-1 data from 2000. These comparisons reveal higher ice velocities on a large glacier in the southeast part of the ice cap (Southeast2 Glacier), which agrees with recent thickening of the stagnant ice into which the glacier drains.

ACKNOWLEDGEMENTS:

Support for this project has been provided by a Natural Sciences and Engineering Research Council of Canada IPY Grant (#334815-2006), NSERC Canada Graduate Scholarship, the Northern Scientific Training Program, the Polar Continental Shelf Project, Canada Foundation for Innovation, Ontario Research Fund, CRYO-EX, the University of Ottawa, and the Canadian Space Agency's SOAR-E program (Project # 5009).

I would like to thank Jamie Davis, Gabe Wolken, Hanna Milne for their help with data collection in the field. I would also like to thank Brad Danielson, both for his help during fieldwork, data collection and sharing of data. I would also like to thank Faye Wyatt for sharing of data and Wendy Clavano for providing a BedDEM of the study site. I would especially like to thank Tyler Sylvestre and Emilie Herdes for their hard work and dedication in the field, and all the lab members of the Laboratory for Cryospheric Research for their support throughout the project.

I gratefully acknowledge the help of Dr. Dave Burgess for providing data comparison, satellite imagery and insight throughout the project, and Dr. Martin Sharp for his insight and help throughout this endeavor. I would also like to thank the thesis committee member Dr. Sawada for his help and comments throughout the thesis process. I also greatly thank Dr. Laurence Gray for providing me with the means to complete this thesis, for his insight and patience and constant help throughout this project.

I would like to thank my supervisor, Dr. Luke Copland, for his support, guidance and help throughout the process, and for the many amazing opportunities that he has provided me.

I gratefully thank my parents for their constant support, love and encouragement throughout this project. Finally, I gratefully thank Amanda Reinwald for her love, encouragement and support throughout this endeavor.

TABLE OF CONTENTS

Chapter 1: Introduction

1.1 Recent Climate Change in the High Arctic:

Over Arctic lands north of 65°N, warming of air temperatures was more than twice the global average from the 19th century to the 21st century (IPCC 2007). More specifically, records from 1900 to 2003 indicate that the Arctic climate has fluctuated between warmer and cooler periods, but since 1960 the overall trend has been one of warming (Figure 1.1) (IPCC 2007, ACIA 2004). Over large portions of Arctic land, air temperatures have increased by as much as 5°C during the 20th century. This warming has been confirmed by a number of independent proxy measures, including: earlier thaw and later freeze up of lake ice in the northern hemisphere (Duguay 2006, Magnuson et al 2000), reductions in mean annual snow-cover extent from 1972-2000 (Dye 2002), and decreases in winter sea-ice extent between 1979 and 2005 (Comiso 2003, IPCC 2007). Seasonally, this warming is more pronounced in winter than in summer (IPCC 2007, ACIA 2004). In parts of western Canada and Alaska, winter temperatures have increased as much as 3-4 °C between 1953 and 2003 (ACIA 2004). Recent observed changes in Arctic air temperatures are presented in Figure 1.2.

In addition to rising air temperature in the Arctic, changes to the precipitation regime have occurred and are expected to continue. This has been attributed to increases in rainfall events occurring in the winter, and to a lesser extent, in the spring and autumn (IPCC 2007, ACIA 2004). With warmer temperatures, more precipitation is expected to fall as rainfall rather than snow in the future. The combination of changes in temperature and precipitation has led to significant consequences for the Arctic environment, as further described below.

1.1.1 Recent Sea Ice Changes:

Sea ice has been monitored with the use of satellite imagery since the 1970s and as such, records of sea ice conditions are well constrained and show decreases in Arctic sea ice extent, thickness and age over this period (Barber et al 2009, Maslanik et al 2007, Nghiem et al 2006, Rigor and Wallace 2004, Serreze et al 2007, Kwok et al 2007, Jeffers

et al 2001). In terms of ice extent changes, Serreze et al (2007) used passive remote sensing techniques to determine a negative trend in Arctic sea ice extent for every month between 1979 to 2006. Since 2001 every year has had a pronounced September minimum ice extent, with 2005 being an extreme case, representing a 21% reduction in ice extent when compared to the mean ice extent for the 1979 – 2000 period. The 1979 to 2006 passive remote sensing records also show an average decrease of ~39 500 km^2 yr^{-1} (+/- 5600 km^2 yr^{-1}) in winter Arctic sea ice extent (Barber et al 2009, Parkinson and Cavalieri 2008). Sea ice thicknesses have also decreased in the Northern Hemisphere by up to 40% in some regions over the last 50 years (Barber et al 2009, Rothrock et al 1999, Hilmer and Lemke 2000). Maslanik et al (2007) use remote sensing methods to determine ice age and thickness from 1982 to 2007. The results show that the amount of the oldest and thickest ice within the multiyear ice pack has declined significantly, with 58% of the multiyear ice now consisting of first-year ice compared to 35% in the mid 1980s.

In situ sea ice observations in the southern Beaufort Sea in summer 2009 found heavily decayed (rotten), very small multi-year and first-year remnant sea ice floes interspersed with new sea ice with significant thaw holes and melt ponds (Barber et al 2009). This rotten ice regime was much different than what was expected in terms of ice volume and strength and the presence of this rotten sea ice regime allowed for wind-generated swells to penetrate further into the multi-year ice pack, further weakening the remaining ice. Thus, although the areal extent of sea ice in 2009 was greater than either 2007 or 2008, the volume of multi-year sea ice was at its lowest extent in 2009 (Barber et al 2009). Changes in sea ice conditions have implications for the Arctic marine, terrestrial and freshwater ecosystems, and impacts for indigenous communities who rely on ice for subsistence hunting, resource exploration, development projects and security and sovereignty.

1.1.2 Recent Permafrost Changes:

Measurements of ground temperatures in Russia, Alaska and Canada have shown a consistent warming trend over the last several decades (IPCC 2007, ACIA 2004). Permafrost temperatures in northern Alaska have increased by 2-3°C since 1980 (IPCC

2007). Nelson (2003) found that in northwestern Canada, the top 30 m of permafrost warmed by up to 2°C between 1983 and 2003. The Geological Survey of Canada and several of its partners have developed a permafrost monitoring network across Canada and results are reported by Smith et al (2005). This monitoring network has revealed a warming of 0.3-0.6°C per decade since the mid-1980s for shallow permafrost in the central and northern Mackenzie Delta region. This permafrost warming has been linked to a general increase in air temperatures. In the High Arctic, results from the monitoring network reveal that shallow permafrost has warmed between 1°C and 4°C per decade, mainly since the mid-1990s. Lewkowicz (2007) investigated detachment failures on the Fosheim Peninsula of Ellesmere Island in the Canadian High Arctic in 2005. The detachment failures were linked to an increase in the number of thawing degree-days during the summer, which in 2005 were at their highest since 1960.

In other regions of Canada (Iqaluit and Northern Quebec) permafrost cooling was observed from the mid-1980s, followed by a warming trend since the mid-1990s (IPCC 2007). For the Russian Arctic, in Eastern Siberia, permafrost temperatures increased ~1°C from 1960-1990, while in the Western Arctic permafrost has warmed between 0.3 and 0.7°C during the same period (Pavlov 1996, IPCC 2007). A pan-Arctic summary of permafrost change is summarized in Table 1-1. Models of future climate change are predicted to increase the active layer thickness and result in deeper thawing of permafrost (ACIA 2004). This could have impacts on drainage patterns, subsidence and thermokarst formation, especially in ice-rich soils. The thawing of ice rich permafrost may also trigger mass movements on slopes and increase the number of detachment failures in permafrost regions (Lewkowicz 2007). This type of permafrost degradation poses significant threats to structures such as roadways, buildings, pipelines, tailing ponds and sewage lagoons, causing serious impact for communities which rely on these structures (ACIA 2004).

1.1.3 Recent Glacial Changes:

Estimates of total glacial ice volume in the Arctic are roughly 3.1 million km^3, equivalent to 8 m of global sea level rise (Dowdeswell and Hagen 2004, ACIA 2004). Most of this

volume is accounted for by the Greenland Ice Sheet, with the smaller ice caps of the Canadian Arctic, Alaska, Svalbard, Iceland, Franz Josef Land, Novaya Zemlya, Severnaya Zemlya and northern Scandinavia accounting for about one quarter of the total volume (ACIA 2004). However, most of the Greenland Ice Sheet is at altitudes that are well below freezing throughout the year, meaning that the smaller ice caps and glaciers are likely more susceptible to mass and area changes in response to precipitation and temperature changes (ACIA 2004). Due to the faster response times of these smaller circumpolar ice caps and glaciers, these may provide a precursor of future change in Greenland.

In general, Arctic ice caps have lost volume since about 1920, coincident with a general increase in temperature throughout the region. There is, however, wide variability between sub-regions in the Arctic. In Svalbard, for example, there was little mass balance change from 1974-2004. Furthermore, glaciers in the western maritime region of Scandinavia had a positive mass balance between 1960-1988, although this is likely linked to the North Atlantic Oscillation (ACIA 2004). In the Queen Elizabeth Islands in the Canadian High Arctic, there was an overall negative glacier mass balance between 1959 and 2003 (Koerner 2005). Specifically, Koerner (2005) used a >40 year period to determine mass balances for the ice caps on Melville Island (-7.24 m cumulative mass balance (cmb)) and Meighen Island (-4.54 m cmb), northwest Devon Ice Cap (-3.54 m cmb) and the White (-5.6 m cmb) and Baby Glaciers on Axel Heiberg Island. All of these ice masses exhibit a weak but significant trend toward increasingly negative balances since the mid-1990s, except for the Meighen Island Ice Cap (Figure 1.3). Summer climate seems to play an important role in the negative mass balances, as winter balances have shown low variability and little change over the period, while warmer summers have increased melt and the depth of meltwater percolation in the accumulation area of the aforementioned glaciers (Koerner 2005).

For the Greenland Ice Sheet, studies show a thickening of the interior of the ice cap (at elevations greater than ~2000 m), while in coastal regions there has been a rapid thinning (Krabill et al 2004, Johannessen et al 2005, Rignot and Kanagaratnam 2006, Rignot and

Thomas 2007, Howat et al 2007a, Thomas et al 2006). Additionally, there is evidence of increased surface melt over the Greenland Ice Sheet. Box et al (2006) found that the duration of the melt season grew by 10 days on average, and that accumulation-area ratio decreased by 3% between 1988 and 2004. Mote (2007) found that 2007 was an exceptionally high melt year in comparison with the 1973-2007 average. This study also found that the recent melt seasons (1996-2007) have all been above the 1973-2007 average. Along with recent increases in melt on the Greenland Ice Sheet, changes in ice dynamics have also been observed (Zwally et al 2002, Rignot and Kanagaratnam 2006, van de Wal et al 2008, Joughin et al 2008). Dynamic changes are linked to increases in supraglacial melt and are discussed further in Section 1.2.1.

1.2 Projected Future Climate Change in the Arctic:

The Arctic Climate Impact Assessment (2004) uses five different model simulations to make climate projections between 60°N and 90°N. For surface air temperatures in the polar region as a whole, the five models project that there will be a warming between 2.8°C and 4.6°C by the late 21st Century. Regional models project that by 2071-2090 average Arctic warming will be >5°C above 1981-2000 baseline temperatures, while in Scandinavia and East Greenland it will be ~3°C, in Iceland ~2°C, and up to 5°C in the Canadian Archipelago and Russian Arctic (ACIA 2004). The Intergovernmental Panel on Climate Change also provides regional projections for climate change. IPCC (2007) reports that by 2100 average temperatures in the Arctic are projected to be 5□C warmer than present (although individually the models vary between 2.7□C and 7.8□C). Models predict that warming will be more pronounced in the winter than in the summer for both land and sea.

Future models of precipitation are generally more variable than those for temperature. The IPCC projects that global precipitation will increase by 10-20% in the next century and that similar to temperature, precipitation change will be more pronounced in the winter than the summer (IPCC 2007). For the Arctic there is discrepancy between models for both seasonal and spatial precipitation patterns, and how the partitioning between snow and rain will be altered in a warmer climate (IPCC 2007). Models of precipitation

increase by 2100 for the Arctic are 15-36% higher than the predicted global average increase.

1.2.1 How climate change affects glacier dynamics:

It has previously been thought that ice sheet response to climate change occurs over hundreds to thousands of years, but recent studies illustrate that glacier and ice sheet response to external forcing may occur over periods of only years to decades (Zwally et al 2002, Van de Wal et al 2008, Joughin et al 2008). During the summer, warmer air temperatures cause melt, creating surface melt pools and a developed supraglacial drainage network. Recent studies have indicated that this surface melt can be transmitted to the base of glaciers and ice sheets, increasing basal lubrication, and ultimately providing a mechanism for the rapid loss of mass via flow acceleration into the oceans (Zwally et al 2002, Joughin et al 2008, Alley et al 2005). In Greenland from 1996 to 1999, differential GPS observations have shown a 5% - 28% seasonal increase in ice velocities (summer over winter velocities) which are strongly correlated with summer melt (Zwally et al 2002, Joughin et al 2008, Van de Wal et al 2008). Summer increases in Greenland ice velocities were also determined from Radarsat-1 interferometry measurements in 2006 and 2007 (Joughin et al 2008). Rignot and Kanagaratnam (2006) used interferometry to determine ice motion of outlet glaciers on Greenland, which showed widespread accelerations between 1996 and 2000 for glaciers below 66□N, and an expansion of the acceleration to 70□N by 2005. From 1996-2006, the ice deficit of the Greenland Ice Sheet doubled (90 km^3 to 220 km^3) and with the acceleration moving further and further north, contributions to sea level rise will increase. Similarly, Howat et al (2008) studied the frontal change and ice dynamics of 32 outlet glaciers along the southeast margin of the Greenland Ice Sheet using Radarsat and ASTER images. They found that there was a substantial seasonality in terms of both speed and retreat. Parizek and Alley (2004) found that the Greenland Ice Sheet is likely to make larger contributions to sea level rise in a warming environment due to the enhanced basal sliding expected with increased surface melt.

Recent studies on other High Arctic glaciers also provide useful insights for understanding seasonal changes in ice dynamics. Copland et al (2003a) found that ice in the ablation zone of John Evans Glacier, Ellesmere Island (a cold polythermal glacier) had summer velocities that were almost double winter velocities, and that internal ice deformation could not account for all of this motion. This suggests that basal sliding is important in the ablation zone of the glacier, and that subglacial water is present beneath this region throughout the year. Measured summer velocities were also faster below a set of moulins and crevasses, indicating that glacier motion is strongly controlled by surface melt in regions where this control was previously believed to be limited (Hodgkins, 1997).

1.3 Project Objectives

As reviewed above, the Arctic climate is changing and causing processes such as permafrost thawing, sea ice reductions (both in terms of thickness and extent) and glacial retreat. Although it is not yet currently understood as to exactly how glaciers will respond to climate warming, recent studies on Greenland suggest the importance of rapid mass loss via increased lubrication at the glacier bed driven by increases in surface melt. Therefore, in order to better understand how glacier dynamics will respond in a warming climate, the objectives of this project are threefold:

I. To determine the spatial and temporal velocity structure of the Belcher Glacier over the short term (~1 year).
II. To determine the ice flux that occurs via the Belcher Glacier and its seasonality.
III. To determine the most comprehensive surface velocity maps of Devon Ice Cap, and determine if and how this motion has changed over the last ~10-15 years.

Devon Ice Cap and Belcher Glacier provide a good location for this study as their extents are well constrained and there have been previous mass balance and ice dynamic studies on the ice cap that can be compared against the results presented here.

This thesis is part of the Canadian contribution to the GLACIODYN project, which involves research partners at the University of Alberta, Natural Resources Canada,

University of Lethbridge, Simon Fraser University, Memorial University of Newfoundland and University of Calgary. GLACIODYN is an international research effort to examine the dynamic response of pan-circumpolar glaciers to climate change and is a contribution to the International Polar Year. The Belcher Glacier and Devon Ice Cap were chosen as an important study region for GLACIODYN as they provide a well-constrained site for understanding changes in glacial dynamics that is likely more responsive to changes in external forcing than either Greenland or Antarctica and may contribute to sea level change on shorter time scales.. The Belcher Glacier is the largest tidewater terminating glacier of the ice cap, with high calving rates that provide contributions to annual mass change.

1.4.1 Study Site:

Devon Ice Cap (DIC) is located on the eastern portion of Devon Island, Nunavut, Canada (Figure 1.4). The ice cap has an area of 14 400 km^2 and an estimated volume of 4110 +/- 140 km^3 (Burgess and Sharp 2004). Between 1959/1960 and 1999/2000 the ice cap experienced a decrease in area of 2.4% (Burgess and Sharp 2004). If the entire Devon Ice Cap were to melt, it would contribute ~10 mm to global sea level rise (Dowdeswell et al 2004).

Dowdeswell et al (2004) measured ice thickness across the entire DIC using airborne Radio Echo Sounding (RES), and produced a DEM at 1 km resolution. Typically, ice is thickest near the interior of the ice cap, with ice depths at the summit approaching 800 m. Ice thicknesses also increase at the major outlet glaciers including the Belcher, Croker Bay, Southeast 2 and Eastern Glaciers (Figure 1.4). These results also reveal that a trough of thicker ice (up to 400 m) extends from the interior of the ice cap to the southern headwall of the Belcher Glacier. This trough provides a significant connection to the interior of DIC that does not occur for many of the other outlet glaciers in that portion of the ice cap. Most major outlet glaciers of Devon Ice Cap are grounded well below sea level, with the Belcher, North and South Croker Bay, Southeast 1 and Southeast 2 Glaciers all having bed elevations as low as 400 m below current sea levels (Boon et al 2010).

The Belcher Glacier basin drains the northeastern portion of Devon Ice Cap, and flows northward into Jones Sound (Figure 1.5). The lower part of Belcher Glacier is constrained within a steep-walled valley, and has a length of ~35 km (Figure 1.6a and Figure 1.6b) (Dowdeswell et al 2004). The glacier represents 50% of mass calved from the ice cap, which in turn represents 15% of the total mass loss (Burgess et al 2005). The lower glacier is linked to its accumulation area and the broader Devon Ice Cap via a network of 12 tributaries ranging from ~1.1 km to ~4.3 km long. Burgess et al (2005) found the occurrence of surface flow stripes on all major outlet glaciers from DIC, including the Belcher Glacier. These are created when ice with high basal speed moves over bed undulations (Gudmundsson et al 1998), and their presence suggests that basal sliding is an important component of total motion. The terminus of the Belcher Glacier is highly crevassed, causing some of the downstream tributaries to be largely inaccessible on the ground.

1.5 Thesis Layout:

The thesis presented here follows a traditional format, however it is planned that chapters 4 and 5 will eventually form the basis of standalone academic journal articles and thus some of the figures used in these sections are repeated in previous chapters. Chapter 2 reviews previous research conducted on Devon Ice Cap to place this study within the current state of knowledge regarding ice dynamics and basal conditions there. Chapter 3 presents the methods used to complete the study. Chapter 4 begins with an evaluation of the methods and an assessment of error, and then goes on to discuss the spatial differences and seasonality of ice motion for Belcher Glacier. Chapter 5 presents ice motion patterns for the entire Devon Ice Cap, and compares them with the results of Burgess et al (2005) to determine if any major changes in ice motion have occurred over the last ~15 years. Finally, Chapter 6 concludes the thesis with a summary of the main findings and a reference list (Chapter 7) can be found at the end of the thesis.

Region	Depth (m)	Period of Record	Permafrost Temperature Change (°C)	Reference
United States				
Northern Alaska	~1	1910s–1980s	2–4	Lachenbruch and Marshall, 1986
Northern Alaska	20	1983–2003	2–3	Osterkamp, 2005
Interior of Alaska	20	1983–2003	0.5–1.5	Osterkamp, 2005
Canada				
Alert, Nunavut	15	1995–2000	0.8	S.L. Smith et al., 2003
Northern Mackenzie Valley	20–30	1990–2002	0.3–0.8	S.L. Smith et al., 2005
Central Mackenzie Valley	10–20	Mid-1980s–2003	0.5	S.L. Smith et al., 2005
Southern Mackenzie Valley & Southern Yukon Territory	~20	Mid-1980s–2003	0	Haeberli and Burn, 2002
Northern Quebec	10	Late 1980s–mid-1990s	<–1	Allard et al., 1995
Northern Quebec	10	1996–2001	1.0	Desjarlais, 2004
Lake Hazen	2.5	1994–2000	1.0	Broll et al., 2003
Iqaluit, Eastern Canadian Arctic	5	1993–2000	2.0	S.L. Smith et al., 2005
Russia				
East Siberia	1.6–3.2	1960–2002	~1.3	Walsh et al., 2005
Northern West Siberia	10	1980–1990	0.3–0.7	Pavlov, 1996
European north of Russia, continuous permafrost zone	6	1973–1992	1.6–2.8	Pavlov, 1996
Northern European Russia	6	1970–1995	1.2–2.8	Oberman and Mazhitova, 2001
Europe				
Juvvasshoe, Southern Norway	~3	Past 30–40 years	0.5–1.0	Isaksen et al., 2001
Janssonhaugen, Svalbard	~2	Past 60–80 years	1–2	Isaksen et al., 2001
Murtel-Corvatsch	11.5	1987–2001	1.0	Vonder Muhll et al., 2004
China				
Tibetan Plateau	~10	1970s–1990s	0.2–0.5	Zhao et al., 2004
Qinghai-Xizang Highway	3–5	1995–2002	Up to 0.5	Wu and Liu, 2003; Zhao et al., 2004
Tianshan Mountains	16–20	1973–2002	0.2–0.4	Qiu et al., 2000; Zhao et al., 2004
Da Hinggan Mountains, Northeastern China	~2	1978–1991	0.7–1.5	Zhou et al., 1996

Table 1.1: *Pan-Arctic summary of permafrost change in the 20th Century (IPCC 2007).*

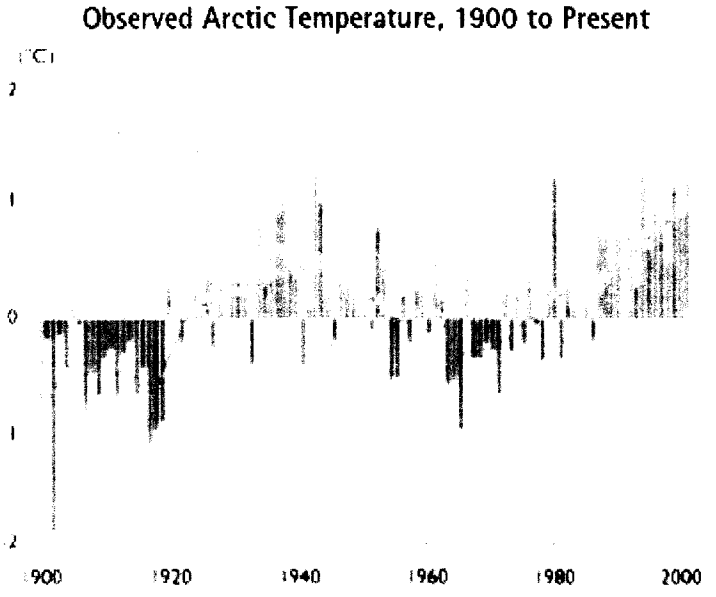

Figure 1.1: *Annual average change in near surface air temperature from stations on land north of 60°N relative to the average from 1900 to 2003 (ACIA 2004).*

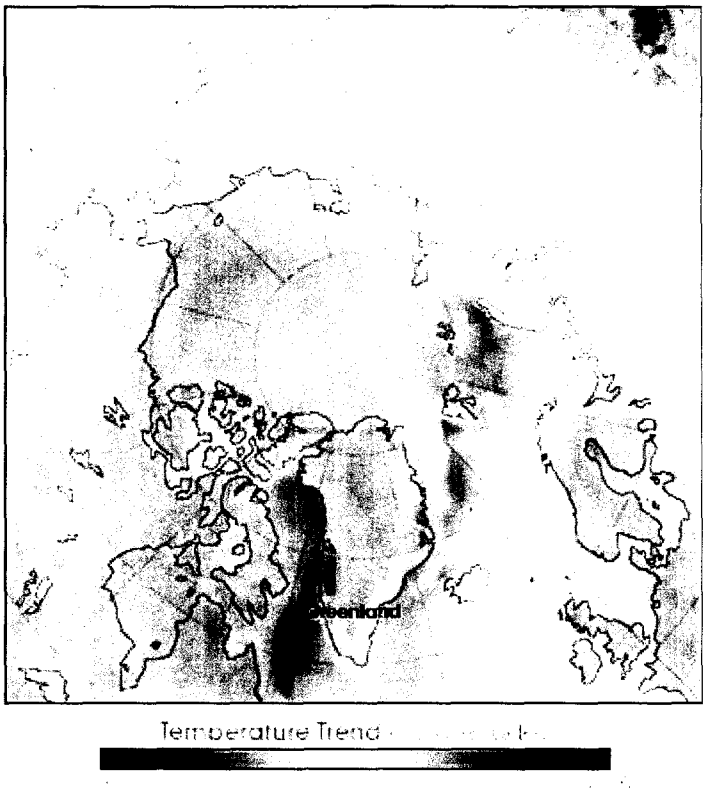

Figure 1.2: *Observed decadal surface air temperature change from 1984-2007(NASA 2007).*

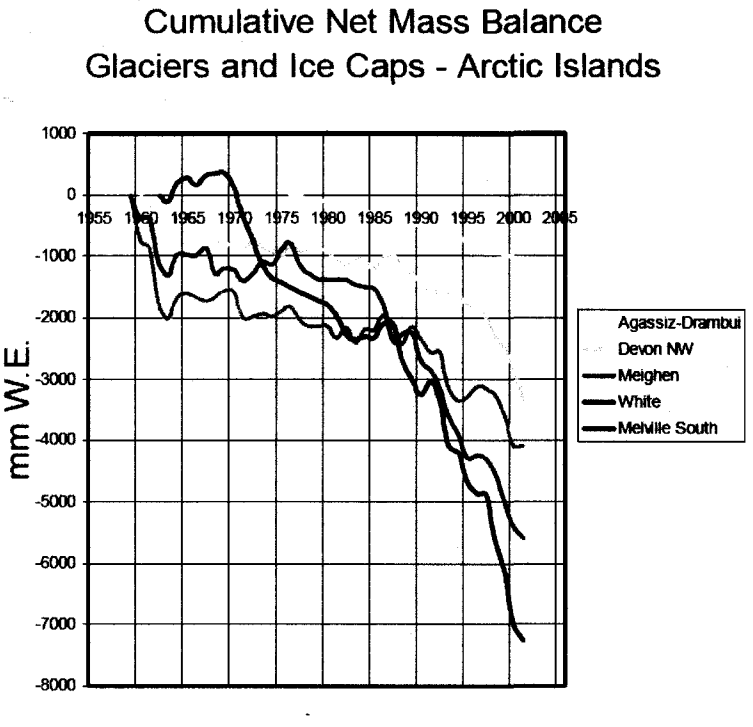

Figure 1.3: *Cumulative net mass balance for ice masses of the Queen Elizabeth Islands (1960-2001) (Demuth and Pietroniro 2008).*

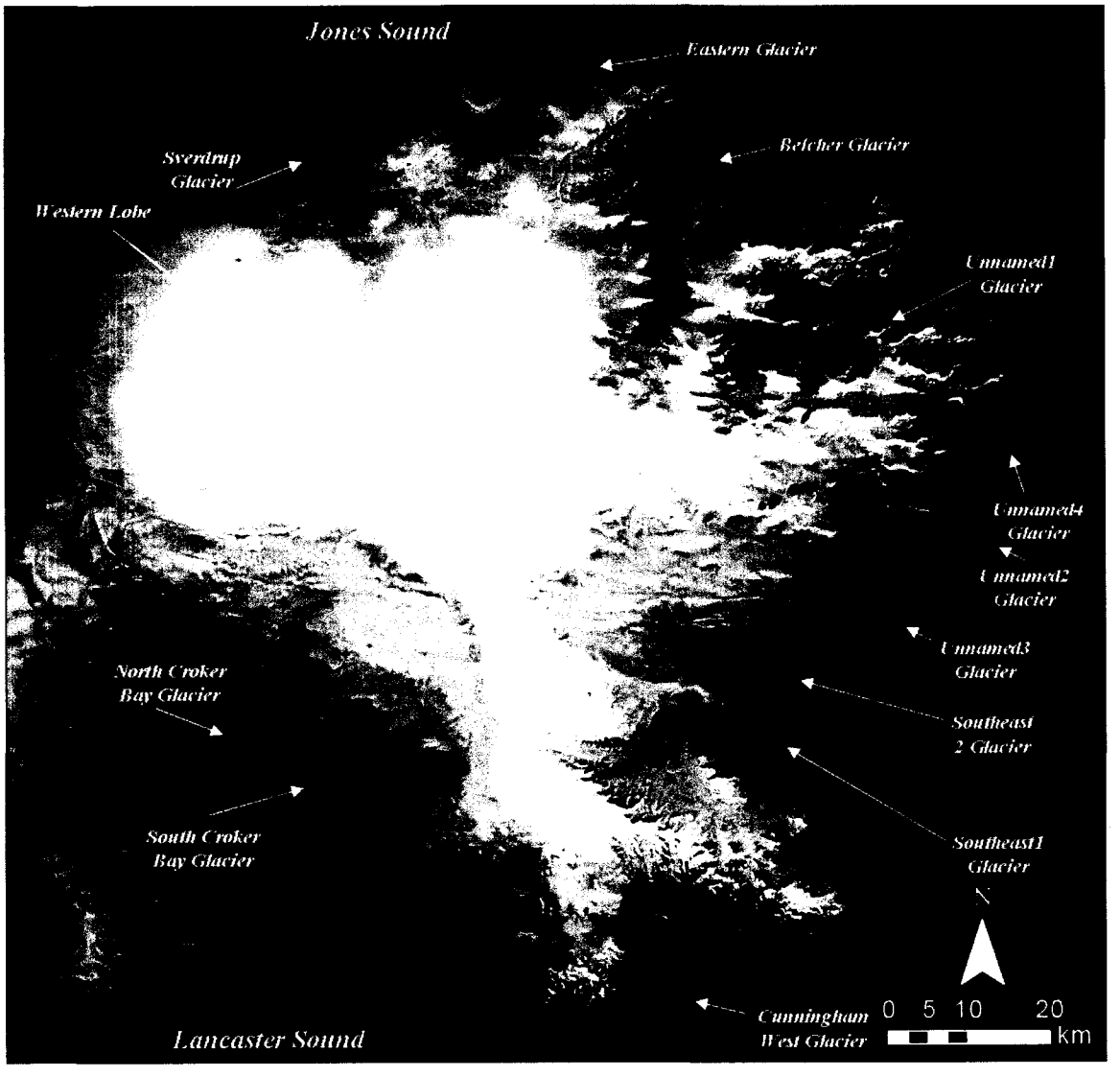

Figure 1.4: *Devon Ice Cap (base image 2000 Landsat ETM+ ortho-mosaic).*

Figure 1.5: *The Belcher Glacier (base image 2000 Landsat 7).*

Figure 1.6a: *Aerial view of the main trunk and tributaries of the Belcher Glacier constrained within the valley walls, May 2008 (View is looking upglacier from the main tributary toward the southern headwall).*

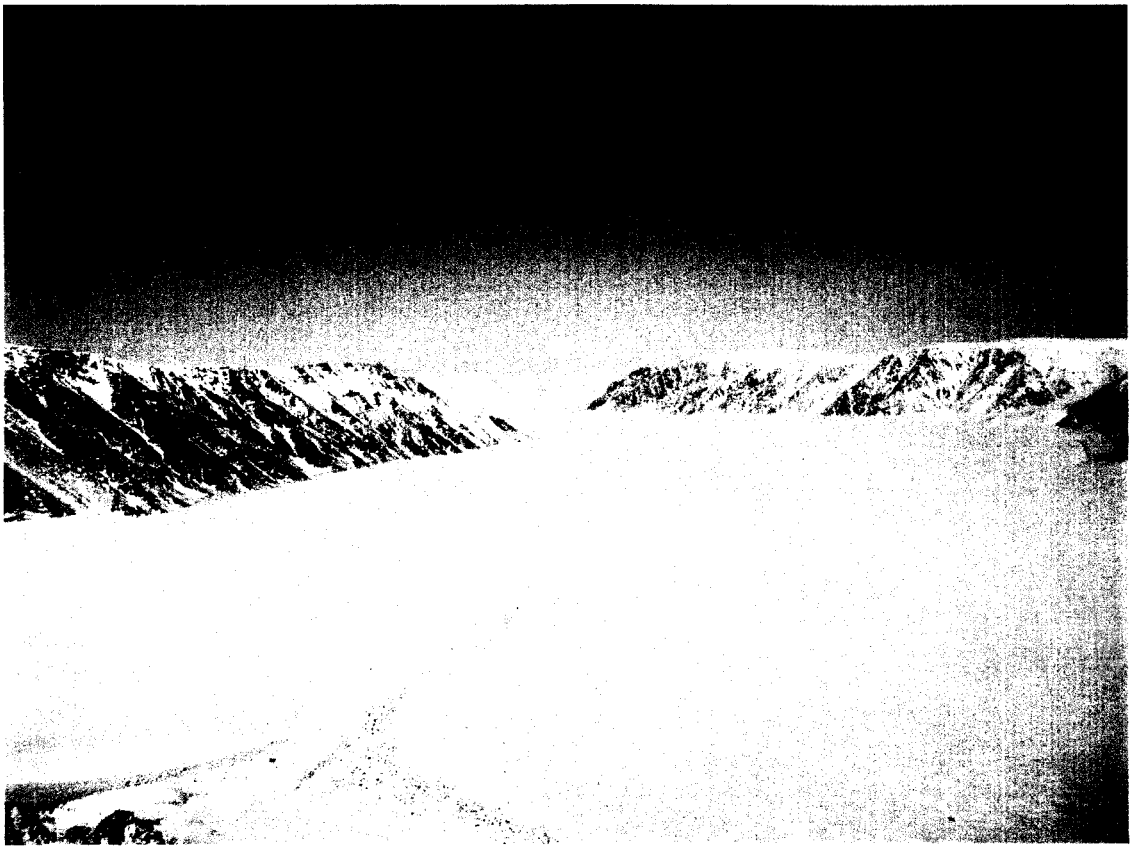

Figure 1.6b: *View of the lower part of the Belcher Glacier and its tributaries constrained within the valley walls, May 2008. (View is looking downglacier from the main tributary toward the terminus).*

Chapter 2: Literature Review

The first part of this chapter provides a review of previous research undertaken on Devon Ice Cap, with a focus on studies of ice dynamics, mass balance, climate and subglacial hydrology. This thesis expands on previous ice dynamics work by producing velocity maps for the entire ice cap (unaffected by satellite look direction issues associated with interferometry), information on how the velocity has changed over the last 10-15 years, together with the first seasonal ice motion maps for the Belcher Glacier basin. The literature review places this current work in context, and also provides a more general review of the links between ice dynamics and subglacial hydrology.

2.1 Historical Research Conducted on Devon Ice Cap (1960s and 1970s)

Boon et al (2010) provides a comprehensive overview of previous research conducted on Devon Ice Cap (DIC). Glaciological research began on DIC in 1961 and has included studies of its geometry, mass balance, ice dynamics and the impact of synoptic weather patterns on its surface melt. Koerner (1970) and Paterson (1976) conducted an early estimate of ice cap area using aerial photographs and determined that it was 15,600 km^2 in size. Early estimates of ice thickness were undertaken near the Sverdrup Glacier and near Croker Bay by Hyndan (1965) using gravimetric techniques, and by Vogtli (1967) using DC resistivity. Ice thicknesses of up to 700 m were determined by these studies, and subsequent studies determined thicknesses of 300-700 m using radio-echo sounding (Paterson and Koerner 1974). Mean ice thickness were found to be different between a southeast transect (568 m) and a northwest transect (426 m) (Koerner 1977) (Figure 2.1).

Records of accumulation and ablation began in 1961 using stakes located on Sverdrup Glacier (Koerner 1966). Between 1962 and 1966 mass balance stake measurements were expanded to include the southeast, southwest and northeast portions of the ice cap, although long term measurements have only been continued in the northwest quadrant up to present day. The findings of Koerner (1966) reveal that net accumulation increases with elevation and that the formation of superimposed ice is an important contributor to net accumulation. Devon Ice Cap has also been an important location for ice coring in the Canadian Arctic that has been used to determine past accumulation rates (Koerner 2005,

Paterson and Waddington 1984). Results from these studies show that accumulation rates have been within 5% of current levels (net accumulation rates vary between 0.22 – 0.245 m w.e. yr^{-1} at the ice cap summit) for the last 1500 years and 10% greater than present for the 3500 years prior to that.

The first ice dynamics study on DIC was conducted by Cress and Wyness (1961) using optical surveying techniques to determine ice displacements along the Sverdrup Glacier. These measurements revealed that ice velocities were faster during the melt season than during the winter, and that ice velocities increased during the course of the day in the summer.

2.2 Devon Ice Cap Climate

Devon Ice Cap is considered a polar desert with mean annual precipitation of <200 mm and surface air temperatures that only exceed freezing for two to three months during the summer (Gardner and Sharp 2007, Boon et al 2010). Snowmelt initiates in early June to early July and the ablation season is characterized by short melt periods interspersed with times of melt cessation due to inclement weather (Boon et al 2010). To understand the contribution of different air masses to summer melt and annual net balance, Alt (1978) classified synoptic weather patterns to determine their impact on summer ice cap conditions from 1961-1974. It was found that strong cyclones over Baffin Bay contribute to decreases in summer melt but increases in summer snowfall, while increased anti-cyclonic activity enhances melt for outlet glaciers but not for the ice cap interior. Alt (1987) determined three regional synoptic weather patterns associated with extreme mass balance years: (I) development of a high-pressure ridge from the south at all levels of the troposphere resulting in high melt; (II) development of a cold trough across Ellesmere Island resulting in suppression of melt and (III) cold polar lows tracking across south/southeast from the Arctic Ocean resulting in summer accumulation. Gardner and Sharp (2007) found that since 1987 the circumpolar vortex has shifted eastward (linked to higher July mean air temperatures), which has increased ridging and surface air temperatures over the Queen Elizabeth Islands and resulted in more extreme melt years and more negative mass balances.

2.3 Recent Research on Devon Ice Cap (1990s and 2000s)

Over the past decade or so, mass balance studies on DIC have been completed by Dowdeswell et al (1997) and Mair et al (2005), and previous ice dynamics research has been completed by Shepherd et al (2007), Dowdeswell et al (2004) and Burgess et al (2005). The following section will summarize the current state of knowledge for the glaciated area of Devon Island.

2.3.1 Previous Mass Balance Research

For the Canadian Arctic Islands, >70% of glacier mass balance years were negative from 1960-1993, and specifically for Devon Ice Cap, the years from 1960-1991 were negative at a 95% significance level (Dowdeswell et al 1997). Negative glacier mass balance can be due to two main reasons: a decrease in precipitation, and/or an increase in summer ablation. For the High Arctic as a whole, prior to 1990, it was unclear as to which mechanism was dominant (ACIA 2004). Since 1990, however, studies have shown that some High Arctic glaciers are losing mass with no clear change in melt, while others are losing mass with a clear increase in melt (ACIA 2004). Thus, the mechanism causing negative mass balance for a particular glacier or ice cap is specific to that region. Studies indicate that for Devon Ice Cap, snow accumulation has remained relatively constant over the last 40 years (Koerner 1966, Shepherd et al 2007), which means that the ice cap is likely losing most mass via accelerated melt (i.e., higher summer temperatures).

A recent study by Mair et al (2005) reconstructed a 37 year mass balance record for Devon Ice Cap by two methods: 1) shallow ice coring to determine snow accumulation rates since a distinctive 1963 marker horizon caused by nuclear bomb testing, and 2) degree-day melt modeling driven by long-term daily air temperature and snow accumulation records. This study showed that Devon Ice Cap (excluding the southwest arm) lost an average of 1.6 +/- 0.7 km^3 of ice per year from 1963 - 2000. These results are consistent with similar mass balance studies of the region conducted by Burgess and Sharp (2004), Koerner (2005) and Shepherd et al (2007). Additionally, studies have found that over the period 1960-2003 warmer summers have increased, and the depth of meltwater percolation in the accumulation zones of QEI Arctic glaciers has also increased

(Koerner 2005). By comparing aerial photography and satellite imagery between 1959/1960 and 1999/2000, Burgess and Sharp (2004) determine changes in mass balance for DIC over the 40-year period. Their main finding is a decrease in ice area of 2.4% over this period, with four main areas of mass change:

I. Retreat of the major tidewater glaciers on the east coast.
II. Indications of a surface lowering in the northeast and southeast regions of the ice cap.
III. Ice advance of ~130 m along 80 km of the northwest margin.
IV. Minor advance of the Sverdrup Glacier and the Croker Bay Glacier basins.

Burgess and Sharp (2004) suggest that much of the ice cap is likely responding to recent climate warming, while the northwestern region of the ice cap is likely still responding to cooler climatic conditions that occurred during the Little Ice Age.

In summary, all studies indicate that in terms of mass balance:

I. Devon Ice Cap is experiencing a net mass loss, but that this loss is not spatially uniform, with the northwest portion of the ice cap experiencing a small mass gain from 1959/1960 to 1999/2000.
II. Overall mass loss is driven by increases in summer melt, while precipitation has remained relatively constant.

2.3.2 Previous Ice Dynamics Research (Devon Ice Cap and Belcher Glacier)

The first ice dynamics research on DIC occurred in 1961 on the Sverdrup Glacier, via the use of optical surveying of stakes drilled into the ice surface (Boon et al 2010, Cress and Wyness 1961). Cress and Wyness (1961) measured surface velocities of ~35 m yr^{-1} before melt and ~65 m yr^{-1} after the onset of melt in the ablation area of Sverdrup Glacier and provided the first evidence that surface ice speeds varied temporally on DIC. Recent research has been completed by Shepherd et al (2007), Dowdeswell et al (2004) and Burgess et al (2005), who determined ice dynamics with the use of remote sensing techniques (Shepherd et al (2007) also used dGPS to determine ice motion). The following summarizes the main results of these studies and provides an overview of

current knowledge of the dynamics of DIC. Table 2.1 provides a summary of the satellite imagery used by each of the previous studies and Figure 2.2 provides the velocity maps produced by them.

2.3.2.1 Shepherd et al (2007)

Shepherd et al (2007) conducted a study of the ice dynamics of DIC using an interferometric SAR (InSAR) method on 1-day and 35-day ERS 1/2 imagery. This study found that 11 major glaciers drain Devon Ice Cap with the fastest flow via Croker Bay Glacier in the southwest portion of the ice cap, and more than half of the mass loss occurring through the southeast portion of the ice cap via glaciers grounded below sea level. Study results were validated using repeat differential GPS measurements of a 23-stake network in the northwest portion of the ice cap (stakes were set out and surveyed in April 1999 and resurveyed in April 2000 and April 2001). These in situ results were on average within 5% of the annual velocities derived from the InSAR method over the same area, except for 5 stakes positioned near the ablation zone of Sverdrup Glacier, where in situ results were within 16% (consistently higher) of the annual velocities and total annual velocities exceeding those expected from creep alone. This suggests that velocities over at least this part of the ice cap are influenced by seasonal changes in basal lubrication (i.e. draining of supraglacial melt to the bed via moulins) (Shepherd et al 2007).

Ice discharge for DIC calculated using velocities from the InSAR method combined with a model of ice depth near the termini of all outlet glaciers showed ice losses of 1.43 +/- 0.03 Gt per year. Overall, ice discharge was 7% higher during the summer than the winter due to the seasonal variation in velocities. Overall, the ice cap contributes 0.003 mm a^{-1} of global sea level rise, about half of previous estimates by Burgess et al (2005) and Mair et al (2005) for the 1960 to 2000 period (Shepherd et al 2007).

2.3.2.2 Dowdeswell et al (2004)

By utilizing a combination of airborne ice penetrating RADAR, analysis of Landsat imagery, and InSAR processing of ERS 1/2 one-day repeat and three-day repeat pass

imagery, Dowdeswell et al (2004) investigated the form and flow of DIC. Their major findings were that the size of the ice cap proper (excluding the stagnant southwest arm) is 12,050 km^2, the largest drainage basin (located in the Southeast portion of the ice cap and including Southeast2 Glacier) is 2630 km^2, maximum elevation is 1921 m and maximum ice thickness is 880 m. All glaciers on the eastern margin have retreated by 1-3 km since 1960, and if the entire ice cap were to melt it would contribute ~10 mm global sea level equivalent. InSAR results show slower, undifferentiated flow in the western and central portions of the ice cap and fast flowing outlet glaciers in the eastern portion. Outlet glacier velocities are 7-10 times higher than velocities in areas of undifferentiated flow at the boundaries between drainage basins, a flow structure typical of Arctic ice caps. The pattern of fast-flowing regions embedded within slower-flowing regions is also consistent with the patterns displayed by outlet glaciers flowing from the Greenland and Antarctic Ice Sheets.

Dowdeswell et al (2004) hypothesize that the reasons for the difference in flow structure between the east and west sides of DIC are because:

I. In the western and central portions of the ice cap the bed is characterized by relatively smooth and flat topography, while faster flowing regions in the east are characterized by much more mountainous bed topography.
II. There is low precipitation and mass turnover in the northwestern portion of DIC (Koerner 1979).

Fast flowing areas of DIC are usually associated with troughs in the basal topography, due to the fact that basal melting occurs first under thick ice located in these areas (Dowdeswell et al 2004). These results are consistent with the findings of Shepherd et al (2007), both in terms of velocity structure for the DIC and for seasonal variations in ice motion.

2.3.2.3 Burgess et al (2005) and Burgess (2006)

The most comprehensive study to date of ice velocities over Devon Ice Cap was conducted by Burgess et al (2005) and Burgess (2006). This study used SAR

interferometry and speckle tracking with ERS-1/-2 and Radarsat-1 data to map the surface velocity over the majority of the ice cap. They found that:

I. The ice cap has very different ice flow dynamics between the east and west. The western portion of the ice cap is drained dominantly by sheet flow, while the eastern portion is drained by fast-flowing outlet glaciers.
II. Roughly 20.5 km^3 of ice was calved from the ice cap between 1960 and 1999, 89% of which was discharged from the eastern margin.
III. The Belcher Glacier basin accounted for 50% of the total ice calved, and is responsible for 15% of mass loss from DIC.
IV. Ice calving accounts for 30% of the total ablation between 1960 and 1999, suggesting the iceberg production can be a highly significant source of mass loss for High Arctic glaciers that terminate in tidewater.

This research also notes that because the outlet glaciers terminate in tidewater, they are potentially very sensitive to changes in climate and sea level. This is because they have continuously high velocities at their termini and their motion is controlled by longitudinal forces that provide little resistance to motion at their snout, with high basal sliding rates due to high water pressures at the bed (Bartholomaus et al 2007, Meier and Post 1987). At the calving front of marine terminating glaciers, accelerated basal motion at the same point over time leads to increased ice discharge into oceans and contributes to sea level rise (Figure 2.3) (Bell 2008, Bartholomaus et al 2007, Zwally et al 2002, Meier et al 2007, Holland et al 2008).

2.3.3 Limitations of Previous Ice Dynamics Research

The aforementioned studies of DIC all provide velocity estimates from SAR interferometry. Shepherd et al (2007) used dGPS techniques to determine ice motion in addition to interferometry, but these were point measurements that provide only limited spatial coverage and no information on the variations in motion between resurveys. A major limitation with the interferometric method is that ice velocities can only be determined in the line of sight of the SAR sensor, meaning that determination of ice velocities in areas where the flow is perpendicular to the SAR look direction are

unreliable (Burgess et al 2005). This means that in order to determine ice motion using interferometry, imagery with different look directions must be combined, and/or information about surface elevations must be used to make assumptions about ice flow. A common practice (one used by Shepherd et al (2007)) is to use the assumption of surface-parallel ice flow (Kwok and Fahnenstock 1996). In this case, by subtracting a model of the interferometric phase due to topography and satellite separation (baseline), the phase information due to motion is all that remains from the interferogram. This leaves only the "motion-only" phase, which is then corrected to the direction of maximum slope as determined from a digital elevation model. In this way, look direction displacements can be turned into down slope displacements.

However, even using these methods does not produce perfect results due to the inability to resolve displacements that are roughly perpendicular to the look direction. Burgess et al (2005) used a DEM to project interferometry results to downslope velocities, but due to the above limitations was only able to estimate surface ice velocities for ~75% of DIC. This limitation of the interferometry method provides good motivation for the use of speckle tracking for this study. Speckle tracking is not dependent on the phase unwrapping required for interferometry, which means that it can measure displacements in both the along-track and line-of-sight directions.

2.3.4 Devon Ice Cap Flow Regimes

From the above studies, a set of four flow regimes relating to ice thicknesses and local driving stresses on DIC have been identified (Figure 2.4) (Burgess et al 2005, Dowdeswell et al 2004, Shepherd et al 2007, Boon et al 2010). Flow regime 1 constitutes a large portion of the ice cap (50%), and includes areas such as the western lobe, the ice cap interior and portions of the southeast section below 300 m asl. Within flow regime 1, ice is assumed to be frozen to its bed, thus limiting motion to internal deformation alone. Flow regime 2 accounts for 22% of the area of the eastern portion of the ice cap and 8% in the west and includes the heads of major outlet glaciers (Croker Bay and Southeast 2). Within flow regime 2 there is likely to be a small contribution of basal sliding to overall ice motion. Flow regime 3 is comprised of the lower reaches of major outlet glaciers

(Crocker Bay, Belcher), and within this regime basal sliding becomes an increasingly important component of total surface motion. In flow regime 4 a large contributor to basal motion occurs from deformation of bed sediments, and this regime is only found at the termini of outlet glaciers (Burgess et al 2005, Boon et al 2010).

2.4 Basal Conditions and Glacier Flow

Glaciers flow under three processes: ice creep, basal sliding and basal deformation. Ice creep occurs when the glacier deforms under its own weight and is a result of the movement within or between individual ice crystals. Ice creep rates are largely dependent on the temperature of the ice, the orientation of the ice crystals and the presence of impurities. Velocities that can be achieved solely due to ice creep are minimal for areas where ice is non-channelized and unconstrained (<10 m yr^{-1}). However, high motion due to ice creep can be achieved in areas where large amounts of ice are channeled into deep, well-constrained bedrock valleys. For example, velocities attributed to ice creep at Jakobshaven Isbrae, an outlet glacier in Greenland, are 235-260 m yr^{-1} (Luthi et al 2002).

Bed deformation refers to glacial motion due to shearing of the sediments underlying soft-bedded glaciers (Willis 1995, Bamber et al 2007, Benn and Evans 1998). In the case of bed deformation, subglacial water discharge either flows along the ice/bed interface or within the underlying sediments and the rate of water movement is dependent on both permeability of the sediments and the water pressure (Knight 1998). If the bed cannot evacuate all the water within such a system, the underlying till becomes saturated and the water pressure beneath the glacier builds. This enhances glacier motion in two ways:

I. Weakening the bed and permitting greater deformation of the sediments.
II. Altering the flow of the water within the till and at the ice/bed interface and causing decoupling of the glacier from its bed. Potentially, if water pressures are high enough this type of drainage can develop into discrete channels and pipes (Willis 1995, Knight 1998, Clarke 1987).

Seasonal changes of ice motion for glaciers on porous till are possible as enhanced motion may be the result of intra-annual water pressures changes at the ice/till interface.

However, these fluctuations may also be due to changes of the deformation of the till due to increasing pore water pressure (Willis 1995, Boulton et al 2001). Experiments by Boulton and Hindmarsh (1987) placed segmented rods into the till below the Breidamerkurjokull Glacier, Iceland, and excavated them several days later. The results showed that the upper 50 cm of till deformed the most, with deformation decreasing with depth. Specifically, segmented pieces of the rod were displaced ~40 cm horizontally near the ice/bed interface and ~0 cm at a depth of ~1 m. These experiments illustrated that the deformation of sediments is greatest at the ice/bed interface for soft bedded glaciers, and that motion of the sediments contributes to overall glacier velocities.

Basal sliding is an important controlling factor of the motion for hard-bedded glaciers (Willis 1995). Water acts to lubricate the interface between the glacier and its bed, with the ice decoupling from underlying bedrock when water pressure at the ice/bed interface exceeds the overburden pressure of the glacier. In many cases, vertical ice motion is detected before horizontal ice motion increases under these conditions (Mair et al 2001, Bingham et al 2008, Willis 1995, Benn and Evans 1998, Knight 1998). Basal sliding has been identified as a means for faster ice motion to occur in a warming climate due to larger volumes of water being transmitted to the glacier bed (Boon et al 2003, Zwally 2002, Bell 2008). Cress and Wyness (1961) were the first to report variations in ice motion at DIC, with faster motion in the ablation area of the Sverdrup Glacier after the onset of the melt season. Shepherd et al (2007) also noted a distinct seasonal variation in velocities between summer and winter on DIC, and hypothesized that these variations were likely linked to subglacial hydrology. As such, it seems likely that the dynamics of outlet glaciers of DIC are controlled by their subglacial drainage characteristics. Thus, in order to understand the causes of seasonal changes and motion of the Belcher Glacier determined here, a broader overview of the drainage controls on glacier flow is necessary; the following provides this context.

2.4.1 Supraglacial and Englacial Drainage

On areas of a glacier surface where melt rates exceed refreezing rates, water will accumulate within the snowpack and produce melt ponds on the surface (Boon et al

2003). These melt pools can connect and may produce a large supraglacial stream network, particularly in the ablation area (Boon et al 2003, Boon and Sharp 2003, Benn and Evans 1998). Moulins are an important part of this network, and are large near-vertical shafts that extend into the glacier and are capable of transmitting large amounts of water from the glacier surface to the glacier interior. Englacial drainage refers to the movement of water within a glacier, with most of this water originating from surface melt that has flowed down through moulins and/or crevasses. Changes to the characteristics of the supraglacial drainage network can therefore have large affects on the nature of englacial drainage (Boon et al 2003, Nienow et al 1998). For example, as the supraglacial drainage network develops throughout the summer melt season, it is possible that old moulins will be isolated from surface melt in favor of newly developed crevasses upstream, creating abandoned moulins.

Water levels within moulins vary temporally, with pressures highest during periods of rapid melt or rainstorms (Boon and Sharp 2003, Benn and Evans 1998, Bartholomaus et al 2007). If the meltwater entering the system is higher than the capacity of the network, then the water levels and pressure within the system increase. Shortly after the peak of the melt season has occurred, the water transport capacity of the englacial drainage system will be at a maximum (because increased water flow melts englacial channels faster than they can close due to creep), meaning that pressure within it is likely to be close to atmospheric, with associated high water levels and low pressures. At the end of the melt season, when surface melt ceases, the englacial drainage network will close due to ice deformation. This occurs in the autumn and throughout the winter until the next summer's melt period, when the process of supraglacial and englacial drainage development begins again (Benn and Evans 1998, Nienow et al 1998, Mair et al 2001, Iken and Truffer 1997).

2.4.2 Subglacial Drainage Networks

Subglacial drainage network development at the glacier bed has recently been found to have a profound influence on glacier velocities (Bartholomaus et al 2007, Zwally et al 2003, Bingham et al 2005, Bingham et al 2008, Benn and Evans 1998). Figure 2.5

summarizes the drainage networks for hard and soft bedded glaciers. The two fundamental types of subglacial drainage networks are discrete and distributed systems. For discrete systems drainage is confined to a few large well-developed channels, while in a distributed system drainage occurs over large portions of the glacier bed as a sheet or through small channels.

2.4.2.1 Discrete Subglacial Drainage

Discrete subglacial drainage is characterized by two types of well developed channels at the glacier bed. The first type of channel is termed Röthlisberger channels (R-channels) and the second type is termed Nye channels (N-channels) (Röthlisberger 1972, Nye 1973, Benn and Evans 1998, Fountain and Walder 1998, Knight 1998) (Figure 2.6). Large R-channels tend to capture water from smaller channels, and in this way produce a large branching network that provides an efficient means of evacuating water from the glacier bed (Sharp et al 1989, Fountain and Walder 1998, Röthlisberger 1972). N-channels incise into the bedrock beneath glaciers where they sit directly on a hard bed, and are particularly common in limestone areas (Sharp et al 1988). The presence of N-channels suggest that basal water flow is consistently focused along the same route. Swift et al (2002) studied the seasonal discharge of suspended sediment within subglacial water flow with the seasonal development of the subglacial drainage network for the Haut Glacier d'Arolla, Switzerland, during the 1998 melt season (Figure 2.7). The results show that water and suspended sediment discharge during the winter months (when a distributed drainage network is present) was ~10,000 m^3 d^{-1}, while in the summer (when a discrete drainage network of R-channels are present) discharge was ~40,000 m^3 d^{-1}. This research reveals the efficiency of subglacial drainage in the winter versus the summer (Fountain and Walder 1998, Swift et al 2002).

2.4.2.2 Distributed Subglacial Drainage

Distributed drainage systems are inefficient at evacuating water from the glacier bed due to the tortuous route that water must follow in order to exit the system. Water films comprise one form of distributed subglacial network, and have been argued to constitute the principal drainage network of glaciers (Weertman 1964, Weertman 1969, Fountain and Walder 1998, Knight 1999, Willis 1995, Benn and Evans 1998). However, this type

of system is recognized to rarely develop to more than a millimeter thick without forming channelized flow or filling subglacial cavities (Benn and Evans 1998, Knight 1999). As such, water films have a limited ability to transport water and appear to be mostly produced from subglacial ice melt. When a water film becomes greater than 4 mm thick it becomes unstable and water will migrate from films into cavities (Willis 1995, Walder 1982).

Linked cavity networks are a second, larger kind of distributed subglacial drainage network. In this system, basal water drains through a network of cavities that develop between the glacier and bed that are linked via narrow orifices. Water transit through a linked-cavity system is slow because of the complex path that the water must follow, and also due to temporary storage in poorly connected cavities. When dye is injected into a linked cavity system, the discharge at the snout is multi-peaked and diffuse in contrast to single, sharp peaks characteristic of channelized systems. This is indicative of the subglacial pattern of splitting and rejoining flow paths in linked cavity systems, as well as temporary storage within cavities (Benn and Evans 1998). If the water pressure in a linked cavity system increases, the orifices will gradually enlarge by roof melt or the system will enlarge to create new links to cavities, this is termed stable orifice growth. If, however, water pressures exceed the capacity of the linked cavity system, unstable orifice growth occurs, which leads to the conversion of the system from linked cavities to a network of interconnected channels (Sharp et al 1988, Kamb 1987, Willis 1995).

2.4.2.3 Switches Between Drainage Systems

Subglacial hydrology is known to switch between distributed and discrete drainage systems throughout the course of a year (Willis 1995, Bingham et al 2005, Bartholomaus et al 2007, Iken and Truffer 1995, Fudge et al 2005, Zwally 2002, Benn and Evans 1998, Knight 1999). Distributed subglacial drainage appears to form a stable system during winter conditions of low water pressures (Nienow et al 1998, Fudge et al 2005, Benn and Evans 1998). Over the course of a melt season, when large amounts of meltwater are generated at the glacier surface and drained to the bed via moulins and crevasses, distributed drainage networks become overburdened and develop into a channelized

system (Bartholomaus et al 2007, Zwally et al 2002, Bingham et al 2008, Copland et al 2003a, Rabus and Echelmeyer 1997). After the melt season, when inputs of water are minimal, channels will close due to ice creep. As these channels close, the efficient drainage network breaks down, and a distributed network re-develops.

Nienow et al (1998) provide a good overview of seasonal basal controls on glacier dynamics for the Haut Glacier d'Arolla. By using repeat dye injections on the glacier surface they found that as the melt season progresses an increasingly efficient channelized subglacial drainage system is established that grows headward at a rate of ~65 m d^{-1}. This upglacier progression works to drain the glacier of basal water, increases the amount of water that it can transport, and in turn decreases the amount water pressure available to facilitate basal sliding. At Engabreen Glacier, Norway, Lappegard and Kohler (2005) monitored water level and pressure at the ice-bedrock interface while water was pumped into the subglacial drainage system. Their results show that during the summer low pressures and high water discharge occurred, inferring discrete drainage. However, in the winter basal water pressures were an order of magnitude higher than in the summer, but water discharges were low. This is indicative of a distributed system, and implies that a seasonal switch in the type of subglacial drainage network had occurred.

Nienow et al (1998) found that subglacial drainage channels developed during one melt season are unlikely to survive until the next melt season. This is because overwinter ice deformation would close drainage channels, leaving a residual distributed drainage network. This study also found that enhanced basal ice motion occurred after inputs of meltwater drainage via moulins and crevasses. During the onset of the melt season, when inputs of surface melt water drain via moulins to the bed but before a fully developed channelized system has developed, the bed will become fully pressurized (water pressure exceeds the ice overburden pressure, causing basal floatation) for a short period. When this occurs, the glacier can decouple from the bed and the potential for basal sliding is great. This type of glacier motion typically occurs at the beginning of the melt season when the drainage network becomes overburdened with melt inputs, although it may also

occur later in the melt season after rapid meltwater inputs (i.e. after heavy rainstorms). Willis (1995) notes that the highest glacier motion occurs when there are high basal water pressures due to the subglacial drainage network being unable to evacuate all the high water inputs from the bed. After high discharge occurs a channelized drainage system develops, thereby de-pressurizing the bed and terminating faster motion (this occurs later in summer).

Some supraglacial drainage through moulins and crevasses may reach the bed away from areas of channelized subglacial flow (Nienow et al 1998). In these cases, it is likely that the quantities of water input are not enough to initiate new subglacial channel formation, but instead drain directly into an inefficient distributed network. When this occurs, the water can act to locally pressurize portions of the bed without creating channelized flow.

2.5 Inter-annual and Intra-annual Variations in Glacier Velocity

Glacier motion is partially determined by the water pressure at the glacier bed, which is in turn related to the drainage network of a particular glacier. Variations in water supply to the glacier bed and temporal changes in the type of basal drainage network can be used to explain the seasonal variations in ice motion (Bartholomaus et al 2007, Bindschadler 1983, Iken and Truffer 1995). Willis (1995) notes that on virtually all glaciers there are variations between winter and summer velocities. For example, between 1979 and 1985, Findelengletscher Glacier in Switzerland advanced about 250 m and retreated thereafter. Iken and Truffer (1997) made observations of surface ice velocity (by surveying 2-3 poles drilled into the ice surface) and subglacial water pressure (with the use of boreholes). Between 1979 and 1983, velocity maximums were achieved in the spring (~0.5 m d^{-1}) and minimums occurred in June (~0.3 m d^{-1}) with a build up of velocities throughout the autumn. Subsequently, from 1983-1994, maximum velocities were achieved in June (~0.4 m d^{-1}) and minimum velocities occurred in the winter (~0.25 m d^{-1}), with a build up of velocities through the winter. This research suggest that changes in basal water pressure between melt seasons is responsible for inter-annual variations in surface ice motion. Large fluctuations in glacier velocity and basal water pressure are

controlled by changes to the subglacial drainage system (distributed/linked-cavity in winter and early summer, and discrete/R-channels in the summer and autumn).

Iken and Truffer (1997) also note that isolated and interconnected cavities may coexist, and the degree to which cavities connect similarly affects glacier motion. When cavities become more and more interconnected, the area of the glacier which is exposed to changes in basal water pressure increases, allowing for larger portions of the glacier to be affected by basal sliding. As such, a basal process that allows cavities to increasingly become connected will cause an increase in seasonal and diurnal ice motion. Similarly, Fudge et al (2009) found evidence for increased basal ice motion of the Bench Glacier in Alaska during the onset of the melt season followed by slow motion after a well-developed subglacial drainage network had been established. Specifically, they found that velocities prior to summer speed up were 1.6 to 2.8 cm d^{-1} and increased to between 50 cm d^{-1} at the beginning of the speed up and 100 cm d^{-1} by the end of the speed up event, after which they returned to pre-summer levels. As such, a progression of subglacial drainage development strongly influences the seasonality of ice motion for particular glaciers and can be used to explain inter-annual and intra-annual velocity fluctuations.

The aforementioned research was conducted on temperate glaciers, which may not be completely analogous for High Arctic glaciers. Muller and Iken (1973) conducted an investigation of the surface ice velocities and the subglacial drainage network of White Glacier (a polythermal valley glacier) on Axel Heiberg Island in the Canadian High Arctic. Based on surveying of 6 stakes on the glacier surface, they found a high degree of seasonality in ice motion related to changes in subglacial drainage. Specifically, summer surface velocities (~12 cm d^{-1}) coincided with marked increases in ablation and were greater than winter velocities (~7.5 cm d^{-1}). They hypothesized that high levels of ablation allow for the decoupling of the glacier from its bed which facilitates greater horizontal motion. The lag time between high rates of ablation and horizontal motion is linked to the evolution of the subglacial hydrology of the glacier (distributed system in the winter, pressurized bed due to ablation early in the melt season, development of channelized flow as the melt season progresses).

Bingham et al (2005) used a dye tracing method to determine of the development of the subglacial drainage network throughout the melt season on John Evans Glacier, a high Arctic polythermal glacier. They found that over the course of a consistently warm melt season the subglacial drainage system developed rapidly and was highly channelized. Conversely, the following year, when the melt season was cooler, a distributed drainage system was more dominant (Bingham et al 2005, Bingham et al 2006). During the time between initial meltwater input to the glacier bed and subglacial water escape at the terminus the bed became pressurized, causing 2-4 days of higher horizontal motion due to enhanced basal sliding (Bingham et al 2006). On John Evans Glacier, Copland et al (2003c) found that meltwater is caught behind the snout by a thermal "dam" in winter and this meltwater is released when surface meltwater penetrates the bed the following summer (usually late June to early July). However, the presence of this dam plays an important role in producing high water pressures (120% of ice overburden pressure) at the bed in early summer. As such, the presence of a thermal dam at high Arctic glaciers is likely to have an important impact on water pressures at the glacier bed which can facilitate higher rates of horizontal motion.

These studies indicate that the relationships between surface motion and subglacial hydrology exhibited on high Arctic polythermal glaciers are similar to those found on temperate glaciers. As such, using the aforementioned research can help to improve understanding of the causes of seasonal changes in ice motion observed on Devon Ice Cap.

Burgess et al (2005)	Radarsat-1	Oct 14-Nov 7, 2000
	Radarsat-1	Nov 20-Dec 14, 2000
	ERS1/2	Mar 15-16, 1996
	ERS1/2	Apr 25-26, 1996
	ERS1/2	Feb 6-9, 1992
Shepherd et al (2007)	ERS1/2	Apr 6-7, 1996
	ERS1/2	May 11-12, 1996
	ERS1/2	Apr 19-20, 1996
	ERS1/2	May 24-25, 1996
	ERS1/2	Apr 6-7, 1996
	ERS1/2	Apr 6-May 11, 1996
	ERS1/2	Apr 7 –May 11, 1996
Dowdeswell et al (2004)	ERS1/2	Mar 15-16, 1996
	ERS1/2	Apr 25-26, 1996
	ERS1/2	Feb 6-9, 1992

Table 2.1: *Summary of satellite imagery used in previous ice dynamics studies of Devon Ice Cap.*

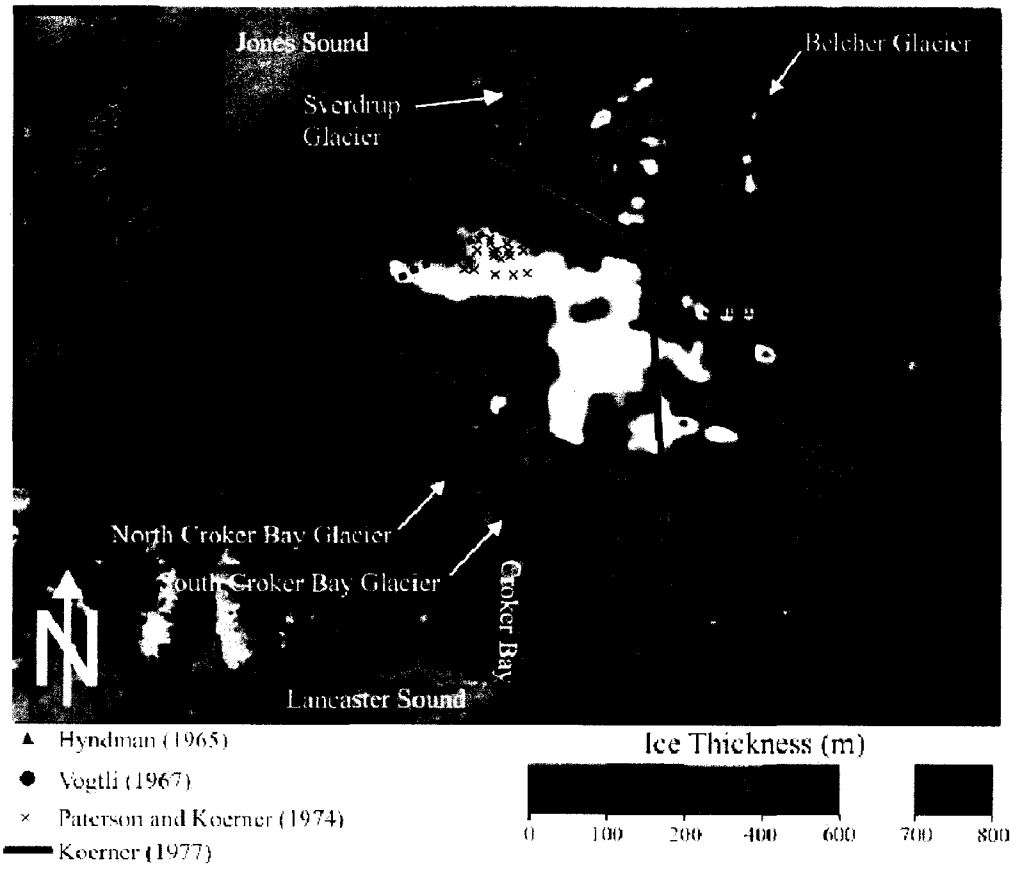

***Figure 2.1**: Devon Ice Cap thickness determined by gravimetric surveys (Hyndman 1965), and radio echo sounding by Vogtli (1967), Paterson and Koerner (1974) and Koerner (1977), and airborne radio echo sounding by Dowdeswell et al (2004) (from Boon et al 2010).*

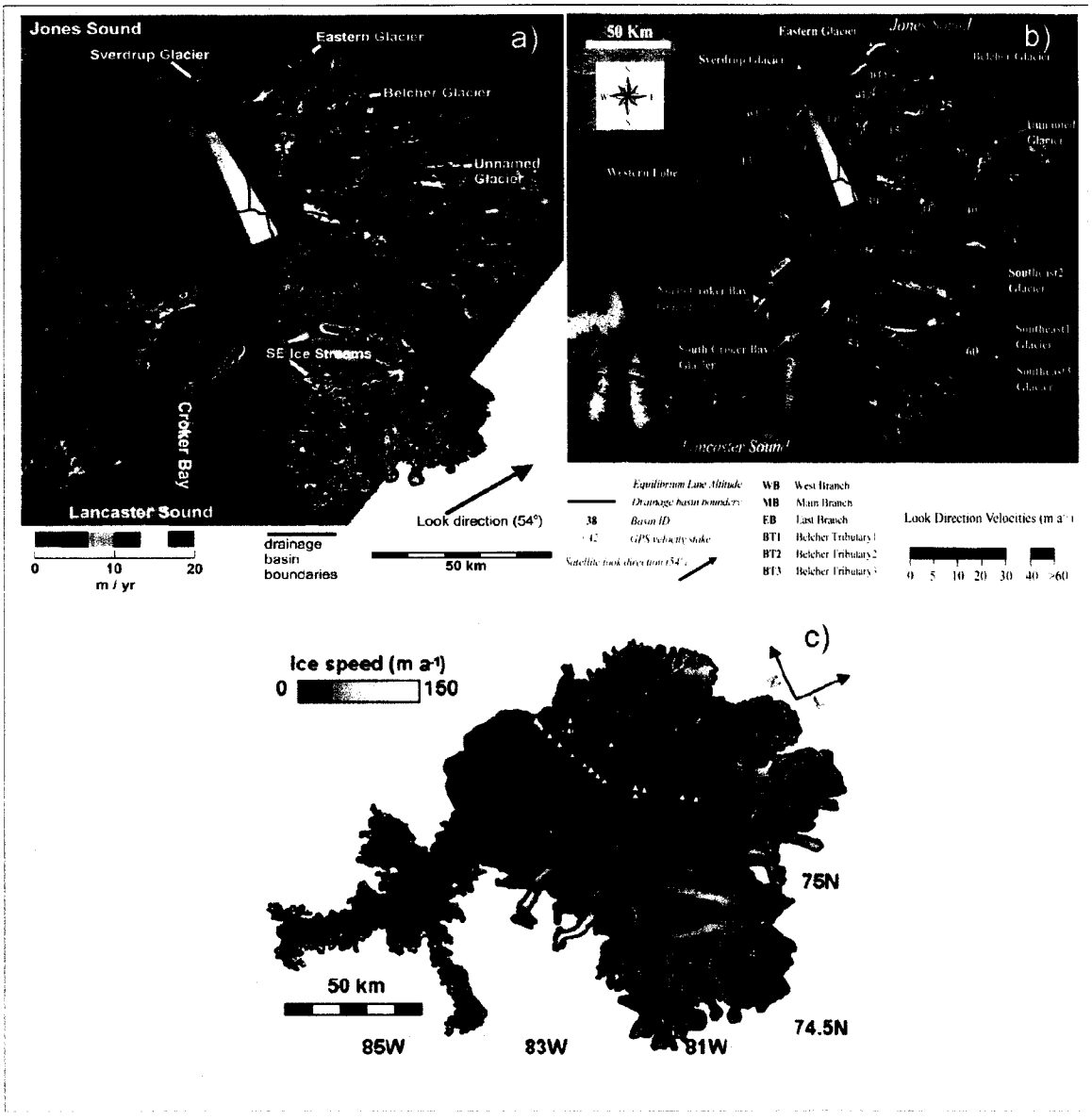

Figure 2.2: *Velocity maps of Devon Ice Cap produced by previous ice dynamics studies: a) Dowdeswell et al (2004) ice velocities determined using interferometry, with displacements shown in line of sight, b) Burgess et al (2005) using interferometry and speckle tracking displacements corrected to downslope displacements, c) Shepherd et al (2007) using interferometry corrected to downslope displacements.*

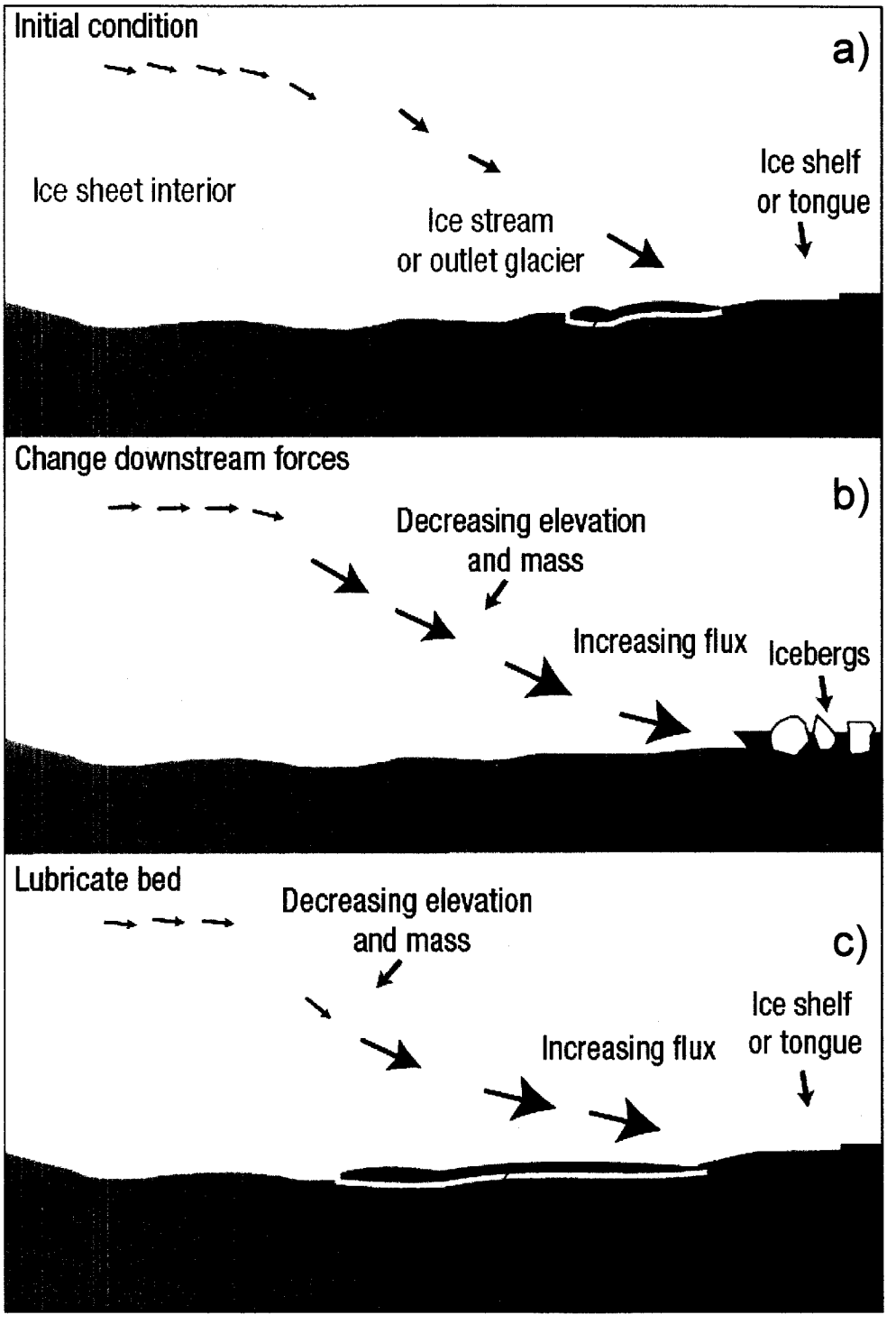

Figure 2.3: *Mechanisms for accelerated ice loss from tidewater terminating glaciers; a) longitudinal compressive force slows the flow of an ice stream; b) removal of an ice shelf or ice tongue producing higher upglacier velocities; c) increase in basal water due to increased summer melt, increased lubrication at the bed, yielding high upglacier velocities (Bell 2008).*

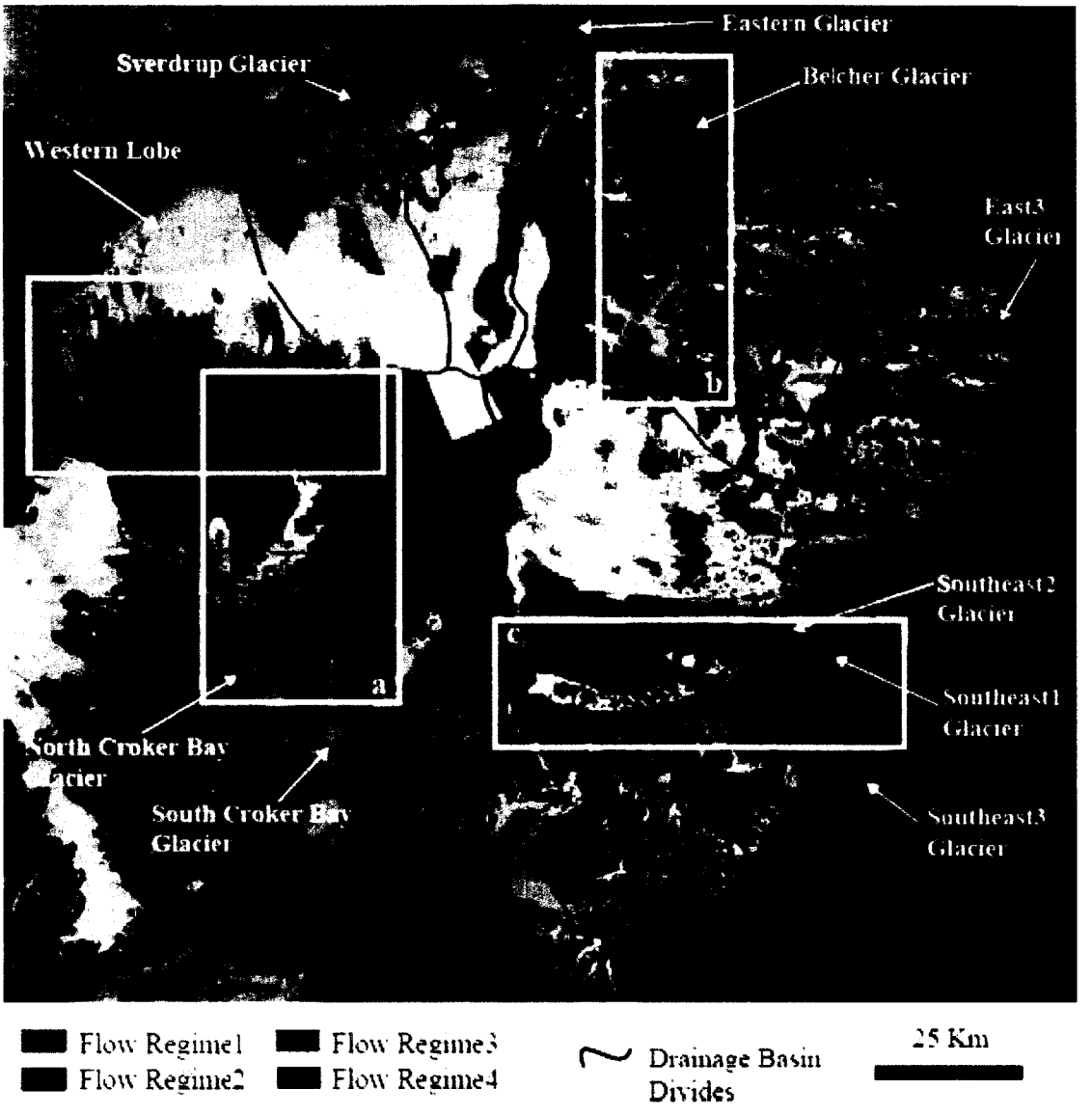

Figure 2.4: *Flow regimes of Devon Ice Cap as described by Burgess et al (2005). Flow regime 1: ice is frozen to its bed and motion is limited to deformation alone. Flow regime 2 basal sliding plays a contributing role in overall ice motion. Flow regime 3 comprises to lower portions of outlet glaciers, basal sliding is an increasingly larger role in overall ice motion. Flow regime 4, located at the termini of outlet glaciers, where basal motion is likely due to the deformation of basal sediments.*

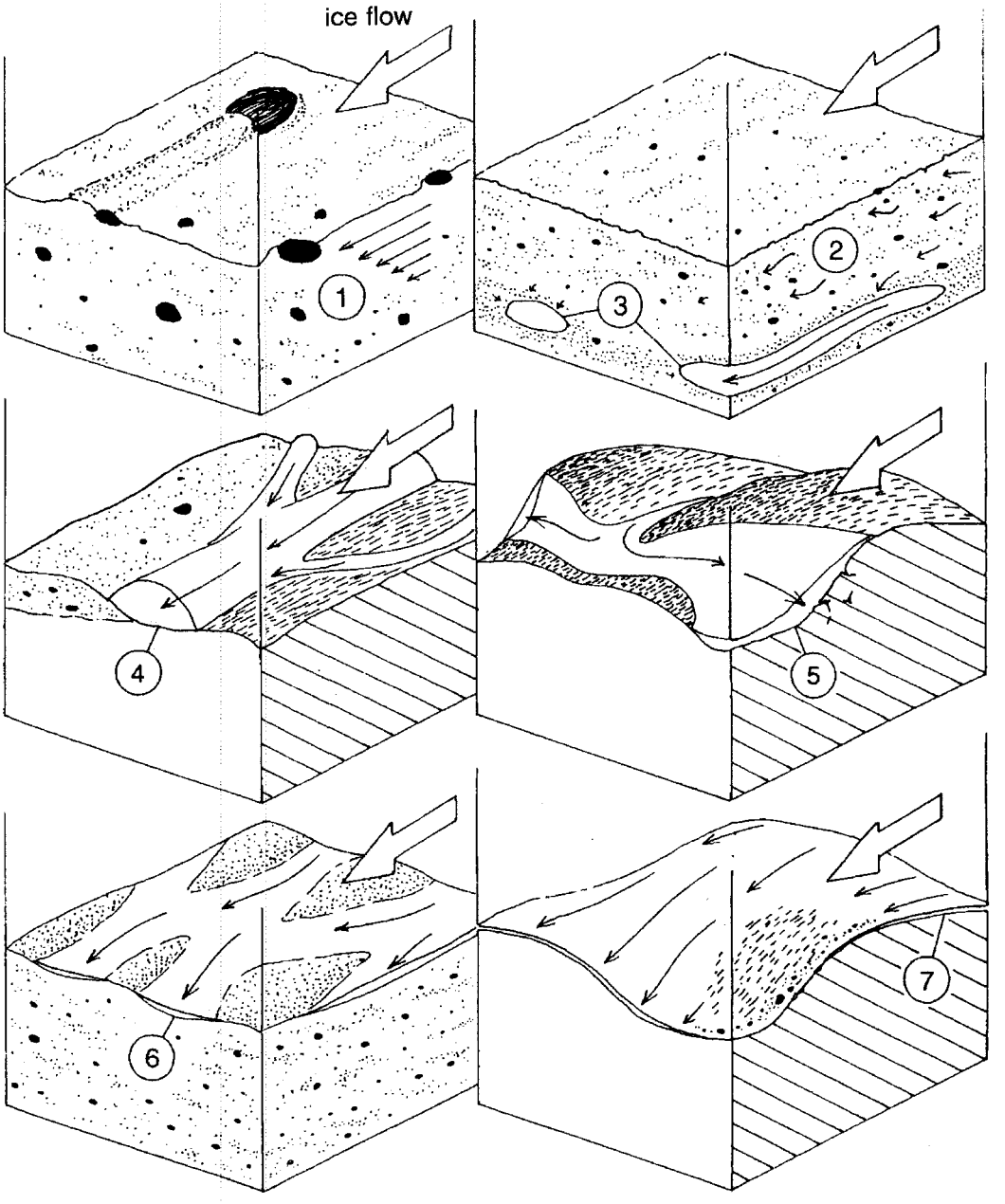

Figure 2.5: *Subglacial drainage networks for soft and hard bedded glaciers: (1) deforming bed; (2) Pore water flow and (3) pipe flow; (4) channel network; (5) Linked-cavity system; (6) Braided canal network; (7) water film at the ice/bed interface (Benn and Evans, 1998).*

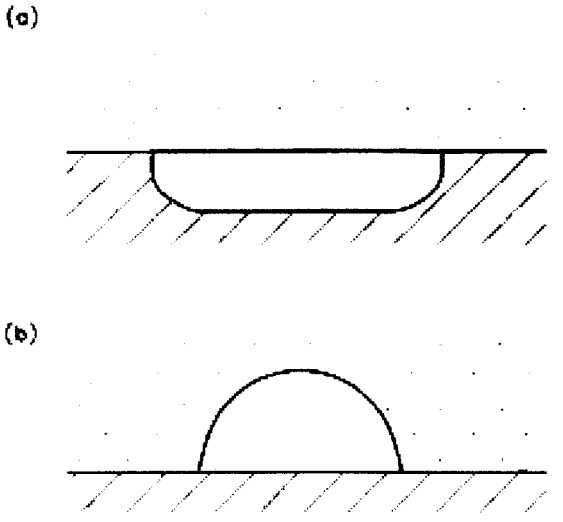

Figure 2.6: *Discrete subglaial drainage: (a) Nye channels incised downwards into bedrock; (b) Rothlisberger channels incised upwards into ice (Knight 1998).*

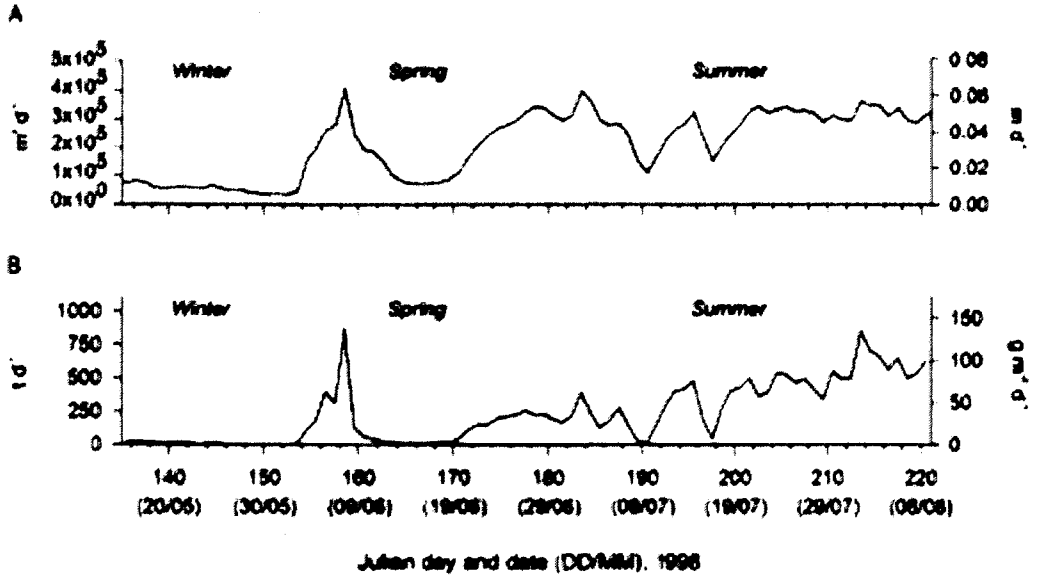

Figure 2.7: *Seaonal fluctuations in (a) water discharge and (b) suspended sediment load at Haut Glacier d'Arolla indicating a change in subglacial drainage (Swift et al 2002).*

Chapter 3: Methodology

In May 2008 fieldwork was conducted on Devon Ice Cap, with a specific focus on the Belcher Glacier ablation area and its accessible tributaries. The fieldwork occurred prior to the onset of surface melt, which ensured that the entire study region was accessible by snowmobile. Field measurements focused on the determination of ice depths and surface ice motion. After fieldwork, speckle tracking velocity maps were produced in Ottawa using MATLAB scripts developed by Dr. Laurence Gray. The detailed methods used are outlined in the following sections.

3.1 Differential Global Positioning System (dGPS) measurements:

dGPS is useful for providing highly accurate (~cm) location data and uses signals sent from satellites to determine precise locations. The GPS method is based on trialateration of precise time signals from a large number of satellites (up to 12 at once). Differences in the time between when the signal is transmitted and received determine how far away the satellite is. By combining this information with the known locations of the satellites, accurate positions can be determined.

dGPS is used for measuring motion associated with a number of geophysical phenomena including plate tectonics, earthquakes, deformation from volcanoes and changes in the earth's orientation (Zumberge et al 1997). The technique can also be applied to determine in situ glacier velocities, and point measurements have been found to be accurate to within a few centimeters (Berthier et al 2005, Joughin et al 2008, Copland et al 2009, Quincey et al 2009). In glaciology, this is typically undertaken by drilling fixed marker stakes into a glacier surface and surveying their position with dGPS (Figure 3.1). The stakes are then resurveyed throughout the study period, and from this the surface motion can be derived. The main error that accompanies this type of survey arises from the fact that the dGPS antenna must be mounted in exactly the same position relative to the marker stake during each survey (Berthier et al 2005). However, this was not an issue for the present research, as the dGPS antenna was screwed onto a metal pole designed to fit snugly inside the top of the marker stakes drilled into the ice surface. This ensured that the antenna was always in the same position between surveys.

This project implemented dGPS measurements on Belcher Glacier in two ways:

I. Trimble NetRS and R7 differential GPS units were installed at semi-permanent stations along the centreline of the Belcher Glacier. The stations are powered by large battery banks and solar panels, and data is retrieved each spring and summer during field visits. Research partners at the University of Alberta (mainly Brad Danielson) completed collection and processing of this data, which created an in situ velocity record for 2008 and 2009. Summer sessions in 2008 collected dGPS data every 15 seconds from late May through late August, in summer 2009 data was collected again every 15 seconds from late May to mid August. Winter sessions collected data every 12 hrs for 1 hr from Sept 2008 – Dec 2008, and again from February 2009 – May 2009. For validation of the speckle tracking results, the surface velocity vectors determined at these dGPS stations were then compared with the vectors determined from the satellite speckle tracking measurements. Temporal subsets of the dGPS data were made to provide in situ surface ice displacements that coincided exactly with the acquisition time of each pair of satellite imagery used for speckle tracking.

II. The second dGPS measurement technique utilized marker stakes that were set out on each tributary of the lower Belcher Glacier basin that could be accessed with snowmobile (Figure 3.2). Trimble R7 units were used to survey the initial position of these stakes between May 6th and May 8th, 2008. The stakes were then resurveyed again on May 24th, 2008, allowing for their displacements to be calculated over a 16-18 day timeframe. These tributary stakes were resurveyed again in May 2009, which allowed annual ice displacements to be calculated. By combining all these resurveyed point locations, the annual motion of the tributaries throughout the study area was determined. Figure 3.2 shows the locations of in situ dGPS measurements on the Belcher Glacier.

There are two ways in which dGPS measurement can be processed: relative processing and precise point positioning (PPP). Relative processing uses a GPS receiver at a known fixed location (base station) to determine the location of all other GPS receivers at

unknown locations in the study site (King et al 2002). Precise point processing (PPP) was a method created by the Jet Propulsion Laboratory, California, which does not require a base station. Instead, it uses very accurate orbital and clock information about the GPS satellite constellation that is released in a final format by the International GPS Service (IGS) 12-18 days after data collection. dGPS data obtained during the 2008 field season was processed using the PPP method via the online application provided by Natural Resources Canada (http://www.geod.nrcan.gc.ca/online_data_e.php). The dGPS data received from the University of Alberta was processed using the relative processing technique utilizing base stations. All ice velocities are corrected to values of m yr^{-1} to account for the differences in time between resurveys.

3.2 Ground Penetrating RADAR

Ground penetrating RADAR (GPR), or radio-echo sounding, has been widely used for mapping the sub-surface properties of glaciers and ice sheets, including bed topography, subglacial hydrology, crevasse detection and internal layering (Copland and Sharp 2001, Dowdeswell and Evans 2004, Woodward and Burke 2007, Irvine-Fynn et al 2006). In glaciology, GPR systems are typically towed behind a skidoo, skier or hiker, thus creating a map of sub-surface characteristics while achieving maximum spatial coverage (Figure 3.3).

In general terms, GPR works by transmitting electromagnetic energy through a medium and detecting when the reflected energy is received (Woodward and Burke, 2007). As the electromagnetic energy travels through the sub-surface material, the energy is reflected at dielectric discontinuities known as reflector horizons (Annan 2002). The energy received back by the GPR receiver is recorded, and an image is built from these returns as the GPR unit is moved across the surface of the material (Figure 3.4).

The frequency used for a GPR survey is determined by the amount of penetration required for a given application, and by the physical properties of the material being surveyed. Low frequencies typically penetrate deeply with low resolution, while high frequencies penetrate to a shallow depth but have a high resolution. For applications such

as mapping subglacial topography, lower frequencies typically ranging from ~5-20 MHz are most commonly used. For applications which require higher resolution, such as reconstructing near-surface snow accumulation and detecting internal firn layers, higher frequencies of ~50-1000 MHz are typically used. However, the depth of RADAR penetration is also dependent on the temperature of the ice via its relation to the dielectric constant and free water content: the same wavelength of energy can penetrate deeper into colder ice (<0°C) than warm ice (~0°C).

To determine ice depths from GPR data, the signal speed through the medium must be known in addition to the two-way travel time that the signal takes between the transmitter and receiver. To determine the GPR signal speed, a common midpoint survey (CMP) is undertaken at the study site. A CMP relies on taking a survey, changing the distance between antennae by a known amount, and repeating (PulseEKKO Pro User Guide 2006). By changing the distance between surveys it increases the signal path for the midpoint reflector (Figure 3.5). The data collected can then be processed and the average velocity to the midpoint reflector can be determined. Once the velocity is known, and if the receiver and transmitter are triggered simultaneously, ice depth can be calculated with the following equation:

$$\text{Depth} = (\text{speed}) \times (\text{time}/2)$$

The speed at which radar energy travels through common materials is well known (Table 3.1). The radar speed through ice depends primarily on water content, density and internal structure, with a study by Macheret et al (1993) showing that typical radar velocities for ice vary from ~0.160 m ns^{-1} to ~0.172 m ns^{-1}. Velocities greater than 0.167 m ns^{-1} are typical of cold ice, while velocities less than 0.167 m ns^{-1} are typical of temperate glaciers.

In this study, a 12.5 Mhz Sensors and Software GPR system was towed by snowmobile (~10 km h^{-1}) along the main trunk and accessible tributaries of the Belcher Glacier, together with parts of the upper accumulation area (Figure 3.6). The 12.5 MHz system has two antennas of ~4 m length each, with a horizontal separation of ~3 m between

them. Data was collected between May 5th-20th, 2008. GPR traces were recorded on a removable flash drive while GPR positions were automatically recorded with an onboard non-differential GPS receiver at every tenth trace. The GPS data records latitude, longitude and elevation values and is accurate to +/- 5 m.

3.2.1 Bed Digital Elevation Model:

Using the GPR data collected in May 2008, together with data collected by J. Kavanaugh (University of Alberta) in May 2007 and previous GPR studies (e.g., Dowdeswell et al., 2004) a new bed Digital Elevation Model (BedDEM) of the Belcher Glacier basin was created for this project by research partners at the University of Alberta (mainly Wendy Clavano). Interpolation was undertaken using Kriging with randomly selected points within sub-regions of the Belcher Glacier to provide the best available estimates of basin-wide ice thicknesses. Errors for the BedDEM range from 20 – 40 m along the main trunk of the Belcher Glacier, although these errors may be higher in areas with sparse data (100 – 200 m). Difficult regions to determine ice thicknesses within the Belcher Glacier basin occur where it bends to an east-west orientation and an area where the main trunk meets the northern tributary (denoted on Figure 3.7) (Clavano, W., personal communication, 2010).

The BedDEM was manipulated in ArcGIS 9.2 to extract ice thicknesses at cross-sections (flux gates) oriented at right-angles to the ice flow direction. Locations were chosen near areas where the GPR measurements were made in May 2008 to minimize potential errors from interpolation. Ice thicknesses for the lower Belcher Glacier are shown in Figure 3.7. In total five flux gates are used, four located along the main trunk of the Belcher Glacier and one along the main tributary. Ice flux is calculated through each gate by segmenting it into 100 m wide sections, and multiplying the ice depth by the depth-averaged velocity for each section. Depth-averaged velocity is usually 80-90% of the surface velocity (Paterson 1994), so for this project 85% of the surface velocity (determined by speckle tracking) was used as the depth-averaged velocity. From summing the sections together, a record of ice flux through each flux gate is determined for each measurement period.

3.3 Remote Sensing Velocity Monitoring:

Remote sensing methods provide a useful way to determine surface ice motion over large, remote areas. Remote sensing methods are attractive for monitoring glaciers as they are relatively cost effective and do not require travel to the field to obtain results. Additionally, remote sensing methods can provide accurate velocities over large areas, particularly when they are validated with ground dGPS measurements. They can therefore address one of the fundamental problems with in situ measurements (e.g., dGPS) that can only provide accurate velocities for single points. Synthetic Aperture RADAR (SAR) provides an excellent remote sensing platform for monitoring ice dynamics in the high Arctic. This is because SAR is an active sensor (a system which transmits its own electromagnetic energy and records the energy reflected back from the Earth's surface), which means that it can penetrate cloud cover and image during the polar night. This is ideal for studying Devon Ice Cap as it allows for remote sensing data to be collected and used throughout the year and in all weather conditions.

SAR works by illuminating the earth's surface with coherent microwave energy, and retains the phase, wavelength and amplitude information during reception at the sensor. Wavelength is a measure of the distance between peaks in the electric field of the transmitted RADAR. The transmitted pulse of microwave radiation is backscattered by the terrain and, on reception by the receiver, two signal components of the received wave are sequentially stored in memory. One component is 'in-phase' with the transmitted wave (the peaks and troughs of the electric field line up) and the other is the 'out-of-phase' component (the peaks and troughs do not line up). The 'phase angle' of the received image pixel can be calculated from the 'in-phase' and 'out-of-phase' amplitude components and is related to the precise range between the entre of the antenna and the phase centre of the pixel..

The retention of phase and amplitude information allows for inferences about the earth's surface properties to be made. Examples of active microwave systems suitable for SAR speckle tracking include Radarsat-1, Radarsat-2, ERS1, ERS2, ENVISAT, JERS and TERRASAR-X. SAR speckle tracking has been found to be a useful technique for

determining the motion of glaciers and ice streams, and has been previously used for studies of ice motion in the Antarctic and on glaciers on Axel Heiberg and Ellesmere Islands in the Canadian High Arctic (Short and Gray 2005, Gray et al 2001).

3.3.1 Theory of Speckle Tracking:

When RADAR interacts with the ground surface, the backscatter created within each individual pixel is defined by the surface properties of the material that is being imaged. However, due to constructive and destructive interference in the returned phase information at the sensor there is a distinctive 'speckle' or 'salt and pepper' look of RADAR imagery. The elementary scatterers, or scattering centres, are the ground surface elements that reflect incoming RADAR energy: if the peaks and troughs of the scattered electric wave from the individual scattering centres coincide then constructive interference occurs which causes an individual pixel to appear bright. However, this almost never occurs in practice and the pixel amplitudes vary because of the scattering process from randomly positioned scattering centres. The result is the intrinsic variation in pixel amplitude from all distributed radar targets which is usually called 'radar speckle'. As long as the elementary scatterers within a pixel of RADAR imagery remain the same between acquisitions and the RADAR viewing geometry is nearly the same, then the speckle pattern in the image should also be very similar. In this sense, it is possible to find the same speckle pattern using a cross-correlation method in two images as long as the elementary scatterers and viewing geometries are similar.

In order for the viewing geometry to be similar, the image acquisitions need to be in the same imaging mode and on the same relative orbit, which typically equates to 24 days for Radarsat 1/2 and 35 days for ENVISAT and ERS1/2 (1 day separation for ERS1/2 tandem mode and 3 day separation for ERS1 and ERS2). For the elementary scatterers to remain the same between image pairs, the ice conditions cannot change substantially. For example, this means that no significant snowfall or surface melt or wind re-distribution of snow can occur within the 24 day orbital cycle if Radarsat images are being used. If no significant change in the elementary scatterers occurs then coherence is said to be maintained. Due to the fact that melt causes phase coherence to be lost, speckle tracking

works best on winter imagery and is not always applicable to summer imagery or to study sites that experience large amounts of accumulation.

This method of determining ice motion is advantageous over SAR interferometry as it is not limited by line of sight problems. The line of sight projections provided by interferometry methods are projections of the actual terrain displacement vector on the line between the sensor and the terrain point. In this case, line of sight displacements cannot be decomposed into horizontal displacements (Kaab 2005a, Joughin et al 1999). Thus the vertical and horizontal components have to be estimated or modeled based on the type of terrain motion being measured (i.e. with the use of a DEM) (Kaab 2005b). The speckle tracking method is advantageous over this method as it can determine displacements in both the azimuth and slant range directions of the image (Short and Gray 2005). The speckle tracking method is also advantageous over 'feature tracking', which uses a similar cross-correlation method to find matches between features in image pairs. Over a homogenous surface such as an ice cap, where the returned amplitude information will be nearly identical over large areas, it is impossible to make matches between features with any degree of confidence. Indeed, feature tracking is only used for determining ice dynamics on glaciers that have many distinctive surface features which can be tracked with a high degree of certainty from image to image (Kaab 2005). Due to the fact that speckle tracking and feature tracking use a similar cross-correlation method to determine ice motion the terms are often used interchangeably in the literature, although this can be misleading.

Speckle tracing takes advantage of being able to ability to determine displacements at sub-pixel accuracy between scenes in an interferometric pair using a cross-correlation method on the speckle pattern, which is sharply peaked. In speckle tracking, single-look complex (SLC) RADAR imagery is very accurately co-registered and the matches are based on speckle, rather than the visible features within the imagery (e.g. crevasses), allowing for this sub-pixel accuracy (Joughin 2002).

3.3.2 Process of Speckle Tracking:

The process of speckle tracking begins with the acquisition of two coarse registered SLC SAR images (Figure 2.7). The process then uses two detected image chips (small subsets of the whole SLC image) and a two dimensional cross-correlation technique to determine displacement of the image chips in the azimuth (along satellite track) and slant range (across satellite track) directions (Short and Gray 2005, Gray et al 2001, Joughin 2002, Strozzi et al 2002). The dimensions of the image chips vary and are tailored based on the region of interest. Short and Gray (2005) found that an image chip size of ~250 to 400 m was appropriate for velocity mapping using speckle tracking on Ellesmere and Axel Heiberg Islands. For this project the image chip size was tested using a variety of sizes from 50 to 400 pixels, with a setting of 100 pixels in azimuth and 50 pixels in slant range providing good results for fine beam and ultrafine imagery. These image chips relate to a ~600 by ~600 m image chip for fine beam imagery and ~200 by ~200 m image chip for ultrafine imagery.

After image cross-correlation is completed on the image chips, a digital elevation model (DEM) of the glacier surface is used to remove topographic information from the range offset calculations. In the case of this research, the Canadian Digital Elevation Dataset (CDED) 100 m (grid spacing) DEM for the Devon Ice Cap was utilized. Because displacements in the range direction are affected by surface elevations, and the baseline of the pair of images being used, the DEM removal is used to convert slant range displacements (the distance measured along a line between the radar antenna and the target) into ground range displacements (the perpendicular distance from the ground track to a given object on the Earth's surface) (Short and Gray 2005). Next, the ground range and azimuth displacements are calibrated using reference points such as rock outcrops or areas with known velocities. These reference points correct potential errors in the displacement measurements (Short and Gray 2004, Short and Gray 2005). Finally, ice motion parallel to the ice surface is assumed and velocities are derived from the corrected displacements, surface slopes determined from a DEM, and the time separation between the image pairs (Joughin et al 1998, Short and Gray 2005).

Potential errors in the speckle tracking technique arise from three main sources (Short and Gray, 2004):

I. Errors arise for small and slow moving glaciers, because this reduces the size of the image chips needed for cross-correlation and increases the random component of error.
II. The method always finds the maximum correlation between the image chips even though the maximum correlation may not represent a true match.
III. Errors due to the assignment of reference velocities and the accuracy of the DEM when used to correct displacements from slant range to ground range. Note that because the perpendicular baselines for Radarsat-2 are well maintained, the DEM errors that can propagate into false motion during the slant range to ground range conversion process are minimized and considered to be insignificant for the research presented here.

Results for the speckle tracking method are expected in improve with the use of Radarsat-2 data, compared to previous studies that have used Radarsat-1 imagery (Short and Gray 2004). First, the improved spatial resolution of the Radarsat-2 sensor (~3 m in ultra fine mode) will mean that the technique can be applied to smaller and slower moving glaciers. Second, orbital maintenance and knowledge is improved on the Radarsat-2 sensor, increasing the number of usable image pairs. Third, the use of quad-polarization imagery should improve speckle tracking as the method can be applied to all four polarizations and combined to produce displacement results, compared to the single polarization available in previous sensors.

The speckle tracking undertaken for this study was completed using a MATLAB script produced by Dr. Laurence Gray. For the reasons discussed above, Radarsat-2 data was used exclusively for this study. Radarsat-2 was launched on December 14th, 2007, and is a C-band SAR imaging system which provides imagery at spatial resolutions of 3-100 m and quad polarization for some beam modes (Figure 3.2). For this study, the speckle tracking algorithms were used on Ultrafine and Finebeam imagery acquired throughout 2009 and 2010 (Table 3.3) Imagery was acquired seasonally over the Belcher Glacier,

while for the entire Devon Ice Cap it was acquired once in March 2009. The southwestern arm of Devon Ice Cap was excluded from analysis as it is assumed to be stagnant as described by Burgess et al (2005). Imagery was acquired through a joint project between the University of Ottawa, the Canada Centre for Remote Sensing (NRCan) and the National Glaciology Program (NRCan). Imagery was also obtained through the Canadian Space Agency's Science and Operational Applications Research - Education (SOAR-E) program (Project # 5009).

3.3.4 Filtering and Interpolation of Results

Results determined from the MATLAB speckle tracking algorithm were exported to a text file, which was added into ArcGIS 9.2 as a point dataset. The point spacing for fine beam mode was ~250 m by ~200 m and ~50 m by ~100 m for ultrafine imagery. The point dataset was then exported as a shapefile and the following criteria were used to assess the accuracy of the results:

I. Motion should be faster in the glacier centre than near the glacier sidewalls (due to marginal friction).

II. Flow direction should be oriented parallel to surface features, such as medial moraines.

III. There should not be dramatic changes in flow direction or magnitude over short distances (i.e., there should be internal consistency within the data).

IV. Speckle tracking results should compare closely to dGPS results

When a speckle tracking match result was determined as being incorrect using the criteria outlined above, the point was deleted in ArcGIS and removed from further analysis. An Inverse Distance Weighting (IDW) interpolation method was used to create a raster dataset of surface ice velocities across Belcher Glacier and Devon Ice Cap from the filtered point shapefile. This raster dataset has 100 m resolution for fine beam imagery and 50 m resolution for ultrafine imagery respectively. IDW provides a conservative approach to interpolating velocities as it cannot exceed values determined by the speckle tracking algorithm. However, if velocities determined from speckle tracking are incorrect and are not removed during the filtering stage, then these velocities will be inaccurately

interpolated across the surface. When this occurs, further filtering is undertaken to remove these inaccuracies.

Material	Radar Velocity (m ns^{-1})
Air	0.30
Water	0.033
Warm Ice	~0.160
Ice average	0.167
Cold Ice	~0.172

Table 3.1: *Radar speed through common materials, adapted from PulseEKKO PRO training materials and Macheret et al (1993).*

Beam Mode	Nominal Swath Width	Approximate Resolution (Range)	(Azimuth)	Approximate Incidence Angle	Polarization
Ultra-Fine	20 km	3 m	3 m	30° - 40°	Single Polarization
Multi-Look Fine	50 km	8 m	9 m	30° - 50°	
Fine	50 km	8 m	9 m	30° - 50°	Single Polarization OR Dual Polarization
Standard	100 km	25 m	28 m	20° - 49°	
Wide	150 km	30 m	28 m	20° - 45°	
ScanSAR Narrow	300 km	50 m	50 m	20° - 46°	
ScanSAR Wide	500 km	100 m	100 m	20° - 49°	
Extended High	75 km	18 m	28 m	49° - 60°	Single Polarization
Fine Quad-Pol	25 km	12 m	8 m	20° - 41°	Quad Polarization
Standard Quad-Pol	25 km	25 m	9 m	20° - 41°	

Table 3.2: *Radarsat-2 beam modes and characteristics from Radarsat-2 brochure (available: http://www.radarsat2.info/about/r2_brochure.pdf).*

Acquisition Date	Beam Mode	Number of Segments	Pass Direction	Polarizations	Resolution
Ma 1st, 2009	Fine Beam (F23)	3	ASC	HH HV	8 m
Mar 1st, 2009	Fine Beam (F3)	3	DES	HH HV	8 m
Mar 2nd, 2009	Fine Beam (F6)	3	DES	HH HV	8 m
Mar 4th, 2009	Fine Beam (F22)	4	ASC	HH HV	8 m
Mar 5th, 2009	Fine Beam (F5)	3	DES	HH HV	8 m
Mar 25th, 2009	Fine Beam (F23)	3	ASC	HH HV	8 m
Mar 25th, 2009	Fine Beam (F3)	3	DES	HH HV	8 m
Mar 26th, 2009	Fine Beam (F6)	3	DES	HH HV	8 m
Mar 27th, 2009	Fine Beam (F3)	3	ASC	HH HV	8 m
Mar 28th, 2009	Fine Beam (F22)	4	ASC	HH HV	8 m
Mar 29th, 2009	Fine Beam (F5)	3	DES	HH HV	8 m
Apr 20th, 2009	Fine Beam (F3)	3	ASC	HH HV	8 m
June 29th, 2009	Fine Beam (F23)	2	ASC	HH HV	8 m
July 23rd, 2009	Fine Beam (F23)	2	ASC	HH HV	8 m
Oct 3rd, 2009	Fine Quad Pol (Q20)	3	DES	HH HV VH VV	8 m
Oct 27th, 2009	Fine Quad Pol (Q20)	3	DES	HH HV VH VV	8 m
Dec 21st, 2009	Ultrafine (U15)	3	DES	HH	3 m
Jan 14th, 2010	Ultrafine (U15)	3	DES	HH	3 m
Feb 8th, 2010	Ultrafine (U15)	3	DES	HH	3 m
Mar 3rd, 2010	Ultrafine (U15)	3	DES	HH	3 m

Table 3.3: *Summary of Radarsat-2 Scenes used in this study to produce velocity maps over the Belcher Glacier and entire Devon Ice Cap.*

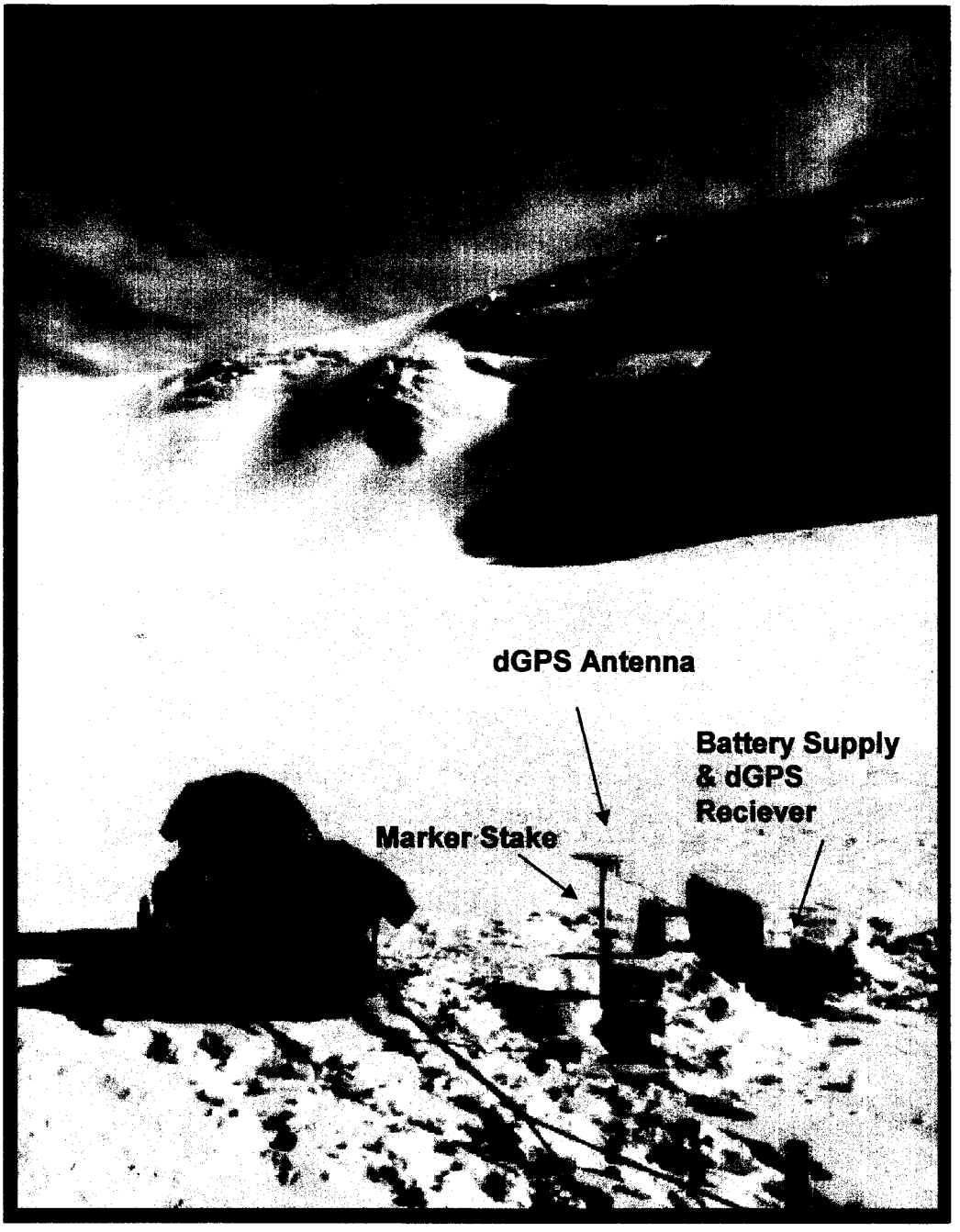

Figure 3.1: *Surveying of marker stakes on the Belcher Glacier using dGPS, May 2008*

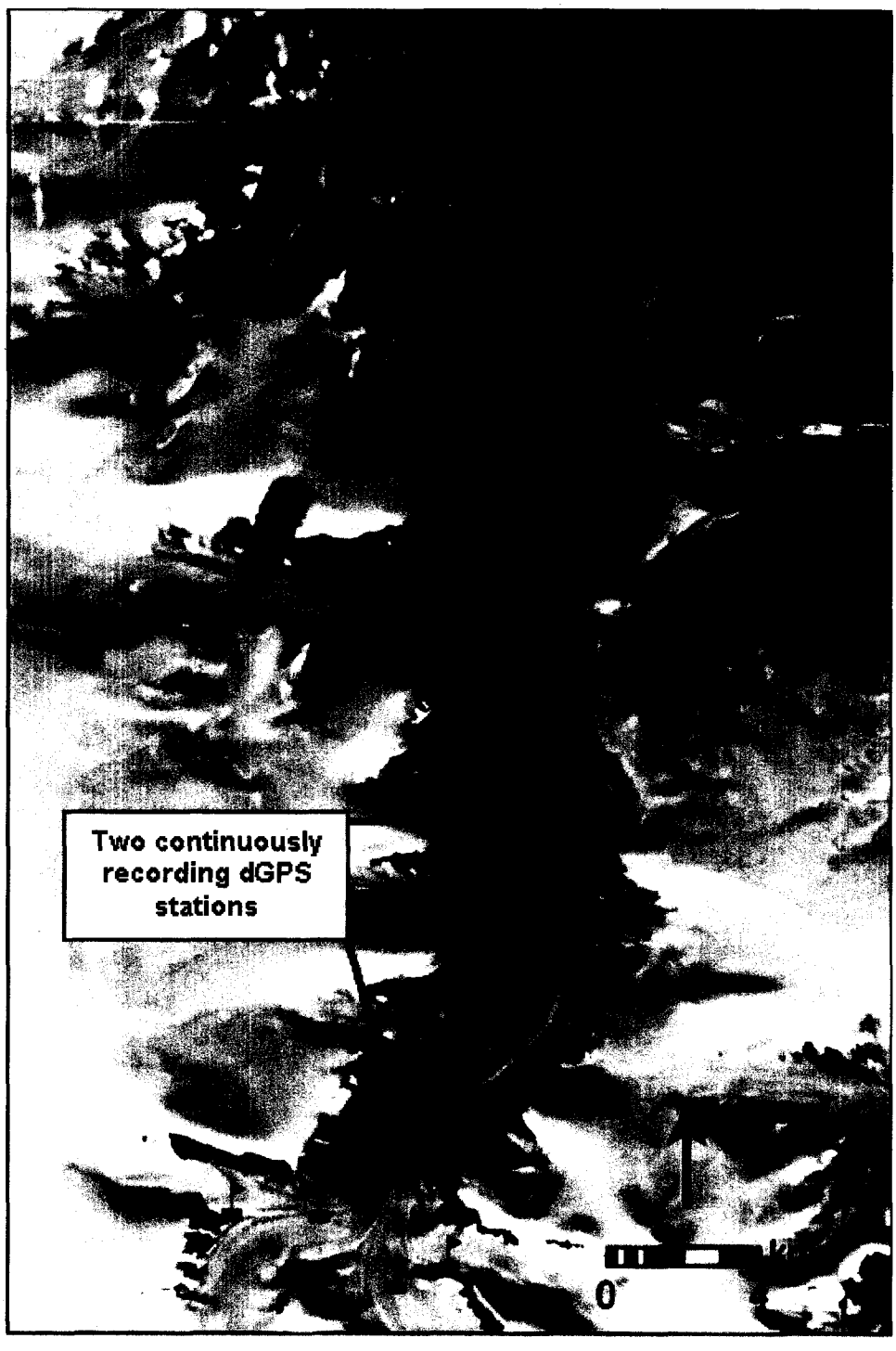

Figure 3.2: *Locations of dGPS marker stakes along the main trunk of Belcher Glacier used to verify the remote sensing velocity results. Blue markers denote locations of tributary surveys completed during May 2008; Red markers denote locations of tributary surveys completed in 2008 and 2009 by University of Alberta research partners; Green markers denote continuously recording dGPS stations (Base image: 2000 Landsat 7).*

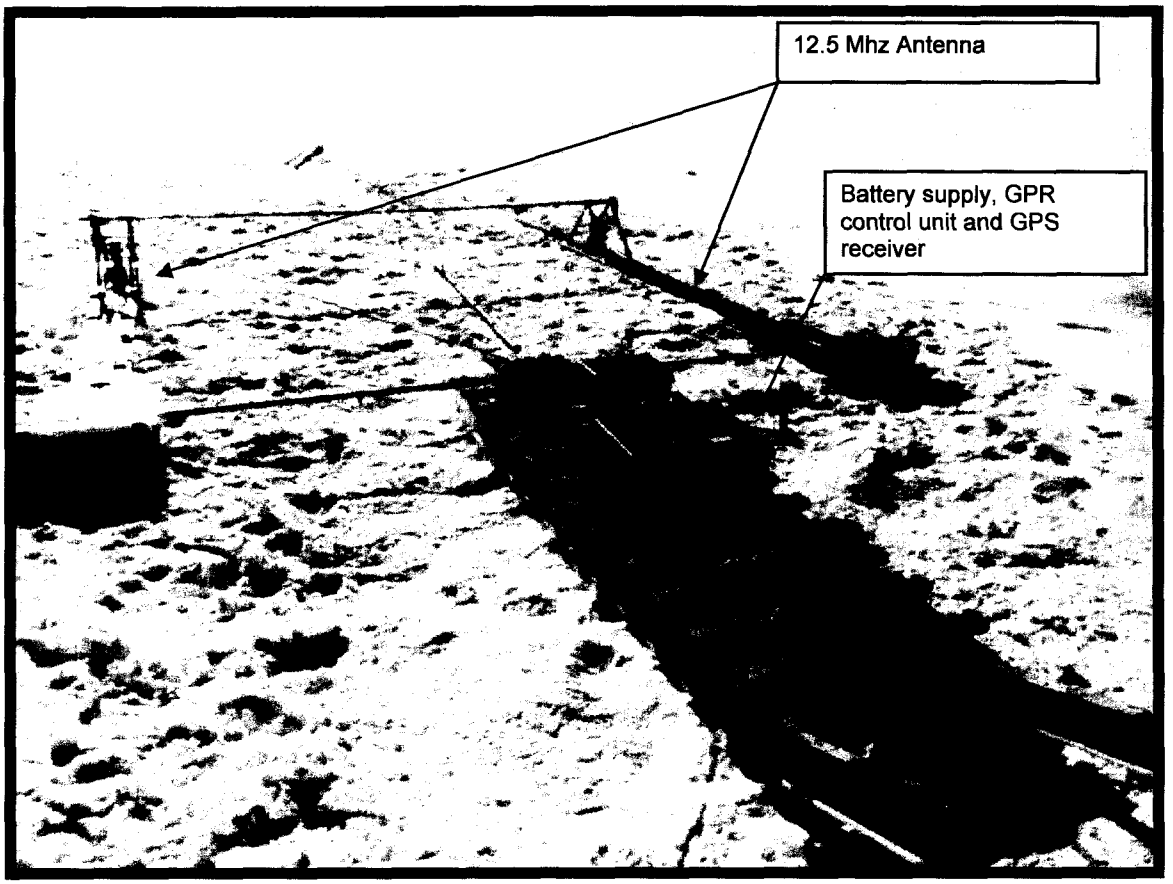

Figure 3.3: *Set up of the 12.5 MHz GPR system used during the 2008 field season.*

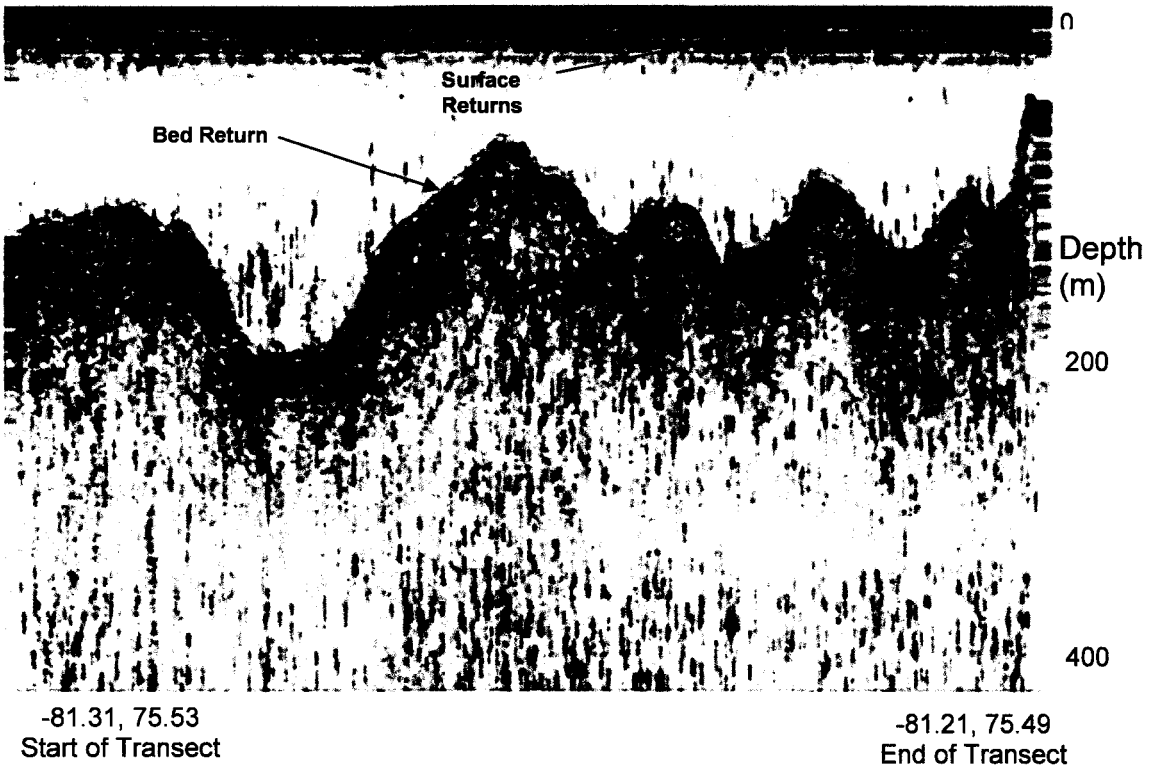

Figure 3.4: *Example of a 12.5 MHz GPR transect taken over a distance of 8 km on Belcher Glacier in May 2008 that shows basal topography (note that surface topographic correction has not been applied)*

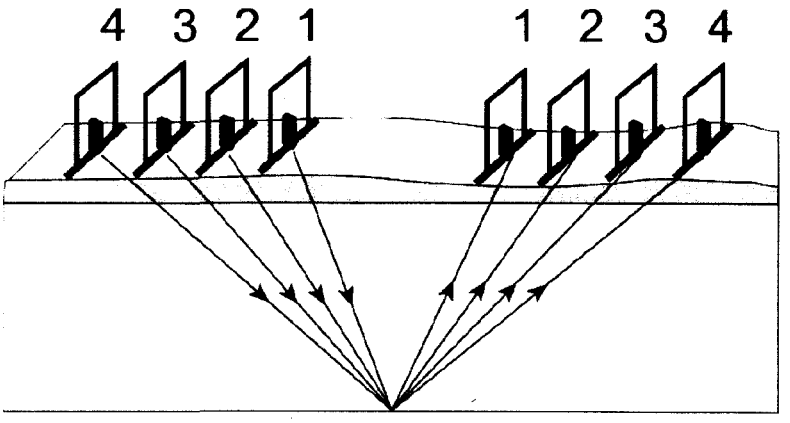

Figure 3.5: *Common Midpoint Survey (PulseEKKO PRO User Guide 2006)*

Figure 3.6: *Locations of 12.5Mhz GPR surveys taken during the May 2008 field season (combined with other datasets) to develop the BedDEM of Belcher Glacier.*

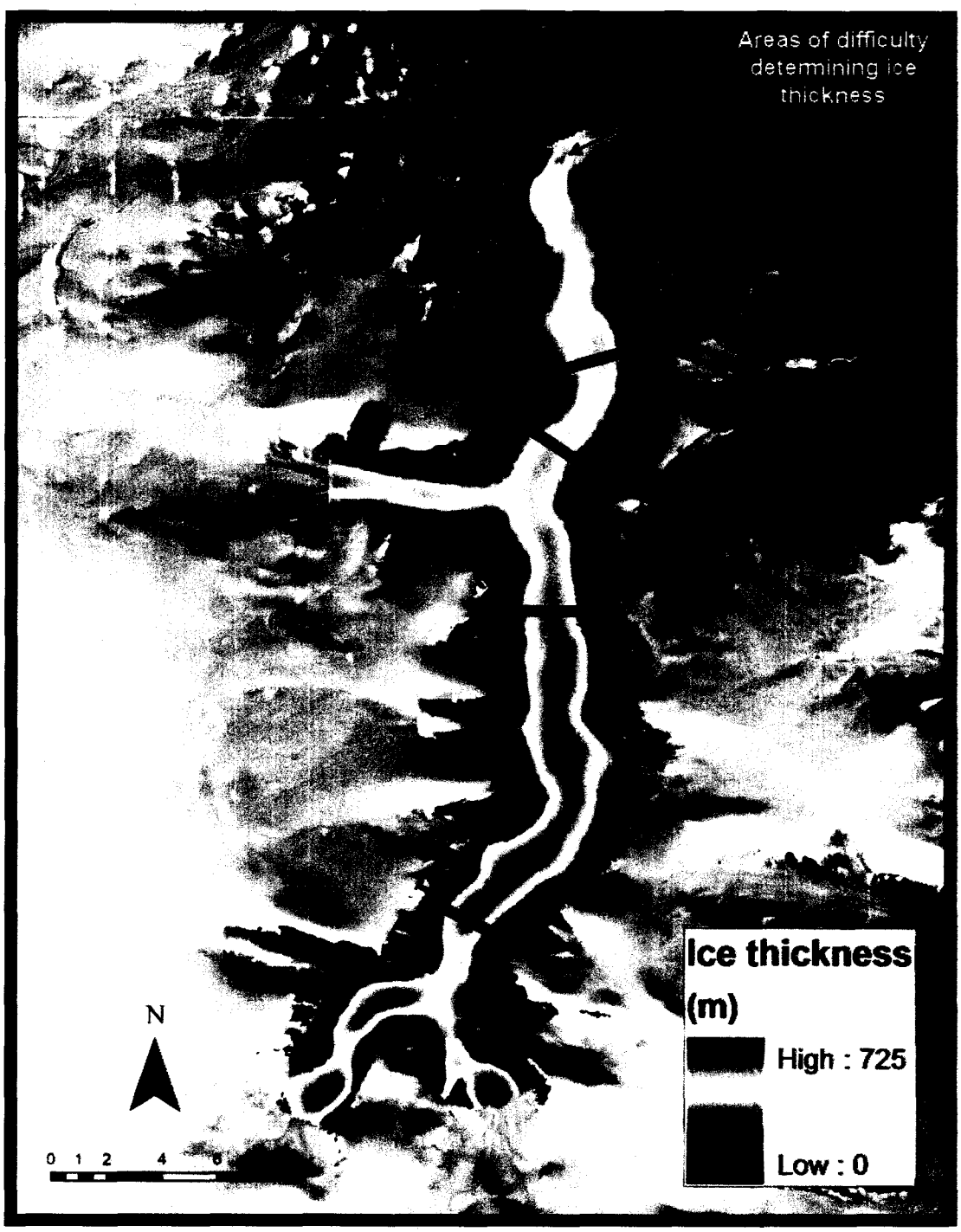

Figure 3.7: *Ice thicknesses for the lower Belcher Glacier basin determined from the 12.5 Mhz GPR in combination with other previous measurements.*

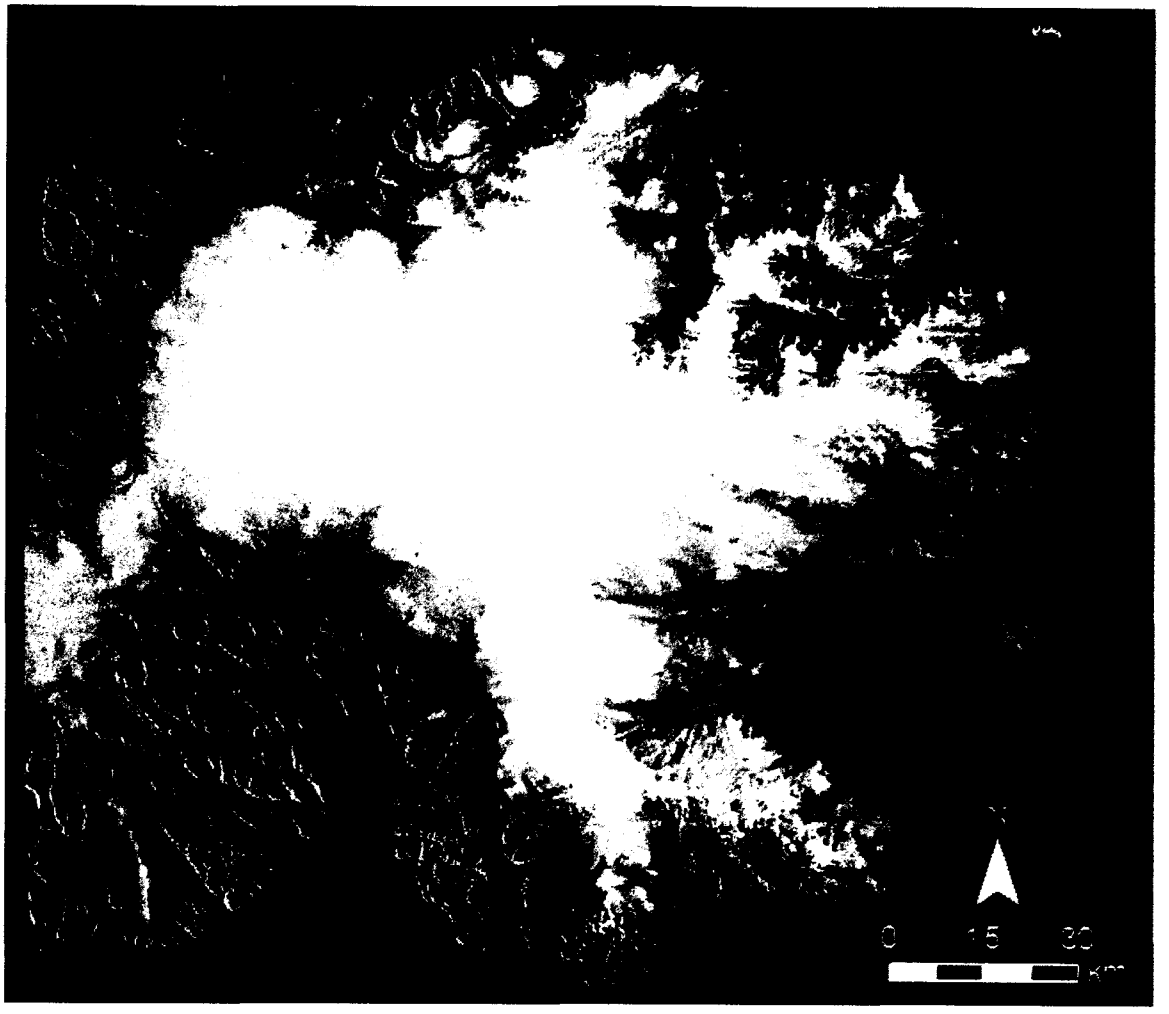

Figure 3.8: *Example of Radarsat imagery over Devon Ice Cap (March 1, 2008 Radarsat-1 ScanSAR Wide image)*

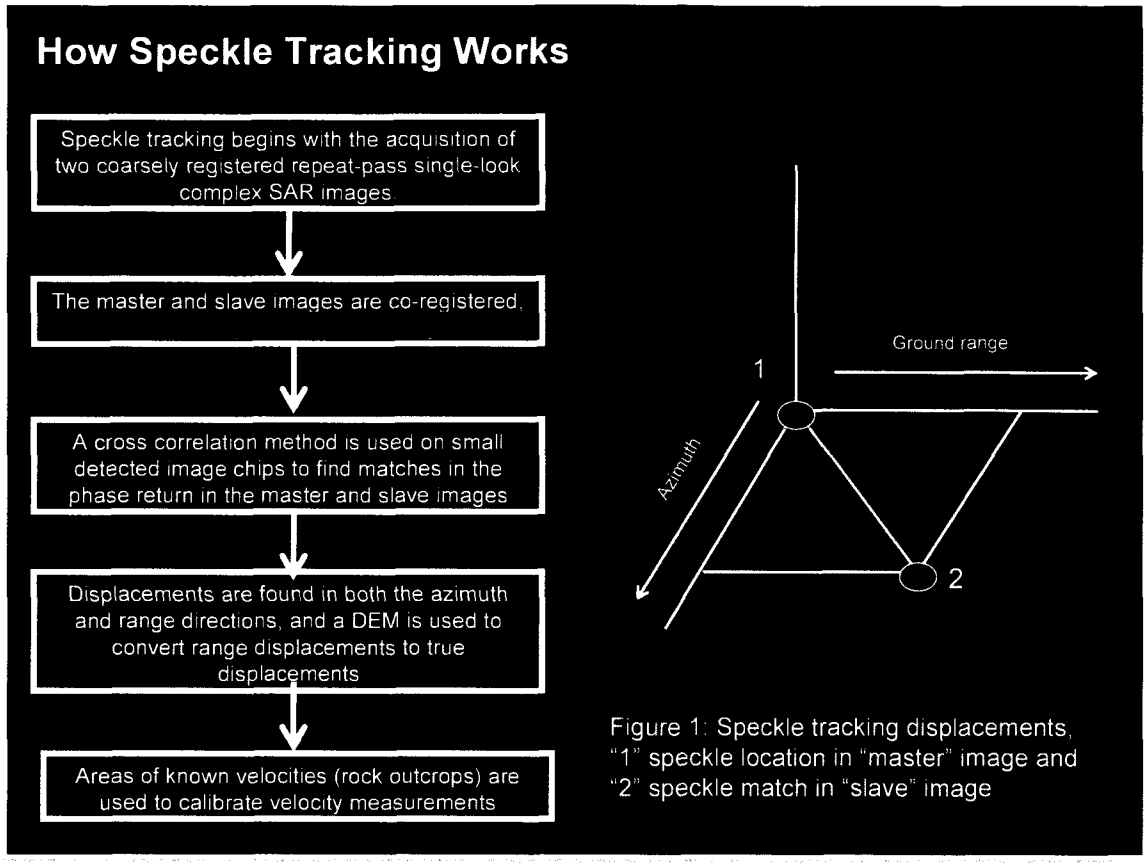

Figure 3.9: *Process of Speckle Tracking*

Chapter 4: Velocity Results for Belcher Glacier

This chapter focuses on the surface velocities of the Belcher Glacier. It begins with a comparison of speckle tracking velocities against independent velocity measures of the Belcher Glacier (in situ dGPS, TerraSar X speckle tracking) and assesses the validity of the method. Next, an evaluation of the errors associated with the method are presented, followed by a detailed discussion of the flow structure of the Belcher Glacier. Finally, the chapter concludes with an explanation of the links between seasonal velocity changes and subglacial hydrology. Two continuously operating (Figure 3.2) dGPS stations acquired surface ice displacements (corrected to m yr^{-1}) along the centerline of the Belcher Glacier during the period that coincided exactly with speckle tracking results determined from March 5-29th 2009 fine beam imagery (also corrected to m yr^{-1}). Although data may be acquired for shorter periods, all velocities presented in this chapter are corrected to m yr^{-1} in order to facilitate comparison.

4.1 Comparison of Speckle Tracking Results with Independent Measures

Velocity maps of Belcher Glacier from different 24-day periods throughout 2009-10 derived from the speckle tracking methods outlined in Chapter 3 are presented in Figure 4.1. In general, each velocity map reveals highest velocities near the terminus with velocity decreasing upglacier. Flow directions follow the valley shape (Figure 4.2). Velocity maps also reveal differences between seasons, with minimum velocities experienced in the autumn (October 3-27, 2009) and highest velocities occurring in the spring (March 5-29, 2009). The terminus region is the only exception to this pattern, with higher terminus velocities occurring in the summer (July 3-27, 2009) and lower velocities occurring in the winter (December 21, 2009 – January 14, 2010) (Figure 4.3). March 5-29, 2009 and October 3-27, 2009 image pairs are Radarsat-2 fine beam (~8 m resolution) while December 21, 2009 – January 14, 2010 and February 8 – March 3, 2010 are Radarsat-2 ultrafine imagery (~3 m resolution). A detailed discussion of the spatial and temporal variations in the velocity structure of Belcher Glacier is provided in section 4.2.

To provide an independent check on the surface velocities derived from speckle tracking, they were compared with the in situ dGPS data collected on the Belcher Glacier. As a second independent check, results were also compared with speckle tracking of TerraSar X imagery over the Belcher basin for March 16th – 27th 2009, which was performed by Noetix Research Inc. utilizing GAMMA software (under a contract to Natural Resources Canada). Comparisons for magnitude of displacements are made between the Radarsat-2 speckle tracking results and both the TerraSar X data (centerline profile) and dGPS data (centerline and across-glacier profiles). For direction of displacements, comparisons are made between the Radarsat-2 speckle tracking results and both the yearly displacements of the in situ marker stakes determined by dGPS, and the continuous dGPS data acquired during periods which exactly overlapped the Radarsat-2 image acquisitions (March 5 – 29, 2009. Note that TerraSar-X orientation results were not provided and as such comparisons were not possible.

At this time it is important to note that there were two regions where no reliable velocities could be determined from speckle tracking. Specifically, loss of coherence occurred on one tributary of the southern headwall in the December 21, 2009 – January 14, 2010 Radarsat-2 ultrafine imagery. This loss of coherence only affected the single tributary and does not affect the results on any of the other regions of the Belcher basin. Loss of coherence also occurred over a second region near the southern headwall in the February 8 – March 3, 2010 ultrafine Radarsat-2 imagery, which caused difficulty calculating ice flux on the southern tributaries for this date (these locations are annotated on Figure 4.1d, and these problems are discussed further in 4.2.1.7).

4.1.1 Magnitude Comparisons: Centerline Velocities

Velocities determined by in situ dGPS are considered to provide the most accurate point measurements of surface ice displacements due to the accuracy of the method as described in Chapter 3. Locations of dGPS observations are shown in Figure 4.5. For the first continuously recording dGPS station with data that coincided exactly with Radarsat-2 image dates (March 2-29, 2009) the displacement was observed to be 60.87 m yr^{-1} while the speckle tracking results at the same location indicated motion of 64.86 m yr^{-1}

(an overestimate of 6.55%). For the second dGPS station the observed displacement was 54.08 m yr^{-1} while the speckle tracking results determined a displacement of 51.02 m yr^{-1} (an underestimate of 5.65%).

Figure 4.4c compares the magnitude of displacements along the centerline of Belcher Glacier determined from speckle tracking of March 5-29, 2009 Radarsat-2 imagery with annual dGPS measurements of the displacement of in situ markers (surveyed in May 2008 and again in May 2009) and speckle tracking determined independently from TerraSAR X imagery between March 16-27, 2009. Figure 4.5 shows the location of annual dGPS observations on Belcher Glacier. Table 4.1 summarizes the annual displacements measured in the field (May 2008 – May 2009) at the dGPS marker stakes with those determined at the same location (within one pixel) for both speckle tracking methods. These results show that the mean difference between the in situ dGPS and the average velocity derived from speckle tracking is -13.27%. Initially, this suggests that the mean velocities derived from speckle tracking tend to underestimate surface ice displacements determined by dGPS. However, this is not unexpected as the mean velocities calculated from speckle tracking of Radarsat-2 imagery did not include any measurements from the summer. Based on continuously operating dGPS stations, summer velocities on the Belcher Glacier are typically ~15% faster than those observed in the winter (B. Danielson, personal communication, 2010), and as such the annual displacement of dGPS marker stakes (which include summer motion) are closely matched to the average speckle tracking results presented here (which do not include summer motion).

The mean difference between TerraSar-X speckle tracking results (March 16-27, 2009) and the speckle tracking results of Radarsat-2 imagery (March 5-29, 2009) is 13.26%, with the Radarsat-2 results tending to provide faster estimates. One potential explanation for this discrepancy relates to the difference in pixel resolution between the two sensors (~8 m for fine beam Radarsat-2 imagery compared to ~3 m resolution for TerraSar-X). In this case, the higher resolution of TerraSar-X provides a larger number of results over the same area as the Radarsat-2 fine beam imagery and is likely to provide fewer

mismatches. Additionally, the different separation times between image acquisitions may play a role in the discrepancy. For Radarsat-2 the orbit cycle between images is 24 days while for TerraSar-X the orbit cycle is 11 days. Figures 4.1a and 4.1d suggest that March is the time of year when velocities are accelerating, the longer acquisition time of the Radarsat-2 imagery means that it may have picked up more of the acceleration than the shorter acquisition time of TerraSar-X.

The TerraSar-X and Radarsat-2 velocities extracted along the centerline profile exhibit the same general structure. Specifically, velocities are highest at the terminus and tend to decrease upglacier, with occasional local fluctuations. The centerline trend is the same for both sensors, with velocity fluctuations occurring on the same regions of the glacier and exhibiting similar magnitudes.

4.1.2 Magnitude Comparisons: Across-glacier Velocities

Table 4.2 compares in situ dGPS measurements of marker stakes (in May 2008 and May 2009) with velocities determined by Radarsat-2 speckle tracking. In general these compare well, with a mean difference between the in situ dGPS results and the average speckle tracking velocity for the cross-sectional profile of -11.92% (i.e., speckle tracking underestimated the annual velocities). However, as discussed in the previous section, this discrepancy is likely due to the absence of the summer speed up in the speckle tracking results.

In terms of variation in the quality of the results across the cross-sections, the speckle tracking results tended to provide better results near the center of the glacier and poorer results near the margins. This difference may be due to the fact that near the glacier margins areas can be shadowed from the incoming RADAR beam, resulting in less consistent phase coherence there. Additionally, there are shear zones near the glacier margins, causing the ice surface in these regions to rotate and change orientation over short distances. This affects the reflected phase information received at the sensor and can thereby affect the correlations that can be made.

4.1.3 Orientation Comparisons

Vector results are also assessed based on the orientation of the annual displacement of the dGPS marker stakes. In this case, the start survey point and the end survey point determined by the dGPS in UTM coordinates are differenced to determine displacements in the easting and northing ranges, from which the direction of displacement is calculated. Table 4.3 presents a comparison between the annual displacements determined by these in situ dGPS surveys and those determined from speckle tracking of Radarsat-2 imagery.

The results show that the directions derived from speckle tracking are generally consistent with those measured in situ with the dGPS. The mean error between the average displacements determined by speckle tracking and the in situ results is 4.81°, with a standard deviation of 3.59°. Speckle tracking vector results near the glacier margins differ more from the dGPS results than they do near the middle of the glacier, likely due to the marginal shear zones affecting the backscatter and phase information returned to the sensor. For points along the glacier centerline (Point ID: 4, 5, 6, 7, 8, 9, 11, 12, 13) there is an average difference of 3.98° compared to the in situ dGPS results, while points nearer to the margins and shear zones (Point ID: 17, 20, 21, 24, 25, 28) have an average difference of 5.66° compared to the in situ dGPS data.

A second method of checking the orientation results relies on the use of physical features produced by ice motion that are visible on satellite imagery. In particular, along the glacier centerline long-term flow patterns establish identifiable flow lines (medial moraines) that run from the southern headwall to the terminus (Figure 4.6). As such, vector results determined over the centerline of the Belcher Glacier would be expected to line up parallel to these (Copland et al 2009, Quincey et al 2009). Figures 4.2 and 4.6 shows that indeed ice motion vector results do closely follow ground features and valley walls, and as such results are likely to be correct.

Some of the differences between the in situ observations and those determined by speckle tracking could be due to the fact that the average annual orientation vector determined by speckle tracking does not include the summer season while the dGPS observations do. However, we have no data available to assess this potential factor.

4.1.4 Error Analysis: Areas of Known Velocities

Another way to assess the validity of the results is to compare areas of known velocity values with the velocities determined by the speckle tracking method. In particular, it is known that rock outcrops have velocities of 0 m yr^{-1}, so the speckle tracking technique should also record zero velocities in these areas. When this does not happen the difference from 0 m yr-^{1} provides the user with an estimate of the margin of error due to co-registration and cross-correlation (i.e., mismatch) errors, and enables quantification of the minimum detectable motion that the speckle tracking technique can reliably achieve.

In this study, velocities determined from the speckle tracking algorithm were compared to single points on 19 rock outcrops along the Belcher Glacier (Figure 4.7). Radarsat-2 speckle tracking velocities determined at the four nearest vectors to an established single point on each rock outcrop were averaged to determine the error (Table 4.4). Results show that apparent velocities (i.e., errors) over the rocks varied between 6.72 m yr^{-1} (February 8 – March 3, 2010) and 10.47 m yr^{-1} (December 2009 – January 2010), and that the average error for all measurements was 8.48 m yr^{-1}.

A second way of determining error is to extract velocities determined by the speckle tracking method over a large bedrock area. In this case, there is a large portion of non-glaciated bedrock on the southern portion of Devon Island near the terminus of the Croker Bay Glaciers which was imaged in fine beam Radarsat-2 image pairs acquired on March 27, 2009 and April 20, 2009 (Figure 4.8). In total, 27,436 velocity measurements over five areas of exposed bedrock were extracted (from a grid spacing of ~225 m between points), and the average velocity was found to be 6.59 m yr^{-1}. These results are consistent with the velocities determined over the bedrock outcrops along the margins of the Belcher Glacier. Additionally, these results represent motion of 43 cm over the 24

day Radarsat-2 cycle, which makes the errors appear larger than they really are when converted to m yr^{-1}.

Based on the two methods for determining ice motion over bedrock, it can be assumed that velocity error associated with the speckle tracking method is 9.48 m yr^{-1} (which represents about 9.58% of the average velocity along the main trunk of the Belcher Glacier). We consider errors of this order to be within an acceptable range for this method, with glacier velocities typically higher than this level on almost all glaciers that experience basal sliding (Willis 1995).

4.1.5 Assessment Summary

In terms of assessing the speckle tracking method, in situ dGPS results and results determined from independent satellite image processing agree well with the speckle tracking results. In terms of magnitude, speckle tracking results determined near the glacier centreline were closer to in situ dGPS results than those near the margins. Overall error is assessed to be ~10% of average ice velocities along the trunk of the Belcher Glacier, and the method reveals internally consistent patterns of higher surface velocities near the terminus and slower velocities progressively further upglacier. In terms of cross-sectional profiles, speckle tracking again reveals expected surface velocity patterns with slower motion near the glacier margins (due to increased friction from the bedrock walls), and an increase to a maximum near the glacier centre (where friction from bedrock is least). For orientation results, the speckle tracking method also agreed well with in situ dGPS observations (average difference is 4.81°) and the alignment of surface flow features. In the December 21, 2009 to January 14, 2010 and February 8 to March 3, 2010 image pairs, velocities were difficult to determine at the southern headwall due to a loss of coherence. As such flux calculations and seasonal variations for this region at this time were more difficult to determine. However, these problem areas are limited to only 3 tributaries, and do not effect the results of the main trunk or other portions downglacier.

Overall, there is high confidence that that the speckle tracking method provides results that can be used to reliably to determine surface ice motion, and we therefore use the

technique throughout the rest of the thesis to determine spatial and temporal variations in ice dynamics for the Belcher Glacier (this chapter) and ice cap wide velocities for the entire Devon Ice Cap (next chapter).

4.2 Overall Flow Structure of Belcher Glacier

Overall, surface ice velocities along the main trunk of Belcher Glacier are highest at the terminus and decrease upglacier toward the southern headwall, ~30 km upglacier (Figure 4.1). From the main tributary to the southern headwall surface ice motion is much more constant, only changing ~50 m yr^{-1} along that length in all seasons. Surface velocities of the main trunk are largely governed by inputs from connecting tributaries. The largest tributary of the Belcher Glacier system (indicated on Figure 4.5), which runs east-west, produces a large increase in ice velocities between where it connects with the main trunk and the terminus.

4.2.1 Seasonal Variation in Ice Motion for Belcher Glacier

Radarsat-2 imagery was obtained throughout 2009 and into 2010 that allowed for the generation of seasonal maps of ice motion for the main trunk of Belcher Glacier for: spring 2009 (March 5^{th}-29^{th}, 2009) (Figure 4.9), autumn 2009 (Oct 3^{rd}- 27^{th}, 2009) (Figure 4.10), midwinter 2009-2010 (Dec 21^{st}, 2009 - Jan 14^{th}, 2010) (Figure 4.11) and late-winter 2010 (Feb 8^{th}-Mar 3^{rd}, 2010) (Figure 4.12).

To facilitate analysis of these results, fluxgates were constructed along the main trunk and tributary of the Belcher Glacier (Figure 4.13). Figure 4.14 provides surface ice displacements along these five cross-sections derived from the speckle tracking. These cross-sections illustrate the seasonality in velocity structure along the main trunk, with each graph showing peak velocities in spring and minimums in autumn. Throughout the winter there is a gradual build-up in velocities, with late-winter values in 2010 approaching those achieved in the previous spring. The cross-sectional profiles also reveal that surface velocities are highest at fluxgate 1 (nearest to the terminus), with a gradual decrease upglacier to the slowest values at fluxgate 4 (closest to the headwall). This illustrates that overall surface velocities are strongly linked to their distance along the main trunk. Finally, the cross-sections show that velocities are lowest near the glacier

margins and highest in the center of the glacier. This is expected because friction from the sidewalls reduces the ice speeds that can be achieved at the margins and provides further evidence that the speckle tracking algorithm has produced reliable results.

4.2.1.1 Belcher Basin Velocity Structure: Spring 2009 (March 5th-March 29th 2009)

Figure 4.1a and Figure 4.9 present the velocity structure of the Belcher basin as determined by speckle tracking of Radarsat-2 imagery for March 5-29, 2009. Of the speckle tracking results presented here, the overall motion of the Belcher Glacier was highest during this spring period (it is likely that speeds were higher during the summer, but lack of coherence between image pairs meant that velocities could only be derived for the near-terminus area then: see Section 4.4). Along the main trunk, velocity maps reveal that the highest surface ice velocities occurred near the terminus (~275 m yr^{-1}) and remained generally high (~100-200 m yr^{-1}) towards the convergence with the main tributary. Upglacier from the main tributary, surface ice displacements are noticeably lower (~25-99 m yr^{-1}) and decrease toward the headwall (~20 m yr^{-1}). Near the convergence of the four southern headwall tributaries surface ice velocities increase to between ~75 and ~100 m yr^{-1}.

4.2.1.2 Belcher Basin Velocity Structure: Autumn 2009 (October 3rd – October 27th, 2009)

Figure 4.1b and Figure 4.10 present the velocity structure of the Belcher basin as determined by speckle tracking of Radarsat-2 fine beam imagery for October 3rd – October 27th, 2009. Out of all the measurement periods, surface ice motion was slowest during Autumn 2009 on all parts of the glacier except for the terminus. It is hypothesized that terminus velocities are higher during the autumn than during any other season due to the fact that annual sea ice minimums occur near the glacier front at this time. Indeed, ice charts produced by the Canadian Ice Service (available from http://ice-glace.ec.gc.ca) indicate open water at the Belcher terminus on September 28, 2009, ice concentrations of 9/10 landfast sea ice at the terminus on October 5, 2009, and sea ice concentrations of 9/10 at the terminus during all other acquisitions (regional ice charts are created weekly and monthly through the winter). This means that in October 2009, at the Belcher Glacier terminus, sea ice is younger and weaker than it is through the winter and into the spring.

As such, the buttressing effect of the sea ice is less in the autumn than any of the other seasons (except summer) which likely allows higher terminus velocities to occur.

On all other areas of the Belcher Glacier away from the terminus, velocities are at a minimum and the areas of faster flow extending upglacier from the terminus are greatly reduced. Velocities between the terminus and the convergence of the main tributary are lower than in all other periods, reaching a maximum of ~125 m yr^{-1} in small patches within this area. From the convergence of the main tributary upglacier to the headwall, surface ice velocities are on the order of 50 m yr^{-1}, with only small limited patches exceeding these velocities. At the convergence of the four headwall tributaries higher velocities do occur, nearing 100 m yr^{-1}. Overall, velocities for the Belcher Glacier are at a minimum during this time along the entire glacier length, with the exception of the terminus.

4.2.1.3 Belcher Basin Velocity Structure: Mid-Winter 2009-2010 (December 21st, 2009 - January 14th, 2010)

Figure 4.1c and Figure 4.11 presents the velocity structure of the Belcher basin as determined by speckle tracking of Radarsat-2 ultrafine imagery for December 21st, 2009 - January 14th, 2010. During mid-winter 2009-2010 surface ice velocities were higher on all parts of the glacier (except for the terminus) compared to autumn 2009. Velocity decreases at the terminus might be linked to the return of landfast sea ice, which creates a buttressing effect against the floating terminus and reduces motion (CIS ice charts indicate 10/10 landfast sea ice at the Belcher terminus with 9/10 ice cover extending entirely across Jones Sound and Baffin Bay).

Upglacier from the terminus, it appears that faster flow propagates in an upstream direction. For example, between the terminus and the main tributary ice motion ranges between 75 and 99 m yr^{-1} during this period, a marked increase from autumn levels. Faster velocities also appear to propagate upglacier from the convergence of the main tributary, with velocities in this small area reaching between 50 m yr^{-1} and 75 m yr^{-1}. For the rest of the area from the convergence of the main tributary to the main headwall, ice velocities remain similar to those in autumn. However, at the convergence of the four

southern tributaries ice velocities are lower than those experienced in spring or autumn, with ice velocities ranging between ~50-74 m yr^{-1}. Overall, during midwinter the terminus has slowed, the main trunk has increased in speed with increased ice velocities propagating in an upglacier direction, but the high velocities have not yet reached the southern headwall.

4.2.1.4 Belcher Glacier Velocity Structure: Late Winter 2010 (February 8th - March 3rd, 2010)

Figure 4.1d and Figure 4.12 present the velocity structure of the Belcher basin as determined by speckle tracking of Radarsat-2 ultrafine imagery for February 8th - March 3rd, 2010. During the late winter, terminus velocities are at a minimum while the rest of the Belcher Glacier experiences faster velocities that extend further upglacier. Between the terminus and the convergence of the main tributary, velocities range between 100 m yr^{-1} and 124 m yr^{-1}. Measured surface ice velocities are higher along the main tributary than in any other season and along the Belcher Glacier trunk south of the main tributary higher velocities propagate upglacier. During all other seasons this area does not achieve velocities higher than 75 m yr^{-1} while during the late winter velocities reach up to 100 m yr^{-1} and accelerated ice motion extends toward the southern headwall. At the southern headwall ice velocities range between ~75-100 m yr^{-1}.

4.2.1.5 Seasonal Centerline Velocity Structure

Figure 4.15 presents the extracted centerline velocities determined by speckle tracking of Radarsat-2 imagery for each season for the Belcher Glacier. Generally, the velocity structure follows the same general trend as discussed above, with higher velocities near the terminus region and a decrease upglacier toward the southern headwall. Figure 4.15 shows that the velocities along the centerline are highest for the March 5-29, 2009 imagery and lowest for the October 3-27, 2009 imagery. Specifically, the average velocity along the entire length of the Belcher Glacier for:

(a) March 5-29, 2009 was 89.91 m yr^{-1}

(b) October 3-27, 2009 was 73.11 m yr^{-1} (-18.67% difference)

(c) December 21, 2009 – January 14, 2010 was 75.58 m yr^{-1} (-15.93% difference)

(d) February 8 – March 3, 2010 was 75.72 m yr^{-1} (-15.78% difference)

(using March 5-29, 2009 as the baseline from which all comparisons are made).

The velocity patterns in the terminus region and the southern headwall region also need to be highlighted. For the terminus region, lowest average centerline velocities (152.46 m yr^{-1}) are achieved in February 8th - March 3rd, 2010, while the October 3-27, 2009, imagery exhibits the highest average velocities (231.44 m yr^{-1}), which represents a velocity decrease of ~29%. The second region of note is the southern headwall region, where again the October 3-27th, 2009 imagery reveals higher velocities than those achieved in the winter. Mean centerline velocity in this region is 48.07 m yr^{-1} in October, while from December 21, 2009 - January 14, 2010 the mean velocity is 41.39 m yr^{-1} and from February 8 – March 3, 2010 mean velocity is 41.93 m yr^{-1}.

For the five flux gates along the main trunk of the Belcher Glacier (Fig. 4.13), seasonal ice discharge was calculated (Figure 4.16). Fluxgate1 experienced the highest flux for the year, with volumes decreasing at each flux gate upstream. The downglacier increase in ice flux is expected as more and more tributaries feed into the main trunk. The flux results also show the seasonality of ice flow through each gate, with the maximum ice discharge occurring in March and the minimum in October. Observations in the winter reveal higher flux in February than in December, illustrating the gradual build up of ice discharge through the winter months. Burgess et al (2005) calculated ice flux for the entire Devon Island Ice Cap to be 20.5 km^3 +/- 4.7 km^3 between 1960 and 1999 (or 0.57 km^3 yr^{-1}). Their study estimated that the Belcher Glacier basin is responsible for about 50% of the total amount of mass calved for the entire ice cap. Thus, according to Burgess et al (2005) the Belcher Glacier is responsible for ~0.285 km^3 yr^{-1} of ice flux at the terminus.

To improve comparison with the work of Burgess et al (2005) a flux gate was created at the Belcher Glacier terminus, although there is only ice thickness data available for the southern portion of the terminus region. To correct for this, we assumed the bed topography follows a parabolic form, and thus the depth values available for the southern

portion of the region are mirrored for the northern portion. The average annual flux calculated at the terminus flux gate is 0.091 km^3 yr^{-1}, roughly 33% of the value estimated by Burgess et al (2005). Reasons for the discrepancy are the differences in ice thicknesses used at the terminus. Burgess et al (2005) used an ice thicknesses determined by Dowdeswell et al (2004) from airborne radio echo sounding with a 1 km resolution. Therefore, Burgess et al (2005) would have an ice thickness of ~250 m for the entire terminus of the glacier, while the results presented in this thesis use a more detailed bedDEM which had an average depth across the terminus of ~165 m. Burgess et al (2005) also determined higher average velocities across the terminus of ~250 m yr^{-1}, while the average velocity across the terminus in this study for the flux gate was ~112 m yr^{-1}. These reasons help to explain the differences between the two studies. Additionally, inter-annual variability may also account for some of the discrepancy between the studies; the Belcher Glacier has been shown to have a strong inter-annual variation (~20%) in its surface ice motion and it may be more appropriate to use a 5 year velocity average for calculating long-term ice flux than a single year (Wyatt, F. Personal Communication, 2010). All flux gates reveal that previous studies have probably over estimated the flux produced by the Belcher Glacier.

4.2.1.6 Seasonal Velocity Structure of Tributaries

Figure 4.17 shows the locations of tributaries of the Belcher Glacier. Tributary velocities as determined by dGPS surveys during the start (May 6th-11th) and end (May 20th) of the 2008 field season and again in late May 2009 are presented in Figure 4.18. The survey undertaken during the 2008 field season provides a good approximation of the spring velocities for the Belcher Glacier tributaries, while the re-survey in May 2009 provides a roughly year long record. These results show that surface ice motion varies considerably between seasons between different tributaries, with some tributaries showing much faster speeds (~30%) in the annual compared to the spring measurements, while others showed decreases in velocity over the annual period (~-30%). Five of the ten surveyed tributaries reveal a ~15% increase of velocities over the annual period as compared to the May 6-11 to May 20, 2008 period (average velocity for all the tributaries was 5.06%), which is consistent with summer speed ups observed at the semi-permanent dGPS stations set out

along the main trunk of the Belcher Glacier (B. Danielson, personal communication, 2010).

Surface ice velocities determined by speckle tracking were extracted along 10 transects across the main tributaries flowing into the main Belcher Glacier trunk (Figure 4.19) (location of transects are shown in Figure 4.17). Results show that seasonal velocity variations are not uniform for each tributary (Figure 4.16). For Tributary A, for example, the highest velocities occur in March and minimums occur in October, with a building of velocities through the winter. In contrast, tributary I shows a rather uniform velocity throughout the year. Indeed, a consistent pattern of tributary seasonal velocity change is difficult to determine.

Tributary interactions are likely to depend to a large degree on the speeds achieved by the main glacier trunk. Results also reveal that it is difficult to determine ice velocities on tributaries using the speckle tracking method due to their commonly narrow nature and being surrounded by stationary bedrock. Because an interpolation method is used to determine ice velocities over the tributary, these stationary rock outcrops will influence the velocities determined using the interpolation method, causing slower velocities to be blended into the tributary results close to the margins. Additionally, because flow along tributary margins causes shearing and associated phase de-correlation in the SAR image pairs, it is more difficult to make speckle tracking matches in these areas.

Ice flux through each tributary flux gate was also calculated for each of the surveyed tributaries that connect the Belcher basin to the ice cap (Figures 4.18). Tributaries D, E, F and G located at the southern headwall are shown to account for a large portion of the ice entering the system. This makes sense as these tributaries are connected to the large trough of thicker ice that extends from the summit of the ice cap (Figure 2.1). Tributaries B, C and I are also large contributors of mass to the Belcher system, while A, H, and J, input relatively small amounts of mass. Spatially, tributary I is the only large contributor of mass located on the eastern side of the glacier. This relationship is expected, as the amount of mass available to the east of the Belcher Glacier is much smaller than the

amount of mass available on the western side due to a much larger accumulation area and higher elevations to the west. Ice discharge through a flux gate is also largely dependent on the size of the tributary. Wider and deeper tributaries are larger contributors than narrower, shallower tributaries.

Seasonal velocities following the same pattern as the main trunk (i.e. maximum velocities in March, minimums in October and velocity build up through the winter) are evident in the results of tributaries B, F and I. Seasonal changes in ice motion are more difficult to distinguish for tributaries at the southern headwall region (Tributaries: D, E F). December velocities are underestimated by roughly 50% as no reliable velocity data was available for that portion of the glacier. Errors are also present in the February headwall tributaries, as there was some loss of coherence between acquisitions, causing confidence in results to decrease. However, these errors are limited to relatively small errors on only three tributaries, and do not impact the flux results on other regions of the glacier.

Results along the main trunk flux gates should roughly equal the sum of ice discharge of the upstream tributaries (Table 4.5). For the most part, results follow this trend, although the sum of the upglacier tributary discharges is generally higher than the ice discharge calculated at a single gate. Reasons for the difference might be that good velocity results are more difficult to ascertain on the tributaries than on the main trunk of the Belcher Glacier, and also due to the loss of ice mass between the tributaries and the main trunk flux gates due to surface melt. February velocities on the southern tributaries seem to be overestimated due to loss of coherence in the region and the consequent need for heavy filtering of the results at this location. Flux results generated on a single tributary are likely to be less reliable for calculating ice flux through the Belcher Basin, and the results are best used for understanding the relevant importance of tributaries to the overall ice discharge. As noted by Short and Gray (2004) it is difficult to determine ice velocities on slower moving, narrow glaciers due to a smaller image chip being needed in these areas to remove the random phase component of error. This may account for the poorer results on the tributaries, particularly the smaller ones.

4.3 Controls on Belcher Glacier Flow

As reviewed in Chapter 2, basal water pressure provides the main control on temporal variations in the flow of temperate and polythermal glaciers (via its control on basal lubrication), making it likely that the large seasonal variations in motion on Belcher Glacier are related to this factor. October minimums occur due to the large amount of meltwater generated during the previous summer's melt season, which cause discrete, efficient subglacial drainage passageways to develop (likely in the form of R channels). This efficient drainage network would allow any water at the glacier bed to be quickly evacuated, with the lack of water input from surface melt causing basal water pressures to be low. As water pressures are reduced, it is difficult to facilitate basal motion as the glacier cannot be decoupled from it bed, and as a consequence ice velocities during this time are at a minimum.

As the autumn progresses into winter, the internal drainage network would close in on itself due to creep. As this occurs the subglacial drainage network typically changes from an efficient channelized system to a linked cavity distributed system. It is likely that a small amount of water remains trapped beneath the Belcher Glacier for the duration of the winter season, with small amounts of new water being produced from basal geothermal heat (Paterson 1994). As the winter progresses into spring, water pressures likely increase as the rate of cavity closing due to ice creep is faster than melting due to subglacial water flow (Iken and Truffer 1997, Lappegard and Kohler 2005, Nienow et al 1998, Fudge et al 2005, Benn and Evans 1998). This would result in an increase in surface velocities as basal water pressures and therefore basal lubrication increases. As more and more water is generated throughout the winter and into the spring from basal melting, basal water pressure would continue to build as this water cannot easily escape from the subglacial system. As this happens greater connectivity between the linked cavity networks would occur and so velocities reach their maximum in the late spring. With the data available for this study the measured velocities are highest in the late spring, but they are likely to be higher in the summer. However, no usable data was available for speckle tracking of the main trunk of the Belcher Glacier during the summer months.

The progressive buildup of water pressure at the glacier bed provides a "priming" for increased motion due to surface water inputs at the onset of the summer melt season. Indeed, at this time, glacier response to surface water inputs is rapid, with a decoupling of the glacier from the bed, followed by horizontal displacement of the glacier (B. Danielson, Personal Communication, 2010). In order for this rapid response to occur, water pressure at the bed must be nearly equal to the ice pressure. This type of water pressure must be generated over the course of the winter, when a distributed drainage network is dominant. In these cases, the influence of winter velocities may be an important precursor for summer speed up events.

4.3.1 Supraglacial Drainage and Velocity Structure

The duration and intensity of the summer melt season will affect the efficiency and extent of the subglacial drainage network. During prolonged, intense melt seasons, the extent and efficiency of a discrete drainage system is likely to be greater than when the melt season is short and less intense. During prolonged melt seasons, most of the water will be effectively evacuated from the basal interface due to the development of large R channels, leaving minimal water pressure available for winter motion. In these cases, patchy areas of faster winter motion are likely to be reduced and the amount of time necessary to generate uniform velocities along the entire glacier surface during the late winter is likely to increase. This reduces the amount of water available at the bed to quickly facilitate motion due to meltwater inputs during the following melt season.

Conversely, after particularly low melt seasons, drainage networks are less likely to be fully developed, and it is probable that some moulins will drain directly into linked cavity networks that do not connect to the main discrete system. At these times, more water remains at the bed at the onset of winter, allowing for uniform glacier motion to be achieved earlier in winter season and increasing the potential of higher water pressures at the onset of the next melt season. In this way, the interplay between winter water storage and summer drainage development could greatly influence the velocities that can be achieved in the following year.

This type of subglacial drainage interplay between high and low melt seasons is similar to the explanations provided by Iken and Truffer (1997) from their study on Findelengletscher, Switzerland. They explain that in melt seasons when an extensive network of small R channels develops they are more readily destroyed in the subsequent winter, promoting the development of an extensive linked cavity network. As a consequence, winter velocities are higher. Conversely, in years of high melt, a more limited network of large R-channels develop. These channels take longer in the winter to close in due to ice creep. Due to this, large amounts of water are evacuated from the bed, causing slower winter velocities. The seasonality of the Belcher Glacier motion can be understood within this framework.

4.4 Seasonal Terminus Velocity Structure

Figure 4.3 shows the seasonal velocity changes recorded at the Belcher Glacier terminus. The Belcher terminus velocity structure differs significantly from the flow in its main trunk. Terminus velocities are highest in the autumn months and decrease throughout the winter and increase again in the spring. High autumnal terminus velocities can be expected due to sea ice minimums that occur at the glacial front at this time. Landfast sea ice present through most portions of the year acts to buttress the terminus in place and reduce motion. When sea ice is removed, this buttressing effect is lost (Reeh et al 2001, Copland et al 2007, Massom et al 2006). Additionally, the terminus is likely to have the largest subglacial channels and highest basal water pressure of any region of the glacier since it has the largest upstream contributing area. Based on the studies of Nienow et al (1998), it is evident that channelized drainage networks typically breakdown fastest upglacier and slowest downglacier, due to the relative size of the channels and because of the meltwater available to keep the channels open. This also means that distributed, linked cavity networks will develop faster upglacier than they will at the terminus. As a consequence, ice velocities will be faster in these upglacier patches than they will at the terminus. This creates higher surface ice velocities on the main trunk at the end of winter and minimum annual velocities at the terminus. As the winter progresses into spring and the water generated along the main trunk nears the ice pressure, the linked cavity network

of the main trunk likely connects to the terminus. When this occurs, large amounts of water are made available to facilitate motion at the terminus, causing increased velocities at this time.

1	75.657	-81.306	206.45	[illegible]	201.91	231.80	199.96	154.62	197.07	-4.54
2	75.659	-81.371	196.30	118.27	190.58	190.97	193.66	129.96	176.29	-10.19
3	[illegible]	[illegible]	117.09	100.16	120.07	89.92	101.64	100.30	102.98	-12.05
4	75.609	-81.433	100.68	106.68	99.33	77.99	96.08	92.16	91.39	-9.23
5	[illegible]	[illegible]	[illegible]	[illegible]	108.26	[illegible]	[illegible]	[illegible]	95.80	[illegible]
6	75.600	-81.422	104.13	109.98	107.45	75.64	89.71	95.01	91.95	-11.69
7	[illegible]	[illegible]	[illegible]	[illegible]	136.01	[illegible]	99.10	[illegible]	95.95	[illegible]
8	75.585	-81.432	111.19	104.84	131.76	74.06	86.98	92.51	96.33	-13.37
9	[illegible]	[illegible]	[illegible]	[illegible]	110.19	67.02	[illegible]	[illegible]	92.48	[illegible]
10	75.560	-81.479	91.21	66.12	63.34	57.25	76.95	93.09	72.66	-20.34
11	[illegible]	[illegible]	[illegible]	[illegible]	72.04	[illegible]	[illegible]	[illegible]	[illegible]	[illegible]
12	75.533	-81.461	65.22	61.82	64.86	40.09	56.25	55.73	54.23	-16.85
13	[illegible]	[illegible]	[illegible]	[illegible]	[illegible]	[illegible]	47.99	[illegible]	51.90	[illegible]
14	75.508	-81.445	58.97	N/D	57.44	47.68	55.81	51.23	53.04	-10.06
15	[illegible]	[illegible]	[illegible]	[illegible]	[illegible]	[illegible]	[illegible]	[illegible]	[illegible]	[illegible]
16	75.419	-81.630	33.74	N/D	29.72	16.05	38.25	23.89	26.98	-20.04

Table 4.1: *Comparison of centreline surface ice velocities determined by speckle tracking of Radarsat-2 Fine Beam (Mar 5-29, 2009 & Oct 3-27, 2009) and Radarsat2 Ultrafine (Dec 21, 2009 – Jan 14, 2010 & Feb 8 – Mar 3, 2010) and TerraSar X (March 16-27, 2009) imagery with in situ dGPS data (May 2008- May 2009). N/D denotes where no data is available. Location of measurement IDs shown in Figure 4.4.*

18	75.603	-81.448	91.56	80.16	61.03	88.63	82.72	78.14	-14.66
19	75.605	-81.408	101.90	107.35	83.25	95.19	88.68	93.62	-8.13
21	75.584	-81.466	74.71	106.39	54.27	67.01	69.28	74.24	-0.63
8	75.585	-81.432	111.19	131.76	74.06	86.98	92.51	96.33	-13.37
24	75.580	-81.401	102.36	68.46	45.72	81.01	83.88	69.77	-31.84
26	75.532	-81.480	61.17	61.17	44.48	45.56	52.60	50.95	-16.70
27	75.532	-81.440	63.71	64.44	42.51	55.10	54.61	54.17	-14.98
10	75.563	-81.503	91.21	63.35	57.25	79.40	93.09	73.27	-19.67
30	75.563	-81.522	79.47	90.68	69.40	56.42	70.64	71.79	-9.67
32	75.559	-81.584	70.93	60.79	57.94	48.14	68.07	58.74	-17.19
34	75.558	-81.566	71.48	71.68	67.26	65.34	69.09	68.34	-4.39

Table 4.2: *Comparison between cross-section surface ice velocities determined by speckle tracking of Radarsat-2 images with in situ dGPS data (May 2008- May 2009). Location of measurement IDs shown in Figure 4.5*

1	75.657	-81.505	[illegible]	[illegible]	[illegible]	[illegible]	[illegible]	[illegible]	[illegible]
2	75.659	-81.371	13.00	19.43	14.22	12.84	6.99	13.37	0.37
3	75.634	-81.435	[illegible]	[illegible]	[illegible]	[illegible]	[illegible]	[illegible]	[illegible]
4	75.609	-81.433	104.42	106.46	109.61	108.01	105.38	107.37	2.94
5	75.605	-81.426	[illegible]	[illegible]	[illegible]	[illegible]	[illegible]	[illegible]	[illegible]
6	75.600	-81.422	109.80	115.00	121.81	113.63	109.87	115.08	5.28
7	75.588	-81.485	[illegible]	[illegible]	[illegible]	[illegible]	[illegible]	[illegible]	[illegible]
8	75.585	-81.432	51.40	51.94	60.06	55.63	52.76	55.10	3.70
9	75.581	-81.443	[illegible]	[illegible]	[illegible]	[illegible]	[illegible]	[illegible]	[illegible]
10	75.560	-81.479	72.25	54.81	102.47	76.65	73.20	76.78	4.53
11	75.538	-81.461	[illegible]	[illegible]	[illegible]	[illegible]	[illegible]	[illegible]	[illegible]
12	75.533	-81.461	91.14	89.87	105.13	96.37	92.51	95.97	1.70
13	75.527	-81.461	[illegible]	[illegible]	[illegible]	[illegible]	[illegible]	[illegible]	[illegible]
14	75.508	-81.445	96.95	103.39	108.22	116.73	89.10	104.36	7.41
15	75.443	-81.331	[illegible]	[illegible]	[illegible]	[illegible]	[illegible]	[illegible]	[illegible]
16	75.419	-81.630	356.72	349.56	357.56	325.17	324.30	339.15	17.57
17	75.602	-81.466	[illegible]	[illegible]	[illegible]	[illegible]	[illegible]	[illegible]	[illegible]
18	75.603	-81.448	111.73	108.82	107.65	120.95	107.51	111.23	0.49
19	75.665	-81.405	[illegible]	[illegible]	[illegible]	[illegible]	[illegible]	[illegible]	[illegible]
20	75.606	-81.393	108.11	107.90	118.75	109.21	109.85	111.43	3.32
21	75.584	-81.465	[illegible]	[illegible]	[illegible]	[illegible]	[illegible]	[illegible]	[illegible]
22	75.586	-81.451	47.12	51.33	57.49	34.06	47.08	47.49	0.37
23	75.582	-81.418	[illegible]	[illegible]	[illegible]	[illegible]	[illegible]	[illegible]	[illegible]
24	75.580	-81.401	53.92	66.48	59.71	58.90	54.01	59.78	5.86
25	75.532	-81.498	[illegible]	[illegible]	[illegible]	[illegible]	[illegible]	[illegible]	[illegible]
26	75.532	-81.480	89.60	92.56	101.01	101.24	89.25	96.02	8.13
27	75.532	-81.480	[illegible]	[illegible]	[illegible]	[illegible]	[illegible]	[illegible]	[illegible]
28	75.531	-81.422	93.76	93.24	125.34	101.59	96.49	104.17	2.57
29	75.569	-81.524	[illegible]	[illegible]	[illegible]	[illegible]	[illegible]	[illegible]	[illegible]
30	75.563	-81.522	40.78	52.90	59.03	53.15	51.79	54.22	13.44
31	75.562	-81.562	[illegible]	[illegible]	[illegible]	[illegible]	[illegible]	[illegible]	[illegible]
32	75.559	-81.584	354.61	356.95	341.04	353.56	359.84	352.85	1.76
33	75.562	-81.569	[illegible]	[illegible]	[illegible]	[illegible]	[illegible]	[illegible]	[illegible]
34	75.558	-81.566	355.68	352.67	342.13	358.10	349.22	350.53	5.15

Table 4.3: *Comparison of ice motion orientation determined from in situ annual dGPS observations compared to seasonal orientations determined by speckle tracking of Radarsat-2 Fine Beam (Mar 5-29, 2009 & Oct 3-27, 2009) and Radarsat-2 Ultrafine Beam (Dec 21, 2009 – Jan 14, 2010 & Feb 8 – Mar 3, 2010) imagery. Location of measurement IDs shown in Figure 4.3*

1	4.34	12.46	11.42	8.15
2	3.26	18.06	9.52	5.79
3	10.57	19.78	17.44	17.68
4	5.46	8.69	16.72	3.21
5	5.11	9.29	6.70	4.40
6	5.58	13.18	8.81	4.43
7	5.60	13.54	16.72	3.21
8	4.43	2.57	9.31	3.28
9	4.63	2.98	10.40	2.14
10	5.85	5.16	8.66	13.94
11	N/A	11.2	11.63	18.20
12	6.37	3.40	15.14	12.01
13	5.81	5.34	14.12	9.92
14	12.05	2.61	8.01	1.64
15	17.4	2.29	7.95	2.02
16	5.79	12.38	6.97	2.73
17	9.29	10.63	8.72	2.76
18	16.79	15.09	7.51	3.67
19	8.19	12.67	7.95	4.26
Mean Error	**7.18**	**9.54**	**10.47**	**6.72**
Overall Mean Error				**8.48**

Table 4.4: *Velocity errors over bedrock outcrops along the margins of Belcher Glacier. Locations of bedrock outcrops shown in Figure 4.7.*

Fluxgate 1	0.0934	0.0715	0.0799	0.0767
Fluxgate 2	0.0871	0.0630	0.0719	0.0747
Upglacier Tributary Flux Sum	**0.1167**	**0.1120**	**0.0964**	**0.1424**
Main Tributary	0.0387	0.0372	0.0397	[illegible]
Tributary A	0.0005	0.0004	0.0005	[illegible]
Tributary J	0.0003	[illegible]	[illegible]	[illegible]
Fluxgate 3	0.0387	[illegible]	[illegible]	[illegible]
Upglacier Tributary Flux Sum	**0.0752**	**0.0692**	**0.0578**	**0.086**
Tributary B	[illegible]	[illegible]	[illegible]	[illegible]
Tributary C	[illegible]	[illegible]	[illegible]	[illegible]
Tributary I	[illegible]	[illegible]	[illegible]	[illegible]
Tributary H	[illegible]	[illegible]	[illegible]	[illegible]
Fluxgate 4	[illegible]	[illegible]	[illegible]	[illegible]
Upglacier Tributary Flux Sum	**0.0488**	**0.0528**	**0.0437**	**0.0578**
Tributary D	0.0214	0.0233	0.0120	[illegible]
Tributary E	0.0169	0.0155	0.0140	[illegible]
Tributary F	0.0037	[illegible]	[illegible]	[illegible]
Tributary G	[illegible]	[illegible]	[illegible]	[illegible]

Table 4.5: *Tributary and flux gate ice flux results along Belcher Glacier (km^3 yr^{-1}).*

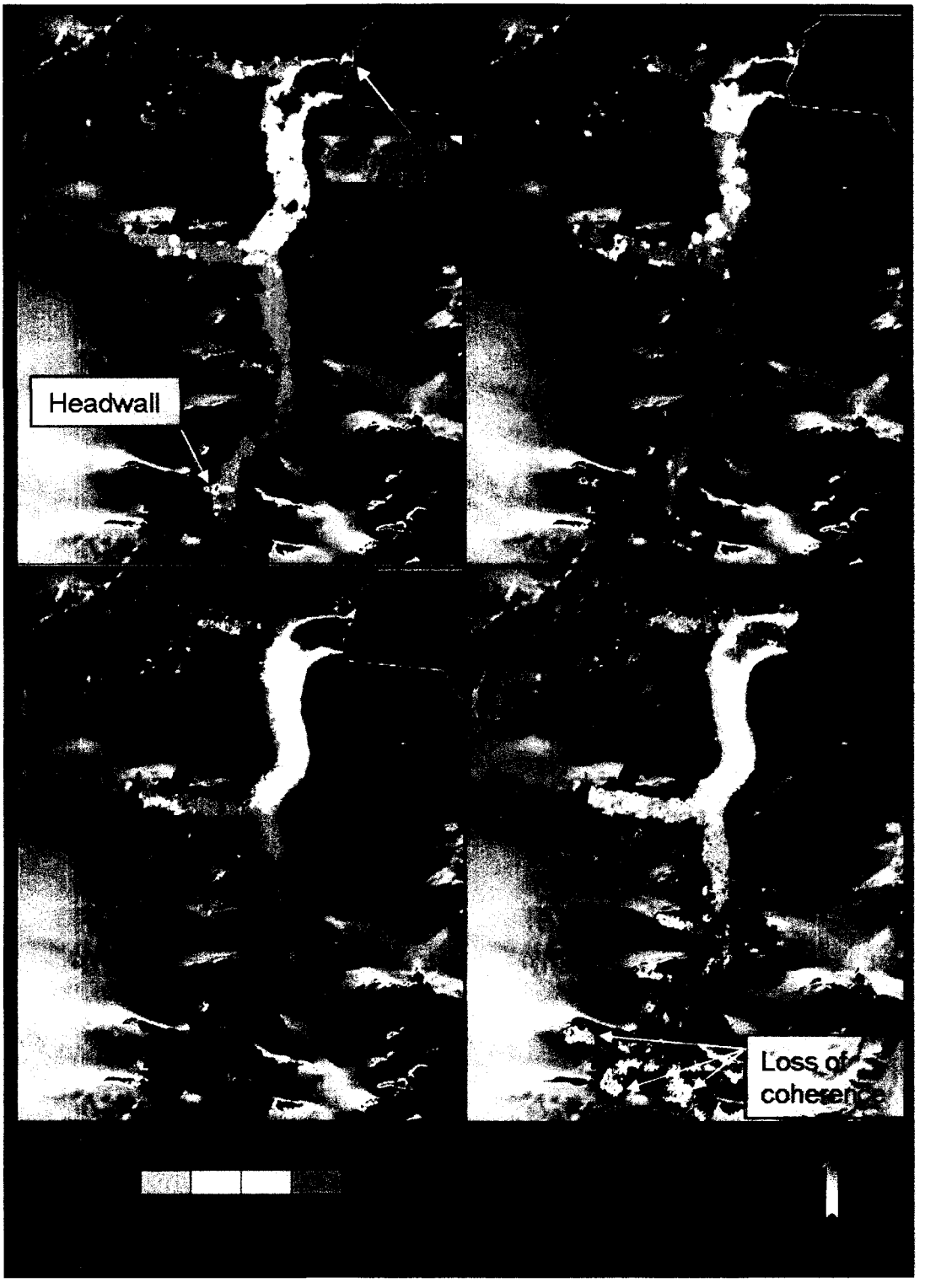

Figure 4.1: *Seasonal velocity maps of Belcher Glacier derived from speckle tracking of Radarsat-2 imagery, a) March 5-29, 2009 (fine beam); b) October 3-27, 2009 (fine beam); c) December 21, 2009 – January 14, 2010 (ultrafine beam); d) February 8 – March 3, 2010 (ultrafine beam).*

Figure 4.2: *Orientation vectors determined by speckle tracking over Belcher Glacier following valley shape (December 21, 2009 – January 14, 2010 (ultrafine beam)*

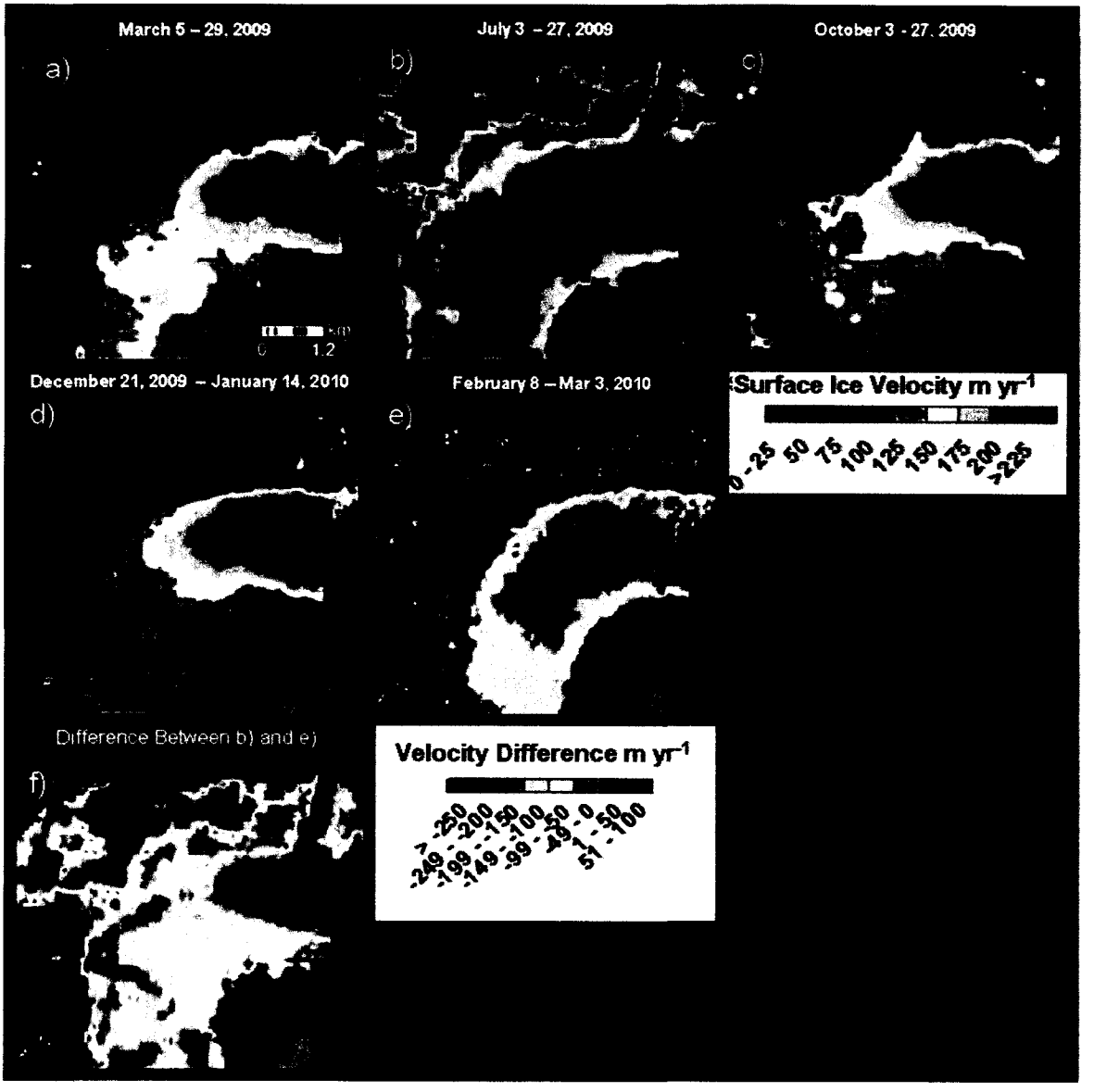

Figure 4.3: *Seasonal velocity changes observed at the Belcher Glacier terminus.*

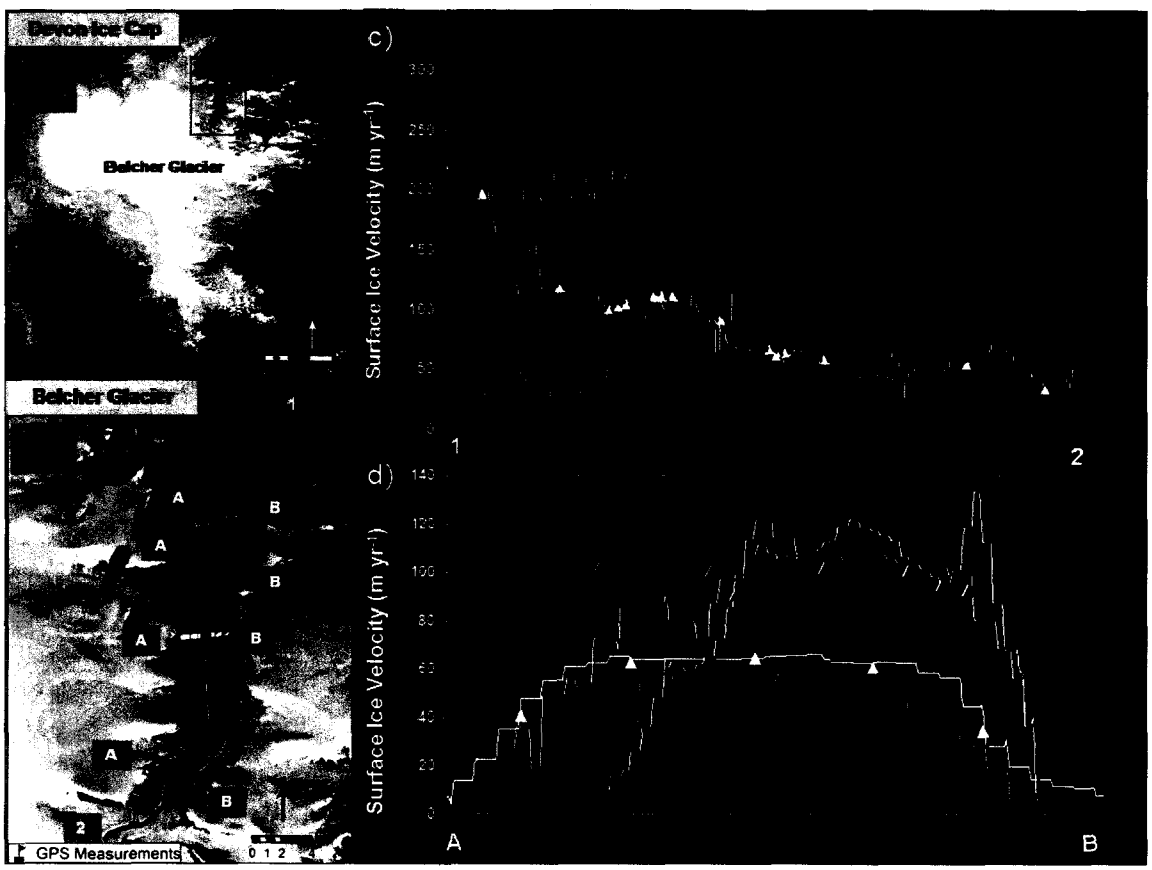

Figure 4.4: *a) Location of the Belcher Glacier on Devon Ice Cap; b) Locations of centerline and cross-section velocities extracted from the speckle tracking results, together with dGPS locations along the main trunk of Belcher Glacier; c) comparison of centerline velocities determined by Radarsat-2 speckle tracking (March 5-29, 2009), in situ dGPS annual ice displacements (May 2008-May 2009) and TerraSAR-X speckle tracking(March 16-27, 2009); d) Comparison of cross-section ice velocities determined by speckle tracking of Radarsat-2 imagery (at each fluxgate) (March 5-29, 2009) with in situ dGPS data (May 2008 – May 2009).*

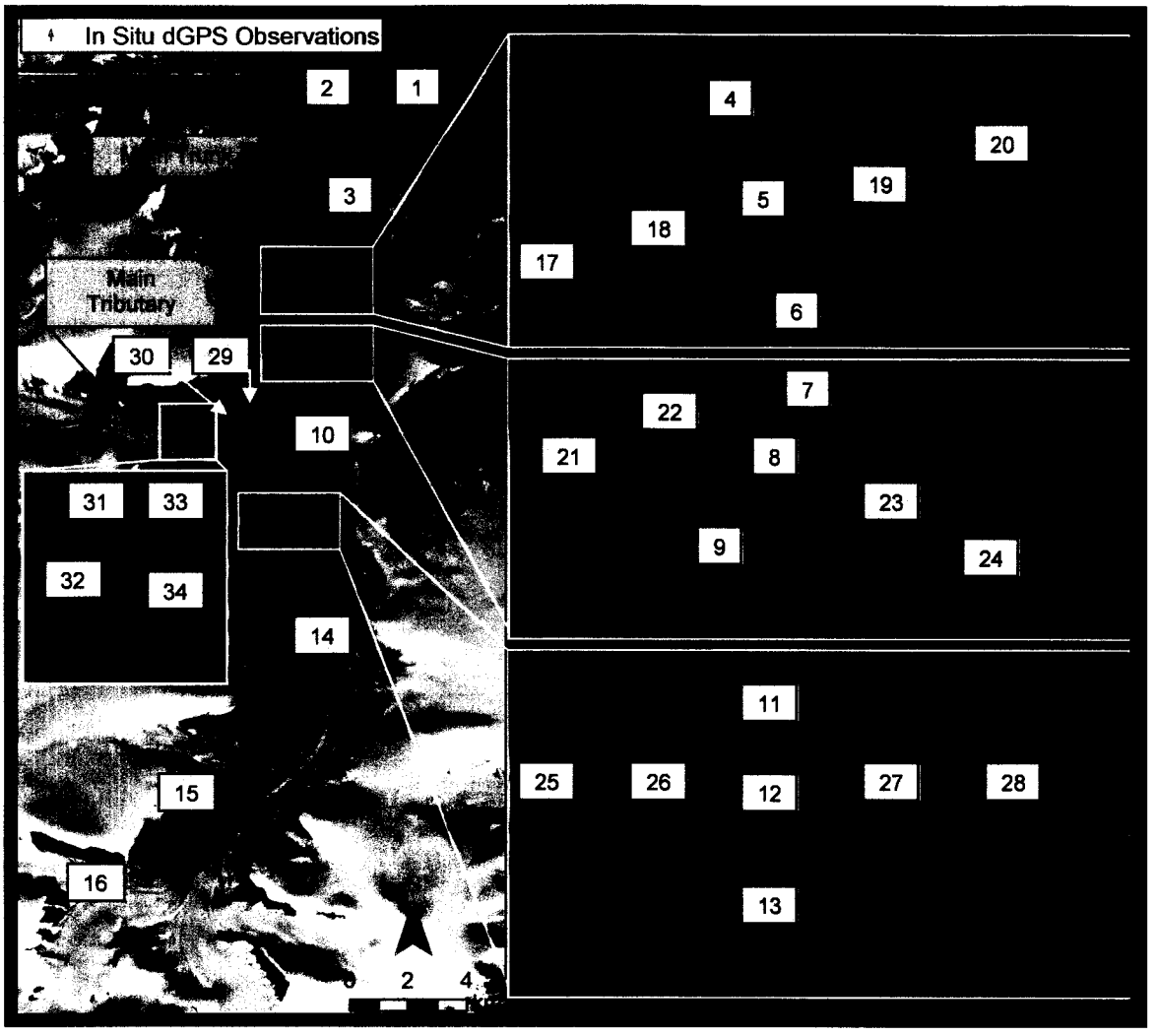

Figure 4.5: *Location of in situ dGPS observations with ID numbers.*

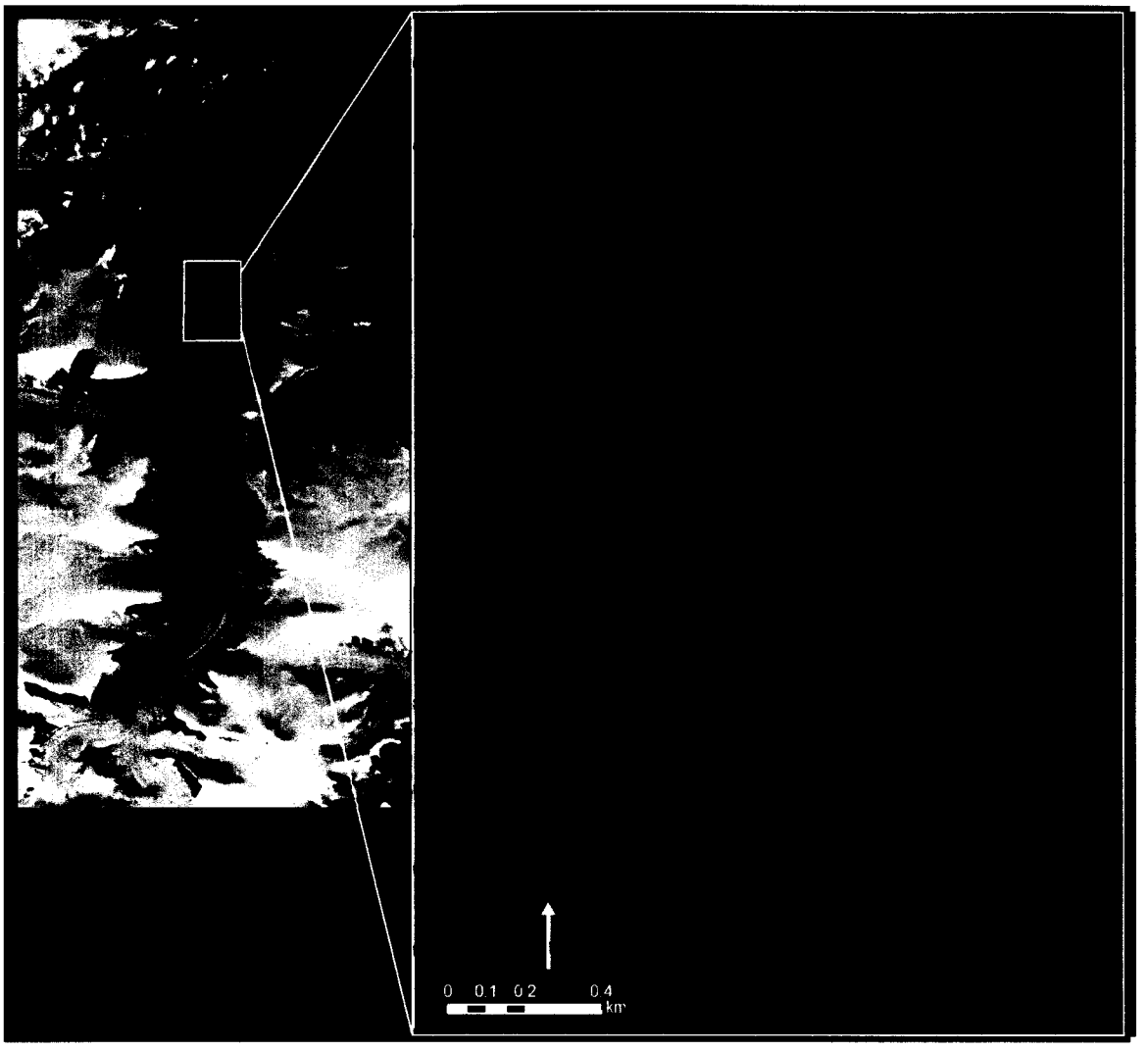

Figure 4.6: *Orientation of flow features (medial moraines) compared with speckle tracking vectors determined from Radarsat-2 Ultrafine (Feb 8 – Mar 3, 2010) imagery (black arrows) and annual displacement vectors of in situ marker stakes measured with dGPS (red arrows).*

Figure 4.7: *Rock outcrops of areas of known velocity (0 m yr^{-1}) used for comparison with results determined from speckle tracking.*

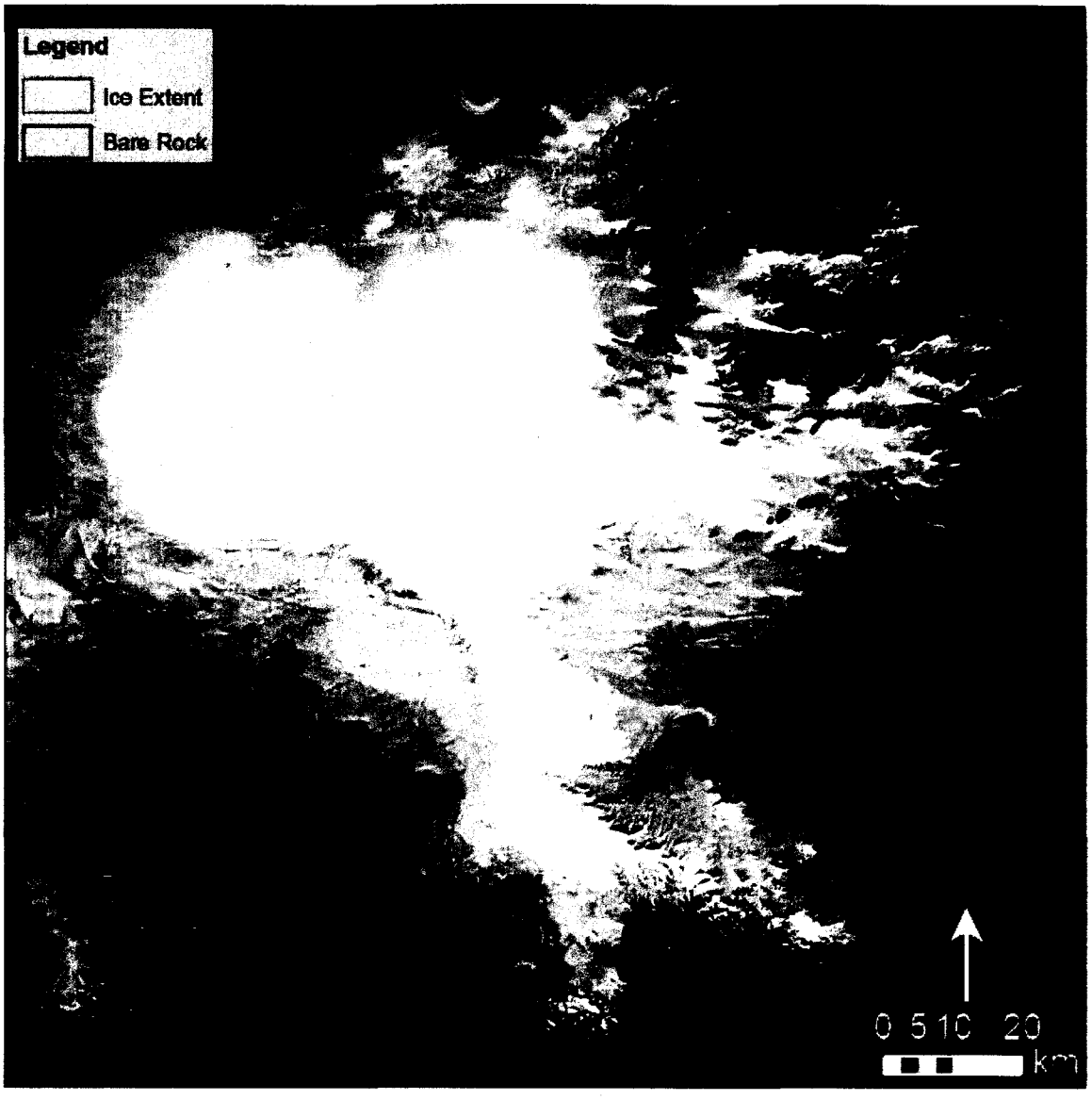

Figure 4.8: *Location of non-glaciated bedrock near Croker Bay used for error analysis (Red dots indicate areas of bedrock outcrop error analysis within the Belcher Basin).*

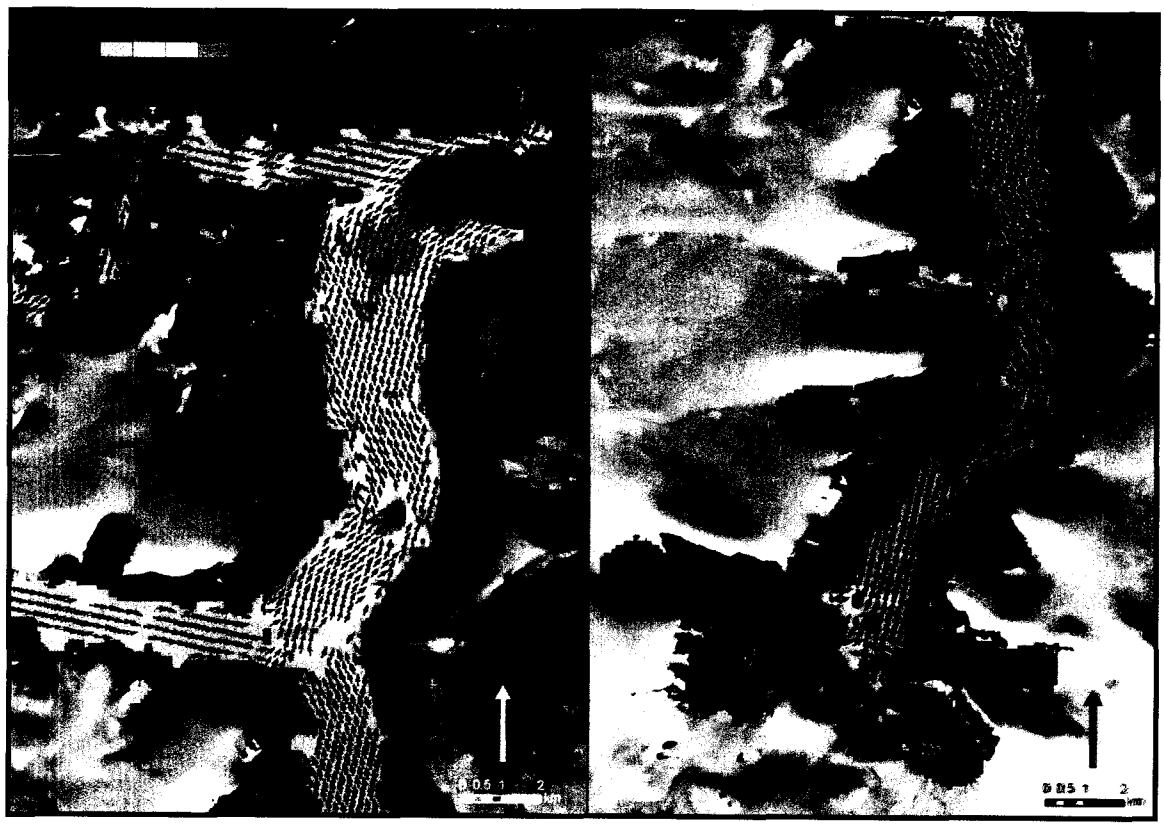

Figure 4.9: *March 5-29, 2009 Belcher Glacier velocity structure with orientation of displacement.*

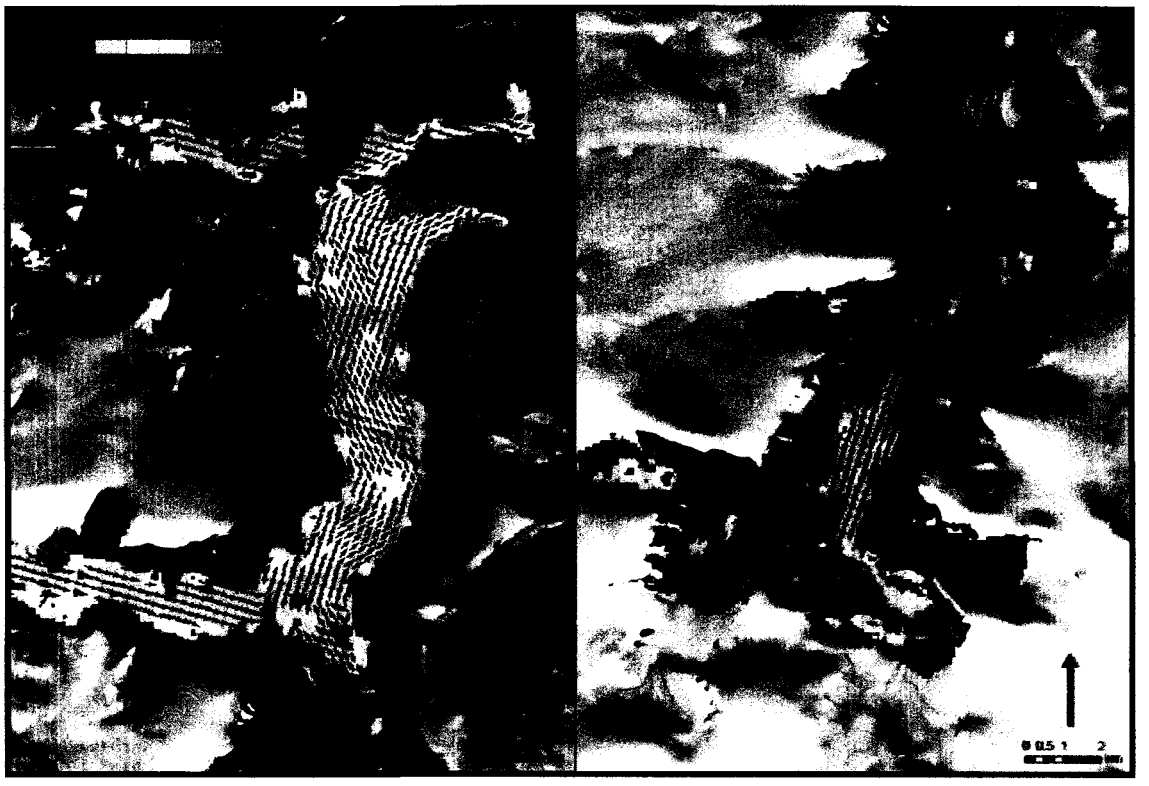

Figure 4.10: *Oct 3-27, 2009 Belcher Glacier velocity structure with orientation of displacement.*

Figure 4.11: *December 21st, 2009 - January 14th, 2010 Belcher Glacier velocity structure with orientation of displacement.*

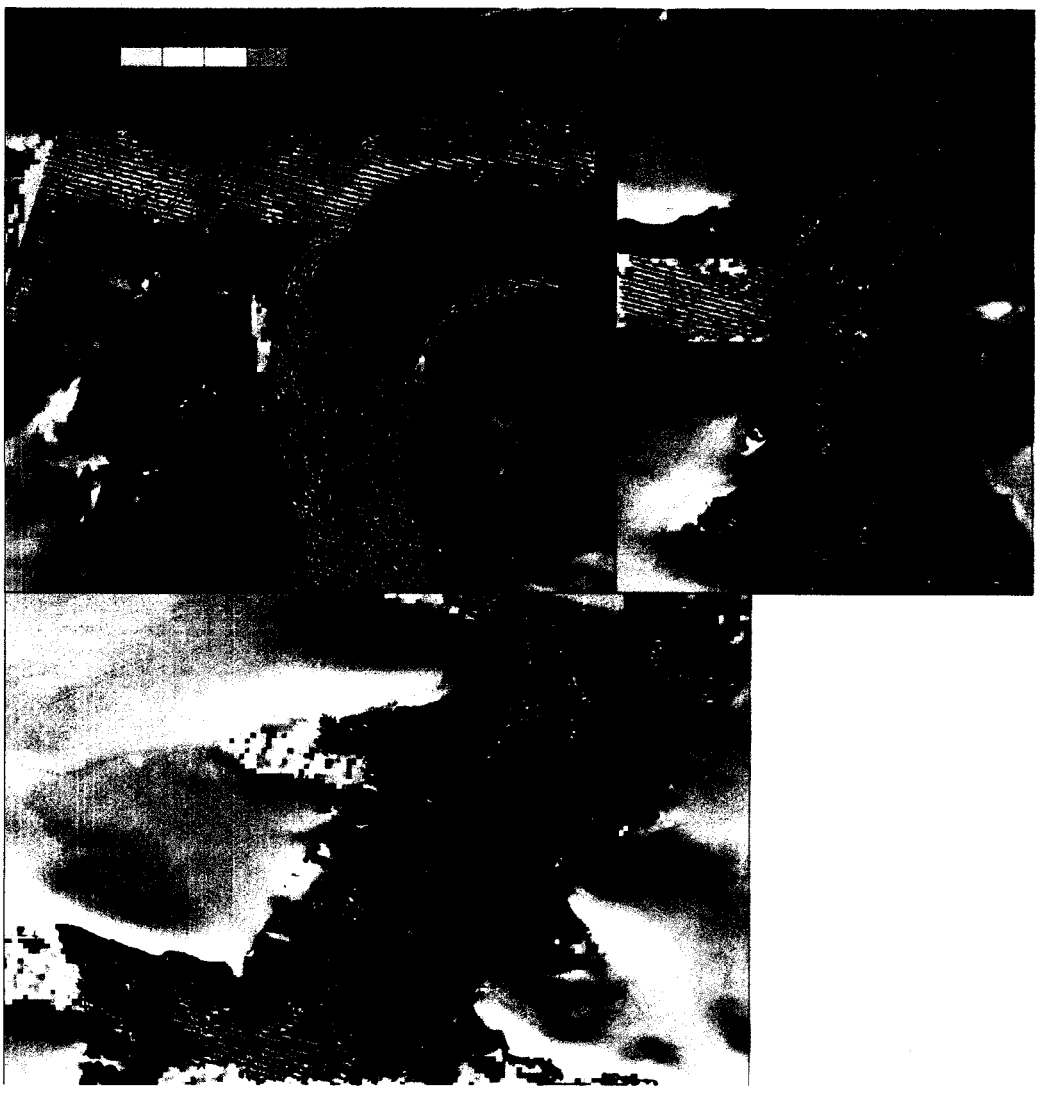

Figure 4.12: *February 8th - March 3rd, 2010 Belcher Glacier velocity structure with orientation of displacement.*

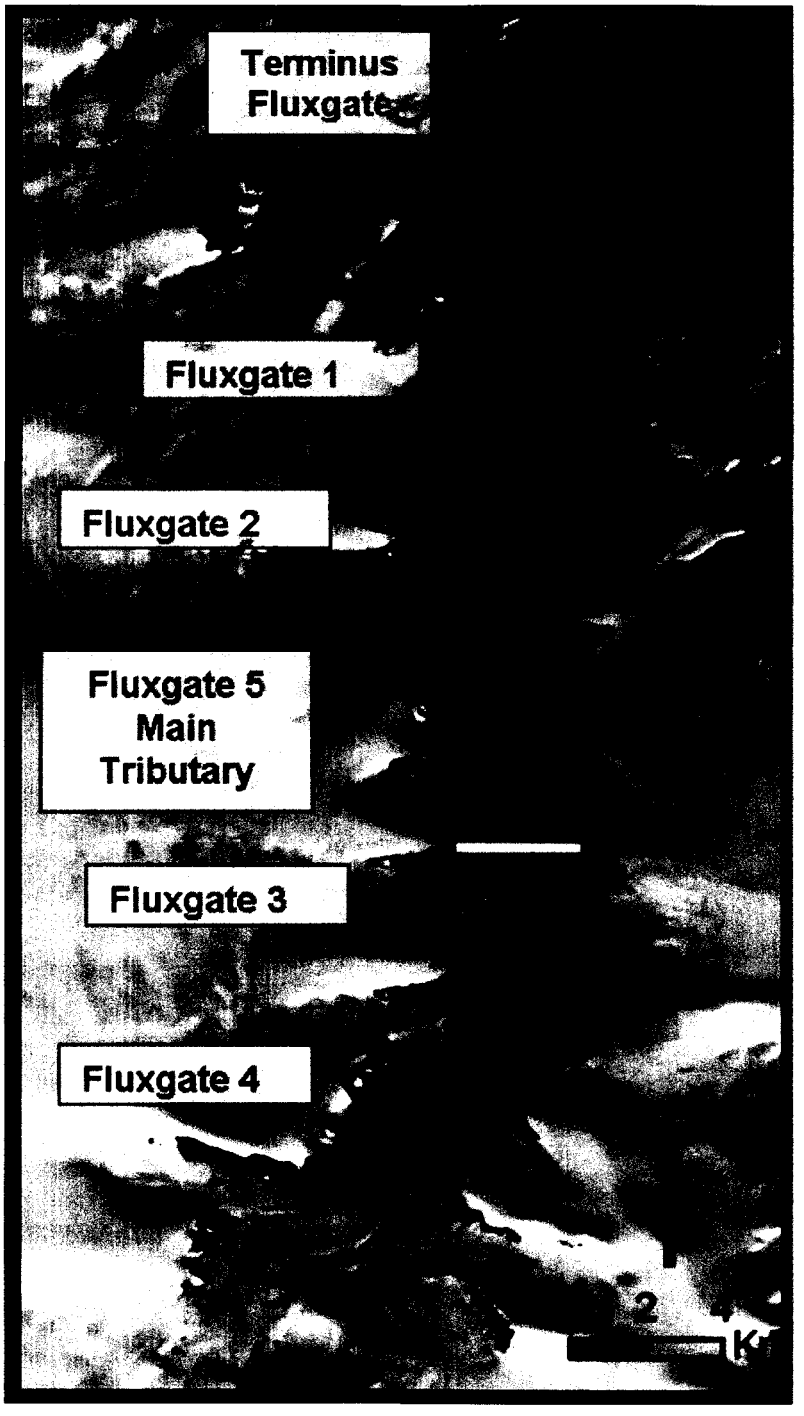

Figure 4.13: *Velocity transect locations along the main trunk of Belcher Glacier.*

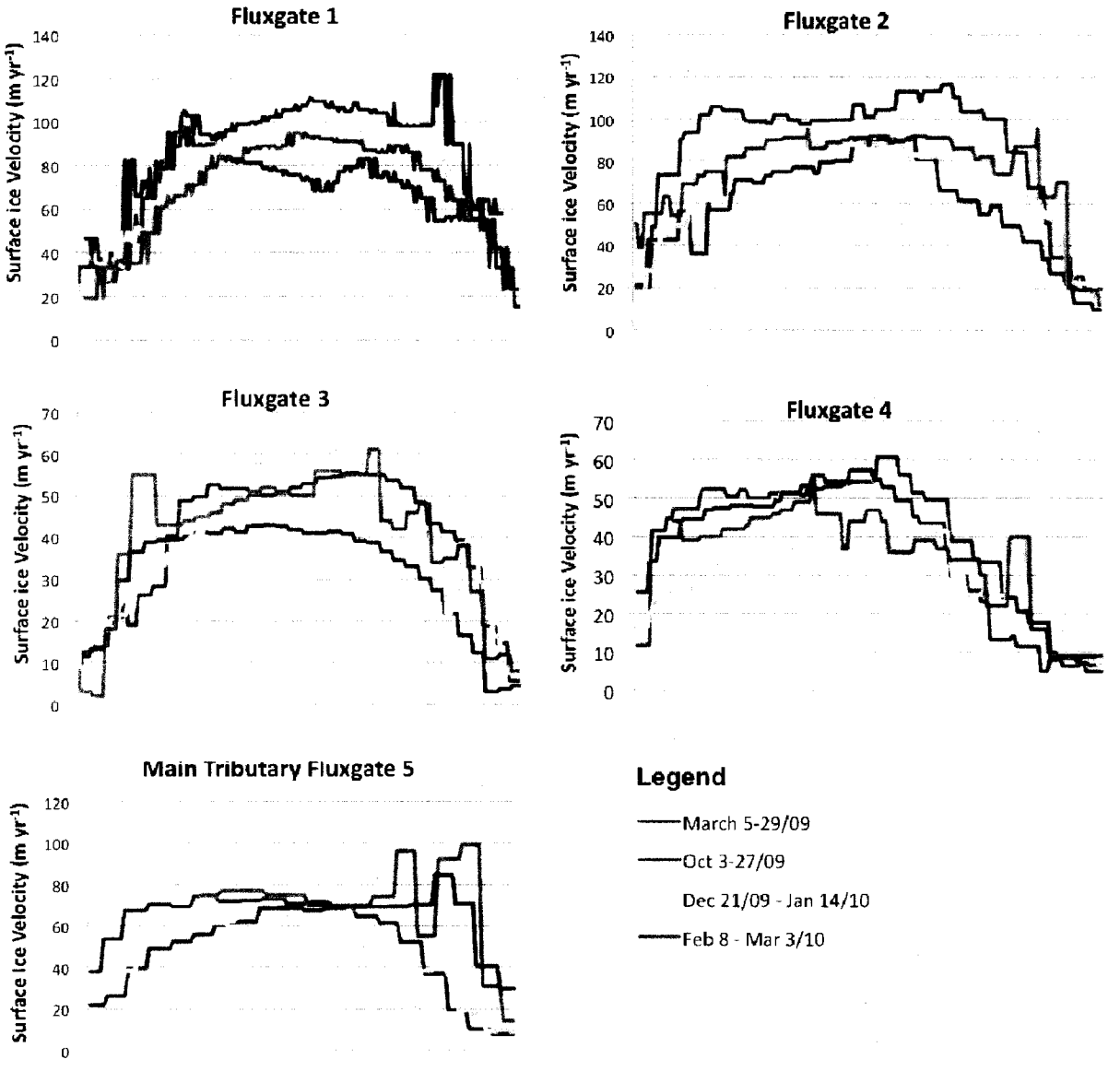

Figure 4.14: *Surface ice velocities determined for the flux gates along the main trunk of Belcher Glacier: a) Fluxgate 1 b) Fluxgate 2 c) Fluxgate 3 d) Fluxgate 4 e) Main Tributary Fluxgate 5. (Note the difference in vertical scale between graphs, velocities are plotted from east to west, on flux gates 1 – 4, and from north to south, for main tributary fluxgate 5).*

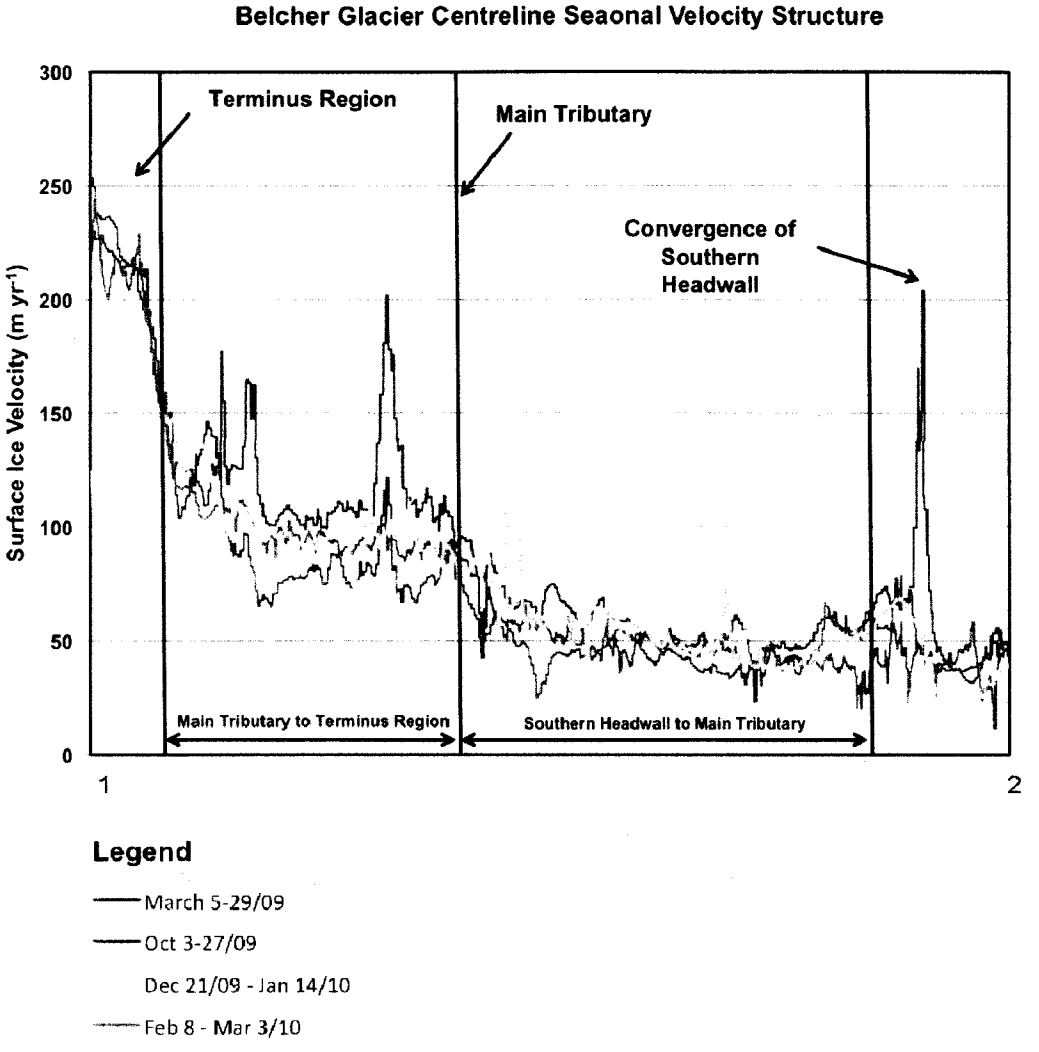

Figure 4.15: *Extracted seasonal centreline velocities along the Belcher Glacier from point 1 to point 2 as denoted on Figure 4.4b (total centerline distance of ~35 km).*

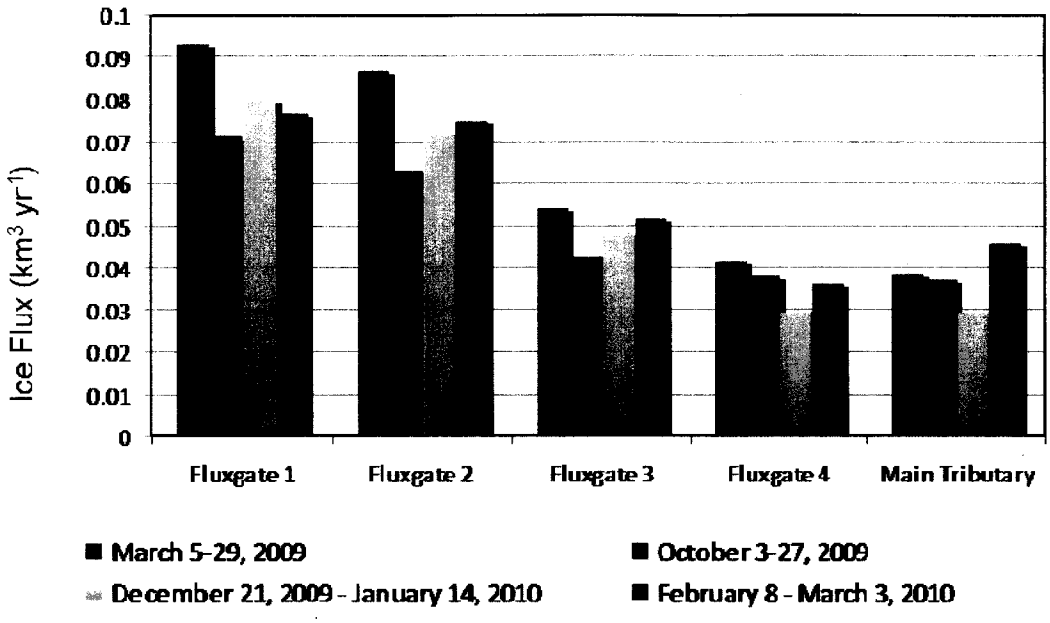

Figure 4.16: *Seasonal ice flux through main trunk flux gates (x-axis labels refers to main flux gate locations as denoted in Figure 4.15).*

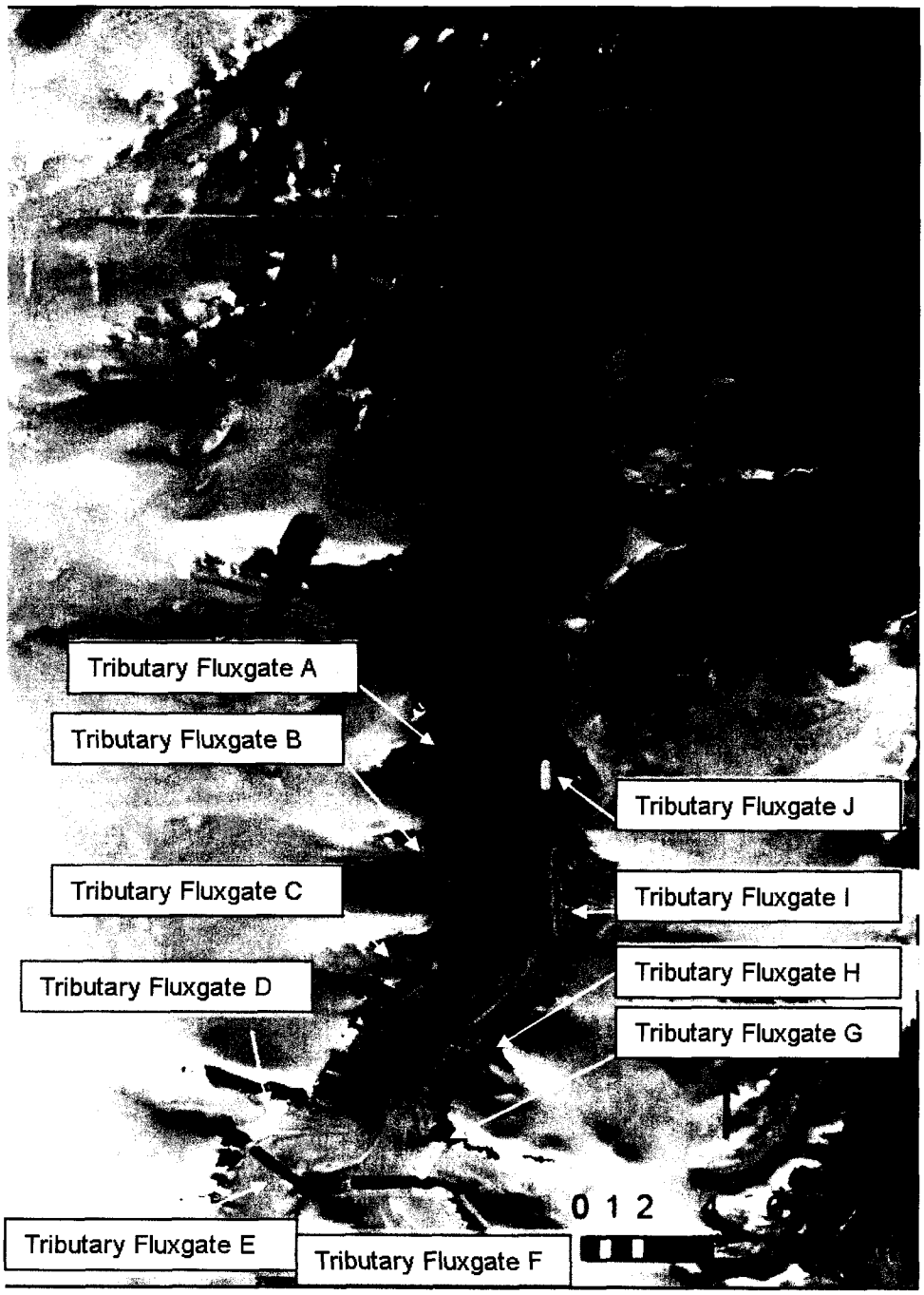

Figure 4.17: *Location of tributary velocity transects.*

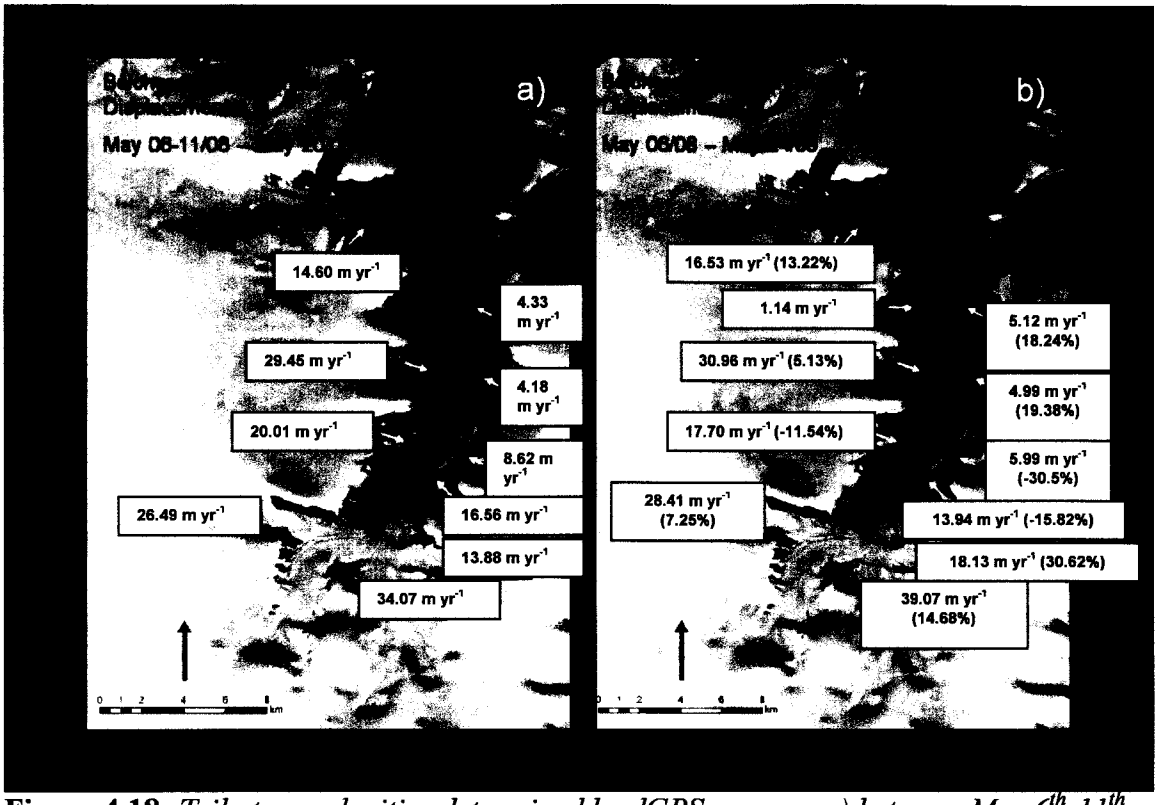

Figure 4.18: *Tributary velocities determined by dGPS surveys: a) between May 6th-11th and May 20th 2008; b) between May 20th 2008 and May 2009 also indicated as % of velocity change.*

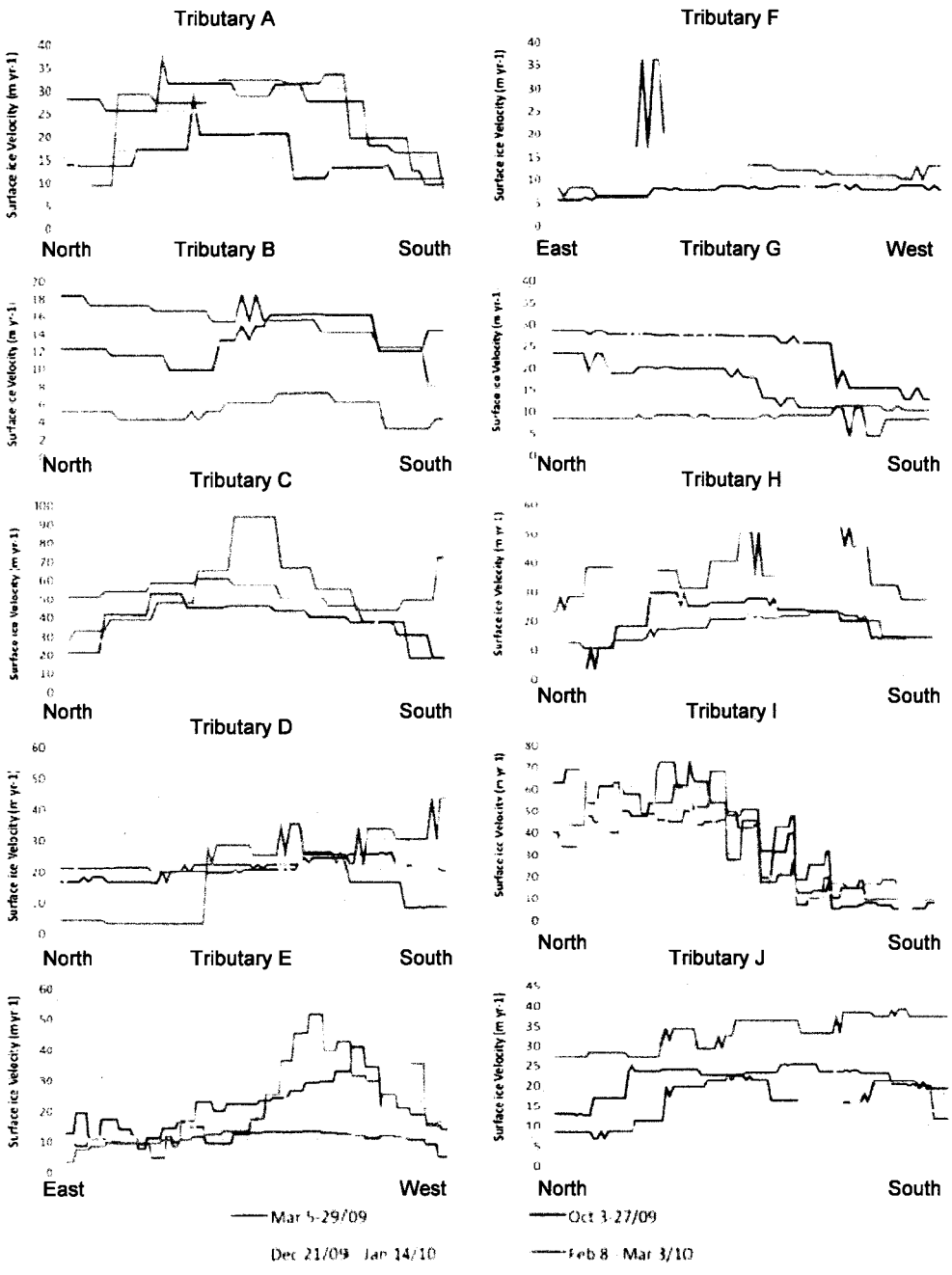

Figure 4.19: *Seasonal surface ice velocities (m yr^{-1}) along tributary cross-sections shown in Figure 4.17 (for north-south oriented tributaries, velocities are graphed from north to south, for east-west oriented tributaries, velocities are graphed from east to west, note differences of vertical scales between graphs)*

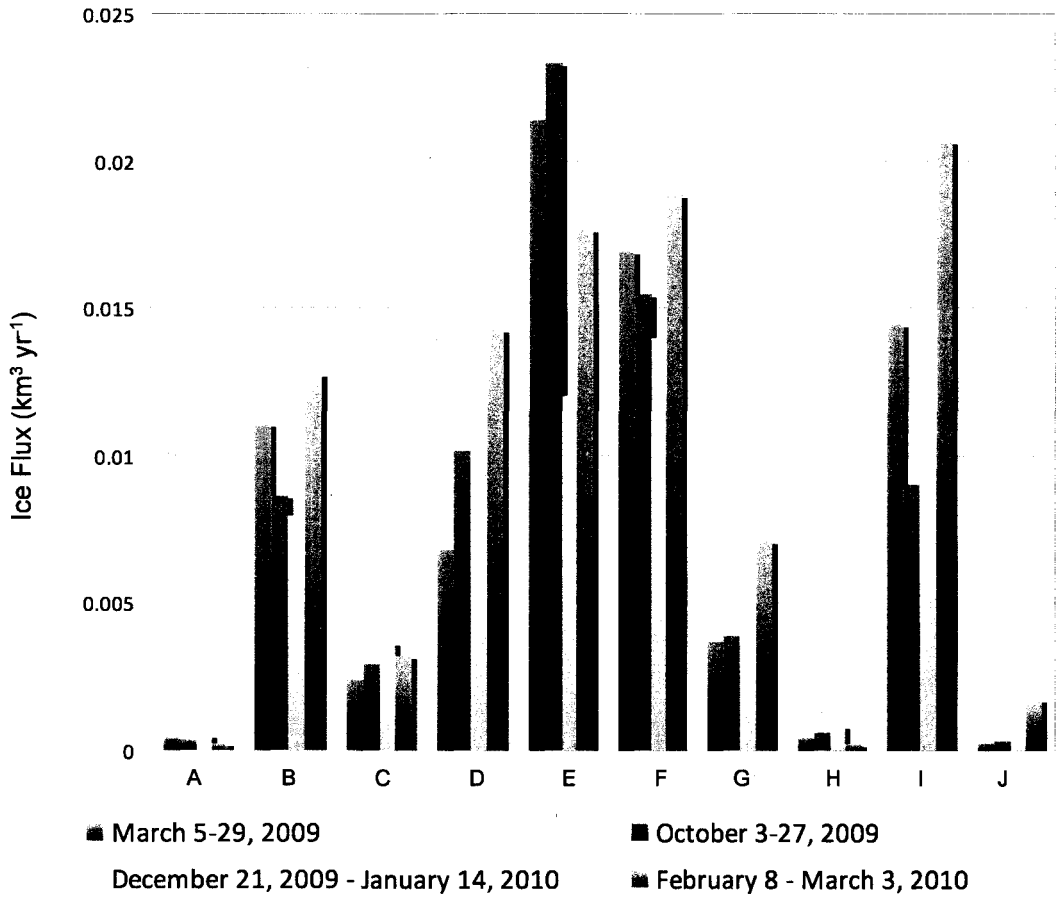

Figure 4.20: *Seasonal ice flux through tributary flux gates (x-axis labels refers to tributary flux gate locations as denoted in Figure 4.13).*

Chapter 5: Ice Dynamics of Devon Ice Cap

As discussed in Chapter 4, we have strong confidence that the speckle tracking method provides accurate velocity determinations when compared against multiple independent checks (stationary rock outcrops, dGPS, surface flow features and TerraSAR-X results). These checks define an accuracy of ~10 m yr^{-1} or better for the method (~10% of surface flow speed for typical glaciers), and as such the technique is now applied to the entire Devon Ice Cap. This chapter begins with a general description of the flow pattern across Devon Ice Cap. For ease of discussion, the ice cap is split into 4 quadrants, and patterns and causes of flow in each quadrant are reviewed. Finally, the chapter concludes with a comparison of previous ice dynamics research carried out on Devon Ice Cap, with a specific focus on the work of Burgess et al (2005) and Burgess (2006).

5.1 Flow Pattern of Devon Ice Cap

Nine Radarsat-2 fine beam mode image pairs of almost the entire Devon Ice Cap (DIC) were acquired in March 2009 (Figure 5.1). March 2009 was selected to determine ice motion over the entire ice cap as the imagery had good coherence (no melt, stable weather between acquisitions) for all scenes. All imagery was processed using Matlab speckle tracking algorithms (as described in Chapter 3) and results were mapped using ArcGIS 9.2. This enabled velocity maps of the entire ice cap and outlet glaciers to be generated. For the purposes of describing the velocity patterns, the ice cap is separated into four quadrants (Northwest, Southwest, Northeast and Southeast; Figure 5.1) that best approximate the flow patterns described by Burgess et al (2005). The Northwest quadrant includes the western, land terminating lobe and the Sverdrup Glacier, while the Southwest quadrant includes the North and South Croker Bay Glaciers that terminate in Lancaster Sound. The Northeast quadrant includes Eastern, Belcher and Unnamed Glaciers, while the Southeast quadrant includes the Southeast1 and Southeast2 Glaciers. The surface velocity patterns of these different regions measured with speckle tracking is described in detail below.

In this chapter, note that velocity figures presented for outlet glaciers of Devon Ice Cap only include arrows showing the direction of motion in fast flowing regions. These

regions have displacements well above the error margins discussed in Chapter 4 (10 m yr^{-1}), and indicate the regions where we have strongest confidence in the results. Areas away from these locations are typically limited to slow-moving, interior regions of the ice cap where motion by ice deformation dominates. The base image for each figure is a Landsat 7 image mosaic created from imagery acquired in July 2000. Speckle tracking results over non-glaciated regions are masked out of all figures. The flow pattern of the entire Devon Ice Cap is presented in Figure 5.2.

5.1.1 Devon Ice Cap Flow Regime Review

Previous studies have identified a set of four main flow regimes for Devon Ice Cap (Figure 2.4) (Burgess et al 2005, Dowdeswell et al 2004, Boon et al 2010). As these are important for understanding the dynamics of the ice cap, a brief review of them is presented here:

Flow Regime 1: Accounts for a large potion of the ice cap (~50%), ice is assumed to be frozen to its bed, and motion is limited to deformation alone.

Flow Regime 2: Accounts for 22% of the eastern portion of the ice cap and 8% of the western portion, basal sliding plays a contributing role in overall ice motion.

Flow Regime 3: Comprises the lower portions of outlet glaciers, basal sliding is an increasingly larger role in overall ice motion.

Flow Regime 4: Located at the termini of outlet glaciers, where basal motion is likely due to the deformation of basal sediments.

5.2.1 Flow Characteristics of the Northwest Quadrant:

Ice flow in the Northwest quadrant is dominated by slow 'sheet' ice motion (<~10 m yr^{-1}). The bed of the western part of DIC is dominated by flat, plateau like topography (Figures 2.1 and 5.3) that likely provides the main control on the type of movement found in the region. Ice motion is governed by the underlying bedrock characteristics (flat, plateau like) and the lack of subglacial water penetration (due to few crevasses or moulins), and as a consequence surface ice motion over the entire western lobe is limited to a maximum of 25 m yr^{-1} (Burgess et al 2005). The speckle tracking results show no discernable flow direction, which is common in areas of slow undefined motion.

Within the Northwest quadrant faster ice motion is found on the Sverdrup Glacier and its two main tributaries, which connect to the western lobe and drain into Jones Sound (Figure 5.4). Maximum ice velocities on the Sverdrup Glacier reach ~40 m yr^{-1} (Figure 5.4a), with the eastern and main tributaries accounting for most of the ice moved through the system (Figure 5.4b & 5.4d). Maximum velocities on the eastern and main tributaries reach ~40-55 m yr^{-1}, and ice flow extends about 9 km into the ice cap interior for the eastern tributary and about 6 km for the main tributary. Part of the eastern tributary also contributes mass to eastern glacier (Figure 5.4d). Ice velocities of the western tributary reach a maximum of ~30 m yr^{-1}, however the tributary terminates before it reaches the lower ablation area of the main Sverdrup Glacier (Figure 5.4c). Inland flow for the western tributary is also low, illustrating that this tributary draws little mass from the ice cap. In comparison with all of the other the outlet glaciers of DIC, the Sverdrup Glacier attains considerably lower overall ice velocities and experiences low velocities at its terminus of ~25 m yr^{-1} (Figure 5.4b).

5.2.2 Flow Characteristics of the Southwest Quadrant:

Ice motion in the Southwest quadrant is dominated by the North and South Croker Bay Glaciers (Figure 5.5). Maximum ice velocity on the North Croker Bay Glacier reaches ~150 m yr^{-1} (Figure 5.5a), while velocities of up to ~225 m yr^{-1} are found on the South Croker Bay Glacier (Figure 5.5b). Ice flow linking DIC to the North Croker Bay Glacier occurs through two tributaries, here termed North Croker Bay Main Tributary (NCB-MT) and the North Croker Bay West Tributary (NCB-WT), with flow predominantly via the NCB-MT. Increased ice flow extends 13 km into Devon Ice Cap along the NCB-MT, which is oriented in a nearly north-northeast direction and channeled through two rock outcrops. The NCB-WT connects to DIC in a near north-south orientation and curves around a rock outcrop connecting perpendicular to the flow of the main trunk of the North Croker Bay Glacier. This change in flow direction may partially account for the slower motion of the NCB-WT in comparison to the NCB-MT, although the underlying topography and upstream contributing area are also likely important. Almost the entire length of NCB-MT is classified within the flow regime 2 as described by Burgess et al (2005), where basal sliding is identified as a component of motion (Figure 2.4).

Conversely, flow regime 2 comprises a much smaller region for the NCB-WT, meaning that much more of the motion over the upper reaches of this tributary is linked to ice creep. Similarly, the ice is thicker and deeper where the NCB-MT connects to the ice cap than where the NCB-WT connects to the ice cap (Figure 2.1, Figure 5.3). As such, the faster motion achieved on the NCB-MT is likely linked to the difference in flow regime and because it has a larger area of the ice cap from which it can draw mass (Dowdeswell et al 2004, Boon et al 2010).

Flow from the NCB-WT extents ~9 km inland. The main trunk of the North Croker Bay Glacier exhibits faster flow near its terminus and extends upglacier ~15 km to the convergence of the two tributaries. For the South Croker Bay Glacier the fastest motion occurs ~4 km upglacier of the terminus and extends nearly 5 km upglacier. From this area of fastest flow, velocities gradually decrease into the interior of DIC over a distance of ~10 km.

In the upper reaches of the Southwest quadrant in areas away from the North and South Croker Bay Glaciers, ice flow is dominated by slow sheet flow, similar to that of the Western Lobe. Surface ice velocities in this area are <15 m yr^{-1} and are likely controlled by the flat underlying bedrock topography of this region, with the bed likely to be frozen to the ground, limiting ice motion to internal ice creep (Burgess et al 2005, Boon et al 2010) (Figure 5.3, Figure 2.4).

5.2.3 Flow Characteristics of the Southeast Quadrant:

Ice drainage from the Southeast quadrant of DIC is dominated by two unnamed glaciers, here called Southeast1 and Southeast2 (Figure 5.6). Both are unique when compared to the flow regimes of the other outlet glaciers flowing from the ice cap, in that both terminate into a near stagnant region ~8 km from the ice front of Hyde Inlet. All other glaciers of DIC experience their fastest surface velocities near their terminus, while Southeast1 and Southeast2 experience their fastest surface velocities near the middle of their main trunks. A potential explanation for this type of flow regime is that ice is being forced from the main ice cap via a narrow bedrock channel that ends in an open plateau-

like manner ~8 km before the ice front. This would allow the ice to stagnate in a similar fashion to the Western Lobe of the DIC. The main trunks of Southeast1 and Southeast2 Glaciers are classified by Burgess et al. (2005) as being within flow regime 2, with some parts of Southeast2 Glacier falling into flow regimes 3 and 4. The stagnant areas which they terminate in are classified within flow regime 1 (Figure 2.4). The bed of the stagnant region which these glaciers terminate into is also relatively flat and plateau like, compared to the main glacier trunks with are constrained within deeper troughs (Figure 5.3). Additionally, theses glaciers draw mass from a relatively large portion of the ice cap, but are channeled through relatively narrow valleys, allowing higher ice velocities to be achieved in the channels.

Unnamed3 is a tidewater outlet glacier located along the northern border of the Southeast quadrant, terminating near the terminus of Southeast2 Glacier (Figure 5.6). The glacier is roughly 18 km long with motion up to 150 m yr^{-1} along the lowermost 9 km of its main trunk. As the glacier turns and connects to the main ice cap, velocities decrease to between 50 and 99 m yr^{-1}. Accelerated flow of this glacier extends ~25 km into DIC, drawing from a large accumulation area and portions of the glacier which extend into the ice cap are classified within flow regime 4.

Previous studies have identified the presence of likely surge type glaciers within the Southeast quadrant of the DIC, specifically the Cunningham West Glacier and the Southeast1 glacier (Figure 5.7) (Copland et al 2003, Burgess et al 2005). Copland et al (2003) used a systematic review of 1959/60 aerial photography and 1999/2000 Landsat 7 imagery to identify surge type glaciers in the Queen Elizabeth Islands. Surging glaciers were identified by the presence of features such as looped medial moraines, heavy surface crevassing, rapid terminus advance and high surface velocities. For the Cunningham West Glacier there was extensive folding of surface moraines between 1959 and 1999 and a retreat of the eastern side of the glacier by ~2 km over the same time period. Surface ice velocities for the Cunningham West Glacier determined by speckle tracking indicate that it is likely not surging at present as current velocities are between ~50-100 m yr^{-1}. These velocities are similar to other nearby glaciers, and higher

velocities are experienced at the terminus only, rather than across the entire glacier as would be expected by surging. Cunningham West Glacier is also found within flow regime 3, where ice motion is linked in large part to basal sliding. As such, higher surface ice velocities are expected.

5.2.4 Flow Characteristics of the Northeast Quadrant:

The Northeast quadrant is dominated by steeper and more dissected bedrock topography (Figure 5.3), with discharge from this region of the ice cap occurring via six major tidewater outlet glaciers (Eastern Glacier, Belcher Glacier, Unnamed1 Glacier, Unnamed4 Glacier, Unnamed2 and Unnamed5 Glacier). Velocities of five of the six outlet glaciers exceed 125 m yr^{-1}, while the other one does not exceed 40 m yr^{-1}. For the Eastern Glacier (Figure 5.8), ice velocities are highest near the terminus (~150 m yr^{-1}) with velocities decreasing to ~50 m yr^{-1} nearly 5.5 km upglacier of the terminus. Near mid-glacier velocities increase to ~60 m yr^{-1} over a span of about 7 km and then decrease to between 25 and 49 m yr^{-1} as the glacier extends into the ice cap. Flow of the Eastern Glacier extends ~8.5 km into the interior of Devon Ice Cap, with a common source shared by the upper Eastern Glacier and the Sverdrup Glacier Eastern tributary (Figure 5.4a). Much of the bed of the Eastern Glacier is grounded below sea level, and thicker ice (~600-700 m) extends for nearly the entire length of the glacier (Boon et al 2010). Additionally, nearly the entire length of the glacier is classified within flow regime 2, which means it is an area of where basal sliding is likely to contribute greatly to observed ice motion. This is the likely the cause for the velocity pattern of Eastern Glacier.

Belcher Glacier (Figure 5.9a) is the largest outlet glacier of the Northwest quadrant and of the entire DIC. The glacier extends ~35 km from its terminus to its southern headwall and connects to the surrounding ice cap via a network of tributaries. The Belcher exhibits higher surface velocities near the terminus (~275 m yr^{-1}) and decreases upglacier (minimum ice velocities are ~40 m yr^{-1}). Previous studies have found that this glacier accounts for 15% of ice loss from the DIC (Burgess et al 2005). The large number of tributaries connecting Belcher Glacier to the interior of DIC allow for large amounts of mass to be drawn from this region. Two main tributaries running east-west, one joining

the flow at the terminus (Northern tributary) and the second converging at about mid-glacier (Main Tributary) have velocities which range between ~50 m yr^{-1} and ~100 m yr^{-1} and extend into the northwest quadrant ~15 km and ~10 km, respectively. Furthermore, these two tributaries allow for large amounts of mass to be drawn from the western portion of the quadrant. From mid-glacier to the southern headwall, Belcher Glacier is connected via nine smaller tributaries, with four of these drawing mass from the western portion of the ice cap, two drawing mass from the south, and the four smallest drawing mass from the east.

The southern headwall of the Belcher Glacier is connected to the main ice cap via a channel of thicker ice (Figure 2.1). Bed elevations are also lower from ice cap summit to the southern portion of Belcher Glacier, allowing the Belcher Glacier to extend into the ice cap and draw large amounts of mass from the interior. Along the entire length of the lower portion of the Belcher Glacier, bed elevations range between 200-400 m below sea level (Figure 5.3), creating a narrow channel of faster moving ice. Similarly, the stretch of Belcher Glacier from the main tributary to the terminus is classified within flow regimes 2 and 3, where basal sliding plays a large role in determining ice velocities. Unnamed5, a small tidewater outlet glacier located ~10 km to the east of Belcher Glacier also draws mass from the northeast quadrant (Figure 5.9b). The amount of mass drawn by this glacier is limited by its smaller size and by the relatively small region of the Northeast Quadrant which it is connected to.

Unnamed1 Glacier is another large tidewater outlet glacier of the northeast quadrant, which also draws large amounts of mass from DIC (Figure 5.10). This glacier is split into northern and southern arms, with the northern arm having considerably slower ice velocities than the southern arm. The north arm portion of the glacier extends ~15 km inland, with slow velocities along this section likely due to its relatively small accumulation region (most mass is drawn from this area by tributaries of the Belcher Glacier). In contrast, the southern arm experiences velocities near the terminus that exceed 175 m yr^{-1} and decrease gradually upglacier. Two main tributaries extend southward off the main trunk of Unnamed Glacier, extending flow ~12 km into the

southern portion of the quadrant. The bed of the southern arm of Unnamed1 Glacier has an elevation ~200 m below sea level (Figure 5.3), is constrained within steep topography (Figure 2.1) and is within flow regimes 2 and 3. Similarly, the bed of the northern arm of Unnamed1 Glacier is ~200 m below sea level, however the ice thicknesses are less than those found on the southern arm, and the tributary is largely classified within flow regime 1. Additionally, the southern arm extends further into the ice cap interior, allowing it to capture more mass. These reasons explain the velocity differences observed between the different tributaries of Unnamed1 Glacier.

Unnamed4 is a tidewater glacier located in the northeastern portion of the Northeast Quadrant, ~2.5 km wide and extends ~20 km into the ice cap interior (Figure 5.11a & 5.11c). The glacier follows the same general flow pattern as the other outlet glaciers of the ice cap, with maximum velocities at the terminus (~175 m yr^{-1}) and minimum velocities upglacier (~30 m yr^{-1}). The amount of mass drawn by Unnamed4 is limited as it is sheltered from the larger portions of the DIC by the faster southern tributaries of Unnamed1 Glacier. The glacier is within flow regime 2, with a bed elevation of ~200m below sea level along its length and ice thicknesses of ~400 m (Figures 2.1, 5.4, 2.4). Ice motion is likely largely controlled by these factors.

The last major tidewater outlet glacier of the region is oriented in a roughly east-west direction, is tidewater terminating, and is termed Unnamed2 (Figure 5.11a & 5.11c). The main trunk of the Unnamed2 glacier extends ~14 km from its terminus inland, where it splits into two tributaries (termed Unnamed2 Northern tributary and Unnamed2 Southern tributary) around a bedrock outcrop. Unnamed2 Northern tributary extends northwest (toward Unnamed1 Glacier) for an additional 14 km, while Unnamed2 Southern tributary extends ~15 km west-north-west into the ice cap interior. Unnamed2 is unique within the northeast quadrant as it is has significantly slower surface velocities along its main trunk and two tributaries (~50 m yr^{-1}) compared to the other outlet glaciers, and there is no marked increase in velocity at the terminus. The terminus region of Unnamed2 Glacier is located within flow regime 4 and the main trunk and Southern tributary of the glacier is classified within flow regime 2. Unnamed2 northern tributary is classified within flow

regimes 1 and 2 (Figure 2.4). The length of the main trunk of Unnamed2 is grounded below sea level and has ice thicknesses of up to 400 m (Figure 2.1 and Figure 5.3). Unnamed2 glacier has very similar basal conditions to other outlet glaciers of the region (Unnamed1, Unnamed3, Unnamed4), but surface ice dynamics do not attain the same high velocities as these glaciers. Reasons for the lower velocities for this glacier could be that its accumulation area is limited by the extension of the other outlet glaciers of the region. Both the Unnamed1 Glacier and Unnamed3 Glacier extend further into the Devon Ice Cap interior and into the same regions as Unnamed2.

5.3 Variation of Ice Cap Flow: East versus West

Results show that ice motion is more variable in the east as compared to the west on DIC, with many more fast-flowing outlet glaciers in the Northeast and Southeast quadrants. In the western half of the ice cap the only glaciers that achieve high surface velocities are the North and South Croker Bay Glaciers, both of which terminate in tidewater. The majority of the western half of DIC is dominated by slower velocities consistent with ice creep (<25 m yr^{-1}). Within this region the subglacial topography is distinguished by a flat, plateau-like form that exists entirely above sea level and therefore causes the ice to terminate on land (Burgess et al 2005).

In the east, speckle tracking results reveal that ice motion is dominated by outlet glaciers draining the ice cap to tidewater margins. Reasons for higher surface velocities in the western regions of the ice cap again relate to basal topography, with the east composed of deep bedrock troughs (Figure 2.1) which allow for basal melt to occur deep beneath the ice causing accelerated ice motion (Dowdeswell et al 1994). Because ice is better insulated under thick ice, it takes less energy to melt ice and generate basal water under thicker ice than thinner ice. There are also many more outlet glaciers located in the east as compared to the west, and many of these outlet glaciers grounded below sea level over their lower reaches (Figure 5.3). In the western portion of the ice cap, only the Sverdrup Glacier, North Croker Bay Glacier and South Croker Bay Glaciers are grounded below sea level, whereas in the eastern portion of the ice cap the Eastern, Belcher, Unnamed 1, Unnamed 2, Unnamed3, Unnamed4, Unnamed5, Southeast1 and Southeast2 Glaciers

(and the entire region of stagnant ice which these two glaciers terminate into) are grounded below sea level.

The difference in bed conditions in the east allows for the development of faster flowing ice regimes within slow flowing ice. Additionally, most of the glaciers on the eastern portion of the ice cap are tidewater terminating, allowing for higher velocities to be achieved in these regions for the reasons described below in Section 5.3.1. Across the entire ice cap, it is likely that basal water pressure plays a large role in governing ice motion. On Devon Ice Cap, surface ablation is negatively correlated with elevation and with distance away from Baffin Bay. In addition, drainage basins on the eastern portion of the ice cap lose more mass to surface ablation than drainage basins in the west because they have larger proportions of their surface area at lower elevations (Burgess and Sharp 2004, Burgess et al 2005, Boon et al 2010). As a consequence, in areas of the ice cap where surface meltwater can be generated (predominantly the east) and be transferred to the bed (through moulins and crevasses), higher surface velocities are achieved.

Surface ice velocities match well with previously identified flow regimes for the Devon Ice Cap as described by Burgess et al (2005) and Boon et al (2010). Regions of higher ice motion as indicated by speckle tracking of Radarsat-2 imagery show higher velocities in flow regimes 2, 3 and 4 where basal sliding and bed deformation have been identified, and lower velocities in areas identified as flow regime 1 where the ice is likely frozen to its bed and motion occurs mainly due to internal ice creep.

5.3.1 Tidewater versus non-tidewater terminating Glaciers

Tidewater glaciers (which account of most of the outlet glaciers of DIC) are able to achieve higher velocities than land terminating glaciers on DIC. Two exceptions exist, the Sverdrup and Unnamed2 Glaciers (although both are grounded below sea level). In theory, tidewater glaciers are able to achieve higher speeds due to the floating nature of their termini, which provides little frictional resistance to flow in comparison to land terminating glaciers (Clarke 1987b, Kamb et al 1994, Benn and Evans 1998). This interaction also allows tidewater glaciers to reach very high speeds within a relatively

confined terminus region. Tidewater glaciers are also able to attain higher velocities on their main trunks because the rapid mass of ice being moved through their floating termini requires mass to be drawn from upglacier (Clarke 1987b). In this way, if velocities increase on tidewater glaciers, a process of rapid mass loss to the oceans and contributing to sea level rise is possible.

5.4 Changes in Velocity Structure of Devon Ice Cap

To assess changes to the velocity structure of the entire DIC over the last ~15 years, the surface ice velocities derived in this study are compared with the results of previous ice dynamic studies on this ice cap.

The following section makes an in-depth comparison between the results determined by this thesis and the work of Burgess et al (2005) and Burgess (2006) (which provides downslope velocity maps for the entire DIC). A detailed comparison was not made with the work of Shepherd et al (2007) as their data was only available as a low resolution grayscale image from their published paper. Nor was an in-depth comparison possible with the work of Dowdeswell et al (2004) as they only presented motion in the satellite look direction. Essentially, Burgess et al (2005) used the same ERS 1/2 data as the Shepherd et al (2007) and Dowdeswell et al (2004) studies (Table 2.1), and as such provides the best available base data to enable comparisons of velocity change over the previous ~15 years. Additionally, the original full resolution dataset (100 m) produced by Burgess (2006) (corrected to downslope velocities with the use of a DEM) was provided to the author for this study (Figure 5.16).

A map of velocity differences between Burgess (2006) and the results of this thesis are presented in Figure 5.13 and data used is summarized in Figure 5.14 and Table 2.1. Burgess et al (2005) used interferometry on ERS1/2 1 day repeat data from spring 1996 and 3 day repeat data from winter 1992 (for the Devon Ice Cap), and speckle tracking of 24 day repeat Radarsat-1 data from Autumn 2000 (limited to the Belcher Glacier terminus).

5.4.1 Basins with Velocity Decreases

Surface ice velocity decreases are evident on a number of outlet glaciers between the results presented here and those obtained by Burgess (2006). Specifically, there is evidence of slowing along the main trunks of the Croker Bay Glaciers (~20-50 m yr^{-1}) (Figure 5.15), a slowing of the southern land terminating glaciers in the Southeast quadrant (Figure 5.16), velocity decreases for Unnamed2 Glacier, and decreases for the northern arm of Unnamed1 Glacier (~20-40 m yr^{-1}) (Figure 5.17) and Eastern Glacier (~10-20 m yr^{-1}) (Figure 5.18).

The Belcher Glacier terminus (Figure 5.19) also represents an area of surface ice deceleration between the two studies, with velocities up to 100 m yr^{-1} slower in this study compared to the findings of Burgess (2006). However, we consider that this velocity decrease is likely due to differences in image acquisition time rather than a true velocity decrease. Burgess (2006) used Radarsat-1 imagery from October 14-November 7, 2000 and again from November 20-December 14, 2000, while the imagery used in this study was acquired March 5-29, 2009. Seasonal velocities for Belcher Glacier determined in Chapter 4 reveal a marked change in terminus velocity throughout the year. Velocities were found to be highest in autumn and at their lowest in late winter. In terms of velocity change, the Burgess (2006) imagery is from the time of the year when terminus velocities are expected to be high, while the imagery used in this study is from a period of expected lower velocities. Therefore, the velocity change is likely due to seasonal differences in velocity at the terminus, rather than significant long-term changes.

5.4.2 Basins with Velocity Increases

Four areas show significant velocity increases during the study period: the terminus of the North Croker Bay Glacier (Figure 5.15), the main trunk of the Belcher Glacier (Figure 5.19) between its terminus and main tributary, Unnamed4 Glacier (Figure 5.20), and Southeast2 Glacier (Figure 5.21). North Croker Bay Glacier has a complex velocity structure, with an apparent slowdown along its main trunk but a significant speed up at the terminus (~20-75 m yr^{-1}). Changes in ice velocity could be due to seasonal differences in ice motion, as the images used by Burgess (2006) are from April 25-26,

1992 while the imagery used in this study are from March 1-25, 2009. However, it is expected that ice velocities would decrease, rather than increase, as the Burgess (2006) data is from later in the spring season than the data from this study. Thus, seasonal differences in image acquisition can likely be discounted as a source of velocity change. Differences in velocity may also be due to look direction issues associated with interferometry since the terminus of North Croker Bay Glacier is oriented roughly perpendicular to the look direction of the ERS1/2 sensors used by Burgess et al (2005). Consequently, it would be very difficult to produce surface displacements for these regions using the interferometric method, suggesting that the large change in speed at this location may be due to differences in methods rather than true velocity change.

Similarly, the apparent velocity increases along the main trunk of Belcher Glacier are more likely linked to line-of-sight problems associated with interferometry than with real surface velocity changes. The portion of the Belcher Glacier which indicates velocity increases between the two studies is again oriented roughly perpendicular to the look direction of the ERS1/2 images used by Burgess (2006). Additionally, the difference in observed ice velocity may also be linked to seasonal differences in image acquisition. Burgess et al (2005) used imagery acquired in February 6-9, 1996 while the imagery used in this study was acquired from March 5-29, 2009. Chapter 4 of this thesis revealed that there may be a large amount of seasonal variation of ice motion over the Belcher Glacier in the winter, and as such, the velocity change identified on the Belcher Glacier between studies may be indicative of seasonal velocity change rather than long term trends.

Velocity increases of up to 100 m yr^{-1} are observed on portions of the southern tributary of Unnamed1 Glacier which connect with the ice cap interior (Figure 5.20). Some of these changes could be due to seasonal differences in motion (acquisitions were on Feb 6-9, 1996 versus March 5-29, 2009), although it is difficult to attribute all observed changes to these differences. This suggests that this portion of the tributary may be becoming a more important region of mass transfer for Unnamed1 Glacier.

Of all the observations of velocity changes presented here, the most dramatic and most certain indicate the acceleration of Southeast2 Glacier (Fig 5.21). Burgess et al (2005) noted that "fast" flow of Southeast1 and Southeast2 Glaciers extends further into the accumulation area of DIC than any other glaciers, as is also evident in this study. Burgess et al (2005) also noted that due to the convex upglacier form of Southeast1, the glacier might be extending further headward (westward) into a region of slow moving ice. A number of independent sources of evidence support this hypothesis. Specifically, Landsat 7 image feature tracking of the Southeast2 Glacier has revealed a consistent speed up of this glacier over the last five years (F. Wyatt, Personal Communication, 2010). Landsat 7 imagery also shows evidence for previous episodes of fast motion for the Southeast2 Glacier based on degraded flow stripes, former marginal shear zones and medial moraines. This indicates that it is a surge-type glacier, and that at some point in the past it ceased moving in either the piedmont area alone or over the entire system (Burgess et al 2005, Boon et al 2010). This suggests that the faster flow has restarted in the upper reaches of the glacier and is propagating downglacier (Boon et al 2010). Preliminary ICESat data (acquired in recent years) reveals a thickening of ice in the stagnant regions that Southeast2 drains into, suggesting that faster flow has recently been initiated (Boon et al 2010, M. Sharp, Personal Communication, 2010). Indeed, the results presented here indicate that the glacier has sped up along much of its main trunk by up to 100 m yr^{-1}, providing further evidence that a surge-type cycle has recently begun.

5.5 Overview of Devon Ice Cap Dynamics

Results show that for the Devon Ice Cap there is a marked difference between ice flow in the west than the east. In the west, motion is slower and ice is drained by 3 outlet glaciers, while in the east ice flow is faster and ice is drained by many more (12) outlet glaciers. Differences in the east/west flow regime are partially linked to regional differences in subglacial topography. In the west, the DIC is underlain by a flatter, plateau like topography while in the east the underlying topography is deeper and steeper. Additionally, a much larger proportion of the eastern outlet glaciers are grounded well below sea level (up to 400 m), with fast flow from these glaciers extending into a larger portion of the ice cap. Faster flow in the east versus west is also explained by differences

in melt which occur between these two areas. The average elevation in the west is greater than in the east, allowing for more melt to be generated in the east than west, and thus more water is available for increased basal lubrication and enhanced motion in the east. Flow patterns also show good agreement with flow regimes as discussed by previous studies (Burgess et al 2005, Boon et al 2010). These results indicate that the flow of the ice cap is largely controlled by water generated at the bed.

The speckle tracking results produced by this thesis show a good general agreement with previous studies of the flow pattern of Devon Ice Cap, although this study refines what has been done before and provides ice motion maps over the entire ice cap which are not limited by look direction issues. However, results reveal that ice velocities at the terminus of some glaciers (Belcher Glacier, Unnamed1 Glacier) are higher than previously reported by Shepherd et al (2007), where they report maximum ice velocities of 150 m yr^{-1} when ice velocities at the terminus of outlet glaciers can be up to ~200 - ~250 m yr^{-1}. In terms of detailed velocity changes, results show a slowing of the North and South Croker Bay Glaciers, Unnamed2 Glacier, the north arm of Unnamed1 Glacier and Eastern Glacier, and velocity increases on the main trunk of Belcher Glacier, the southern arm of Unnamed1 Glacier, Southeast2 Glacier, Unnamed4 Glacier and the terminus of North Croker Bay Glacier. However, the Southeast2 Glacier is the only glacier where there is high confidence that acceleration has occurred. This may be in the start of a surge cycle, and velocity increases along this glacier are in good agreement with other independent studies of speed up for the region mentioned earlier.

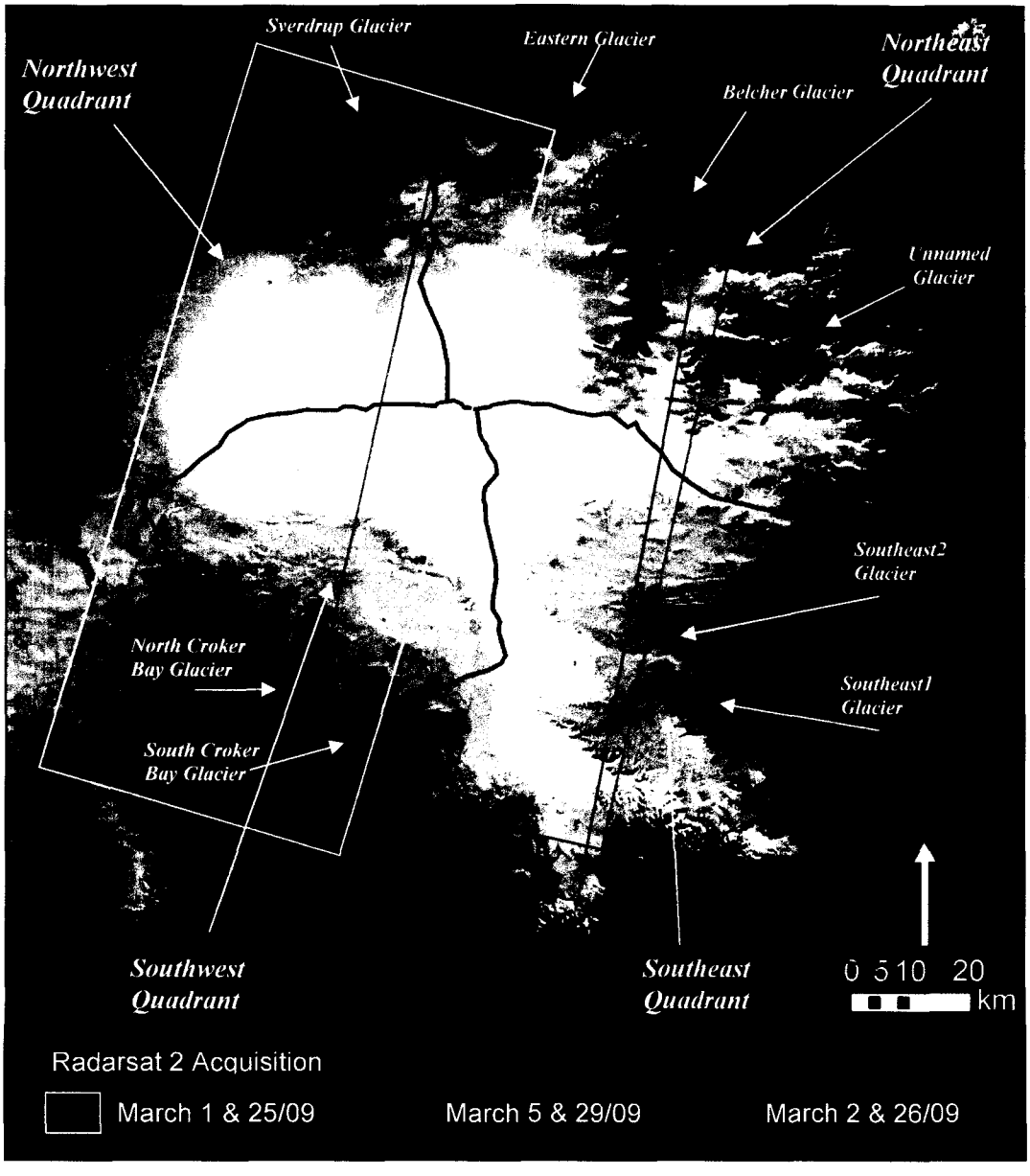

Figure 5.1: *Footprints of Radarsat-2 Fine beam mode imagery acquired for the entire Devon Ice Cap in March 2009. Note that each elongated footprint represents three individual, adjacent scenes (Base image 2000 Landsat 7 Mosaic)*

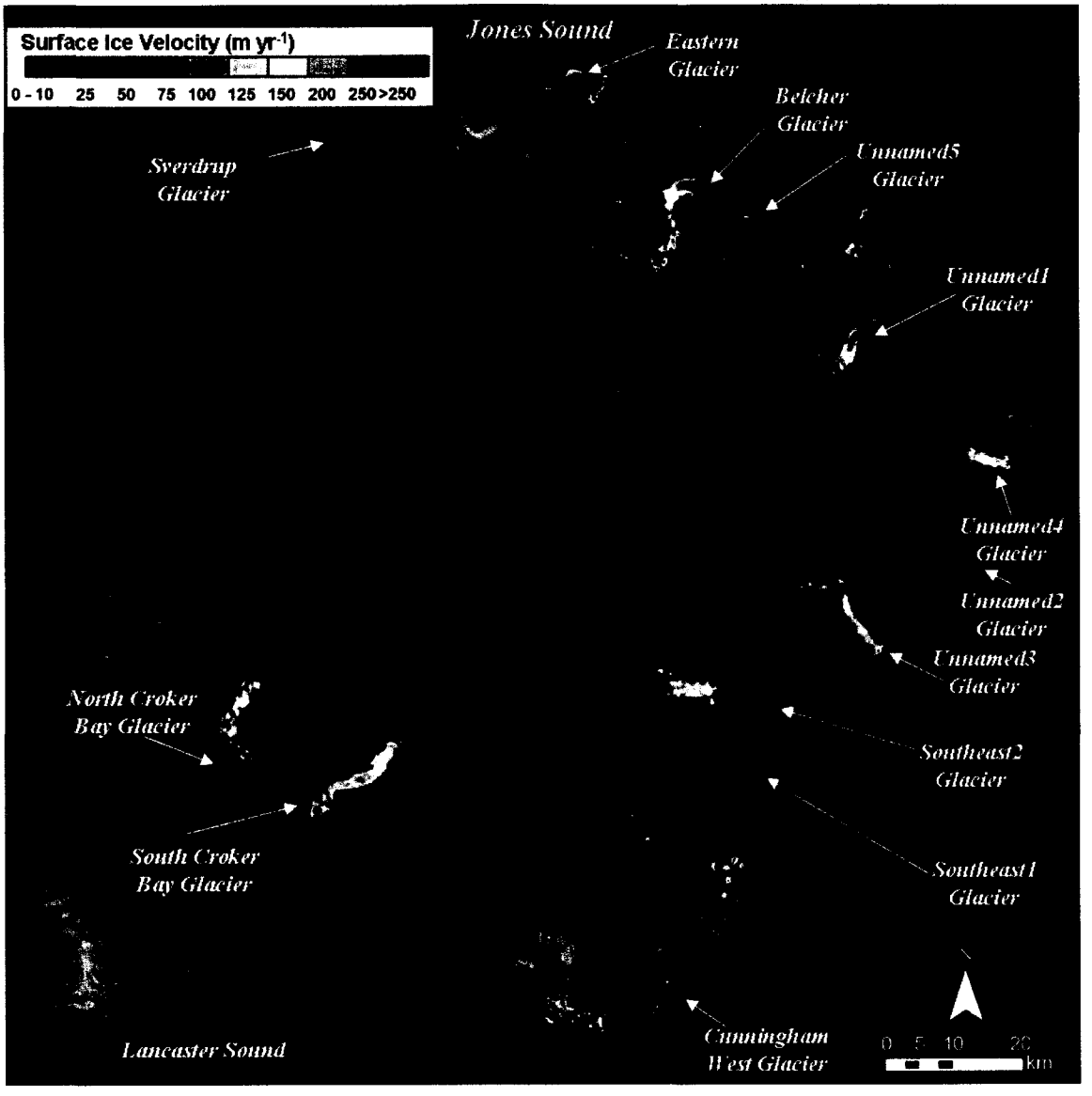

Figure 5.2: *Surface ice velocities across the entire Devon Ice Cap determined by speckle tracking of Radarsat-2 fine beam mode imagery acquired in March 2009.*

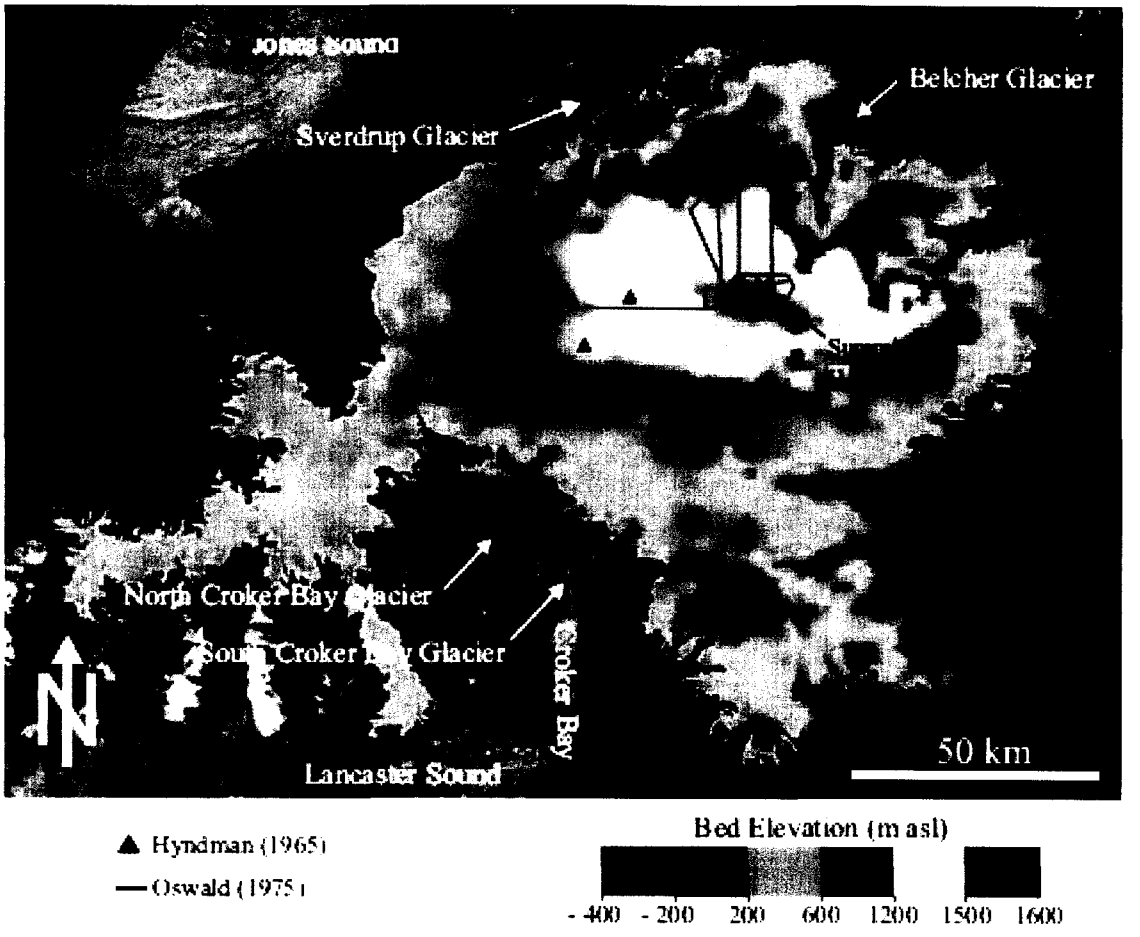

Figure 5.3: *Bed elevation map across the Devon Ice Cap as determined from airborne radar surveys by Dowdeswell et al (2004) and bed condition measurements (Oswald 1975, Hyndman 1965) (From Boon et al 2010)*

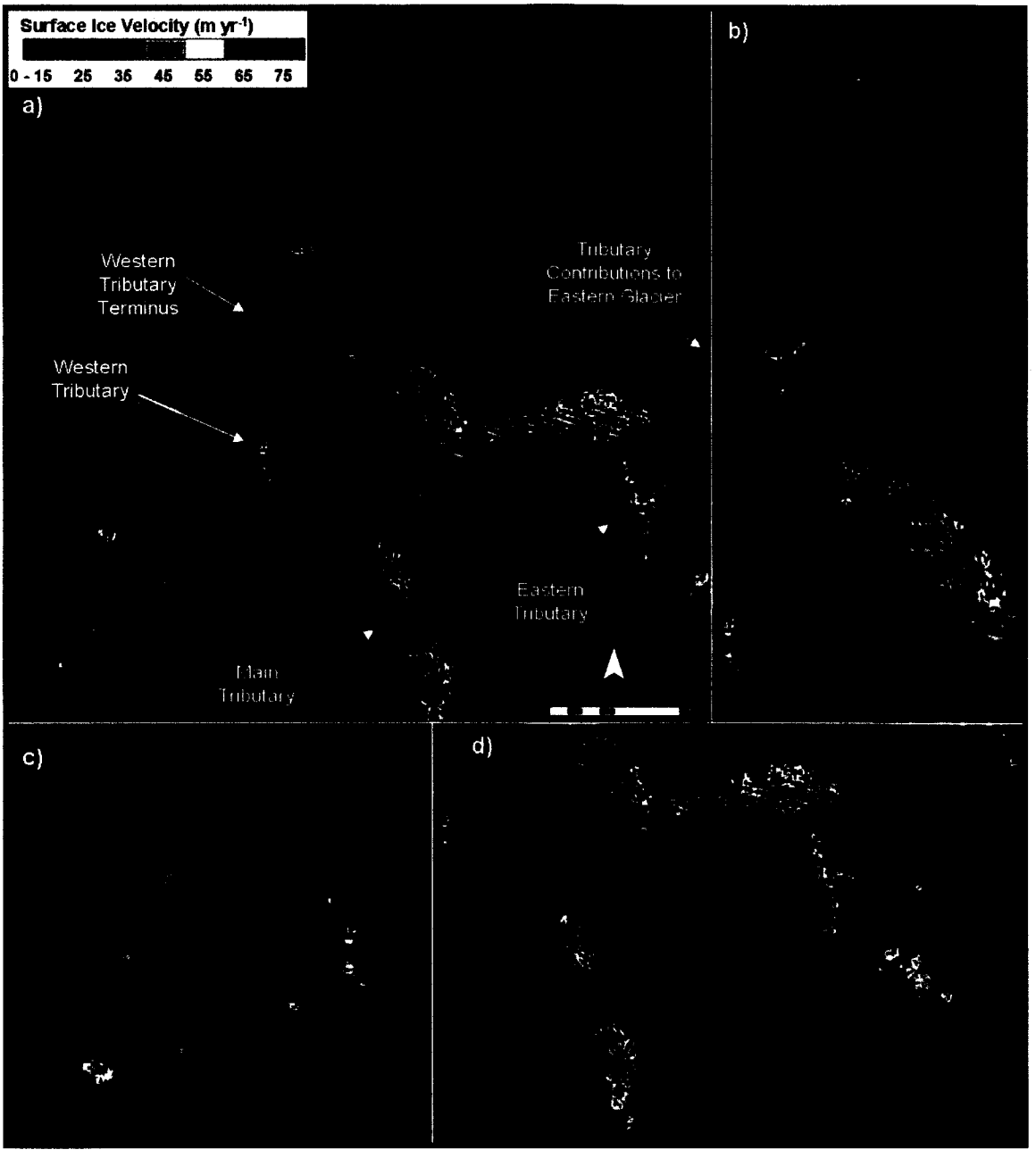

Figure 5.4: *Surface ice velocities determined over Sverdrup Glacier basin: a) surface ice displacements over Sverdrup Glacier and its tributaries; b) zoom-in of Sverdrup Glacier main trunk: c) zoom-in of western tributary; d) zoom-in of main tributary and eastern tributary. (Note difference of velocity scale from previous figures)*

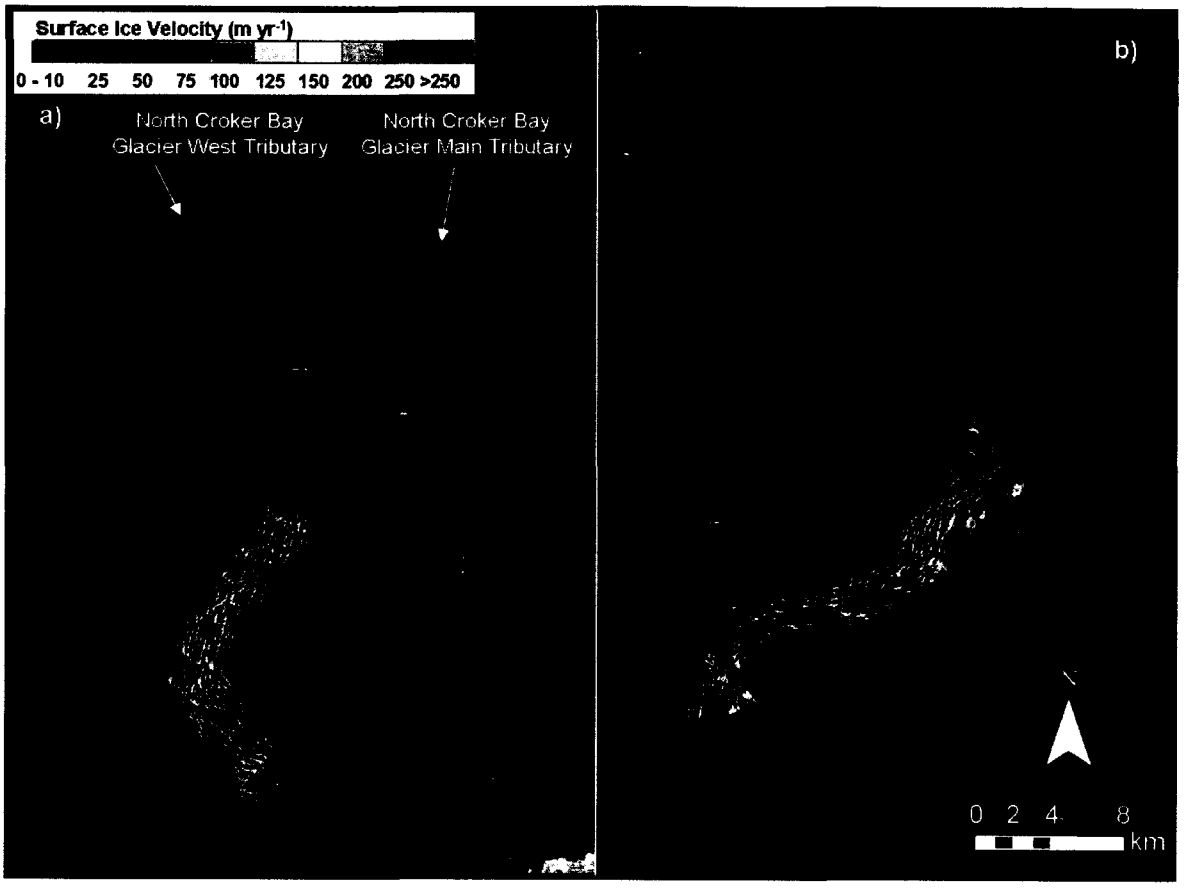

Figure 5.5: *Surface ice velocities determined over: a) North Croker Bay Glacier: b) South Croker Bay Glacier.*

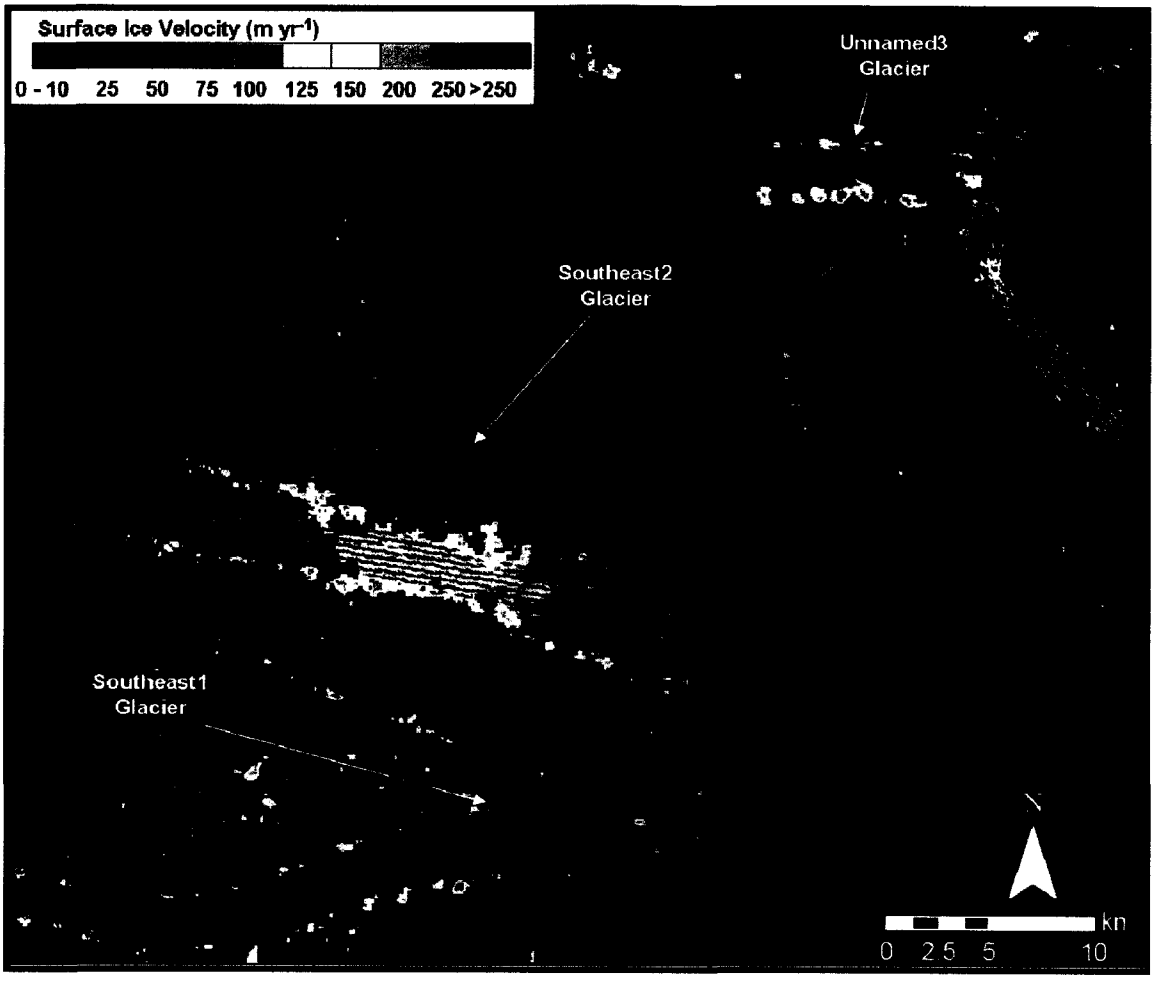

Figure 5.6: *Surface ice velocities determined over Southeast1, Southeast2 and Unnamed3 Glaciers.*

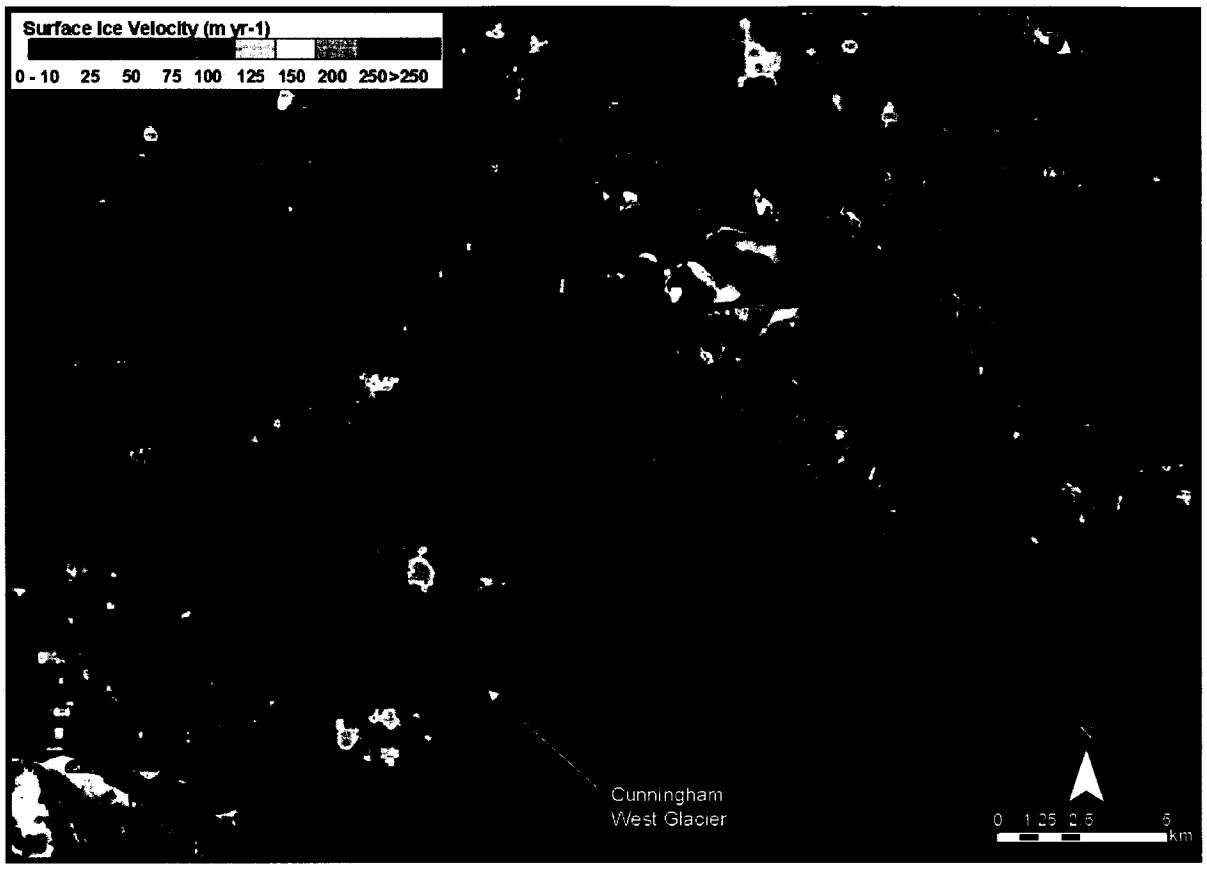

Figure 5.7: *Surface ice velocities determined for the southern glaciers of the Southeast quadrant.*

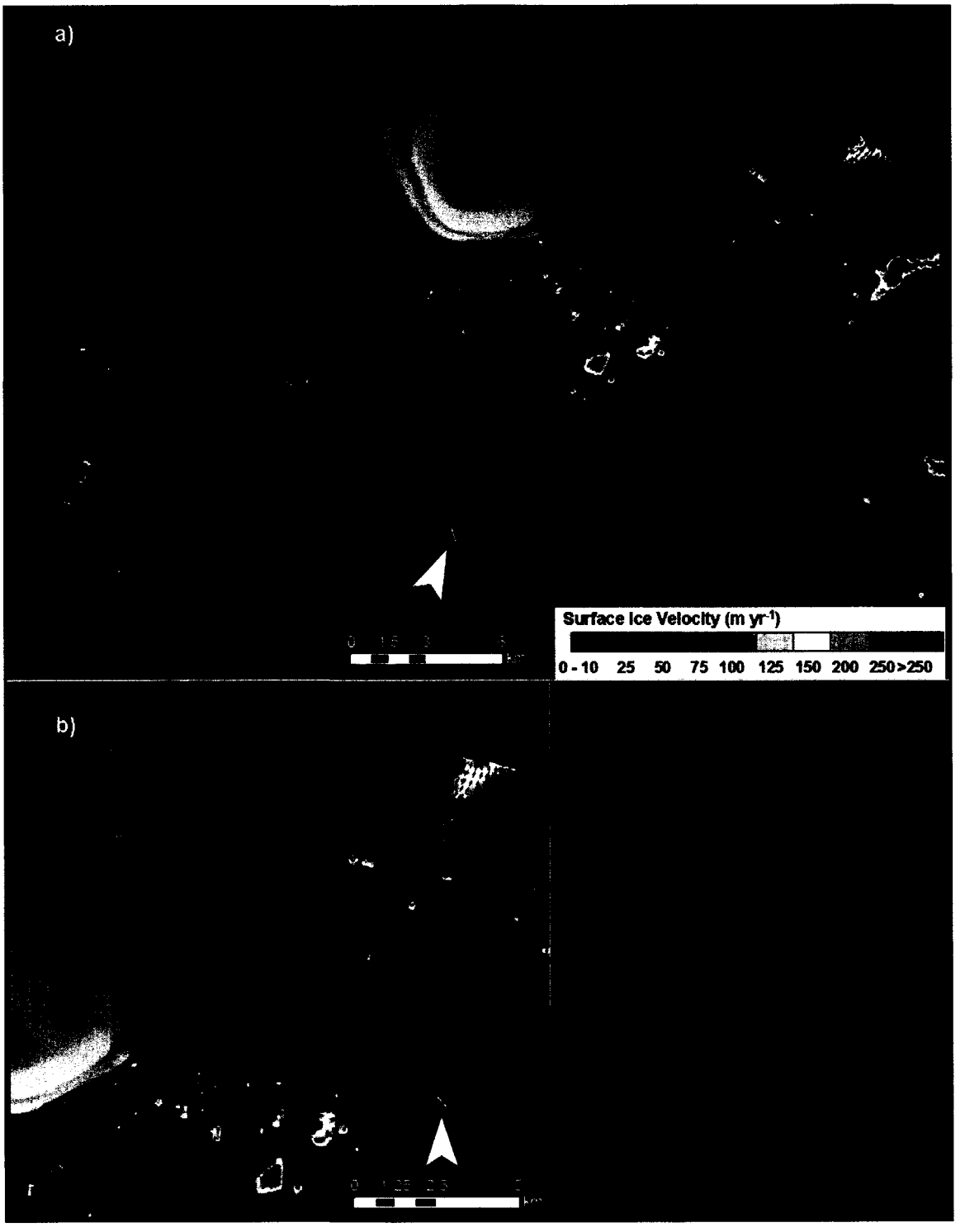

Figure 5.8: *Surface ice velocities along the Eastern Glacier: a) ice motion along the entire length of Eastern Glacier (including upper parts of Croker Bay Glacier); b) surface ice motion near the terminus of the Eastern Glacier.*

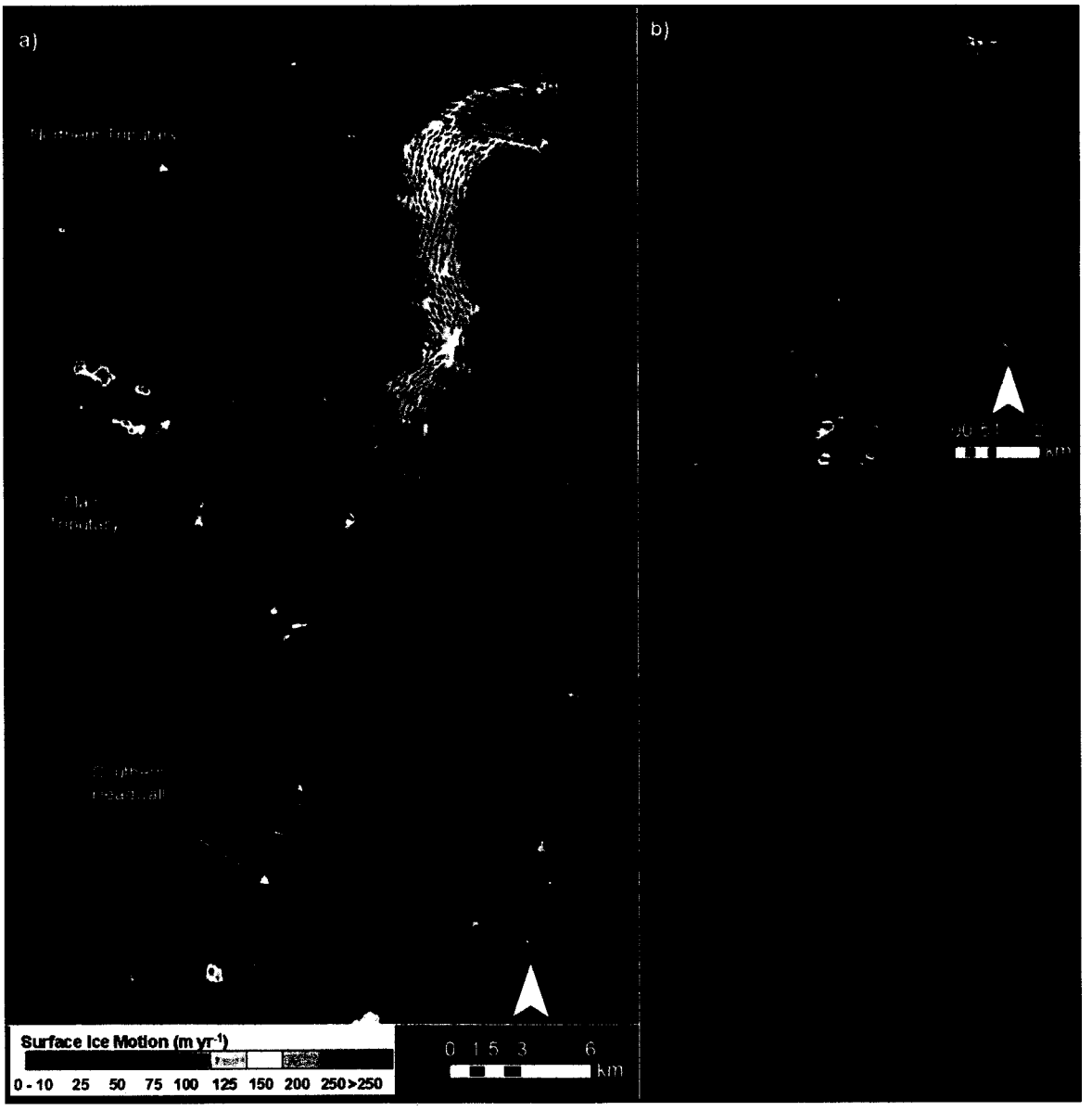

Figure 5.9: a) *Surface ice velocities along the Belcher Glacier; b) Surface ice velocities along Unnamed 5 Glacier*

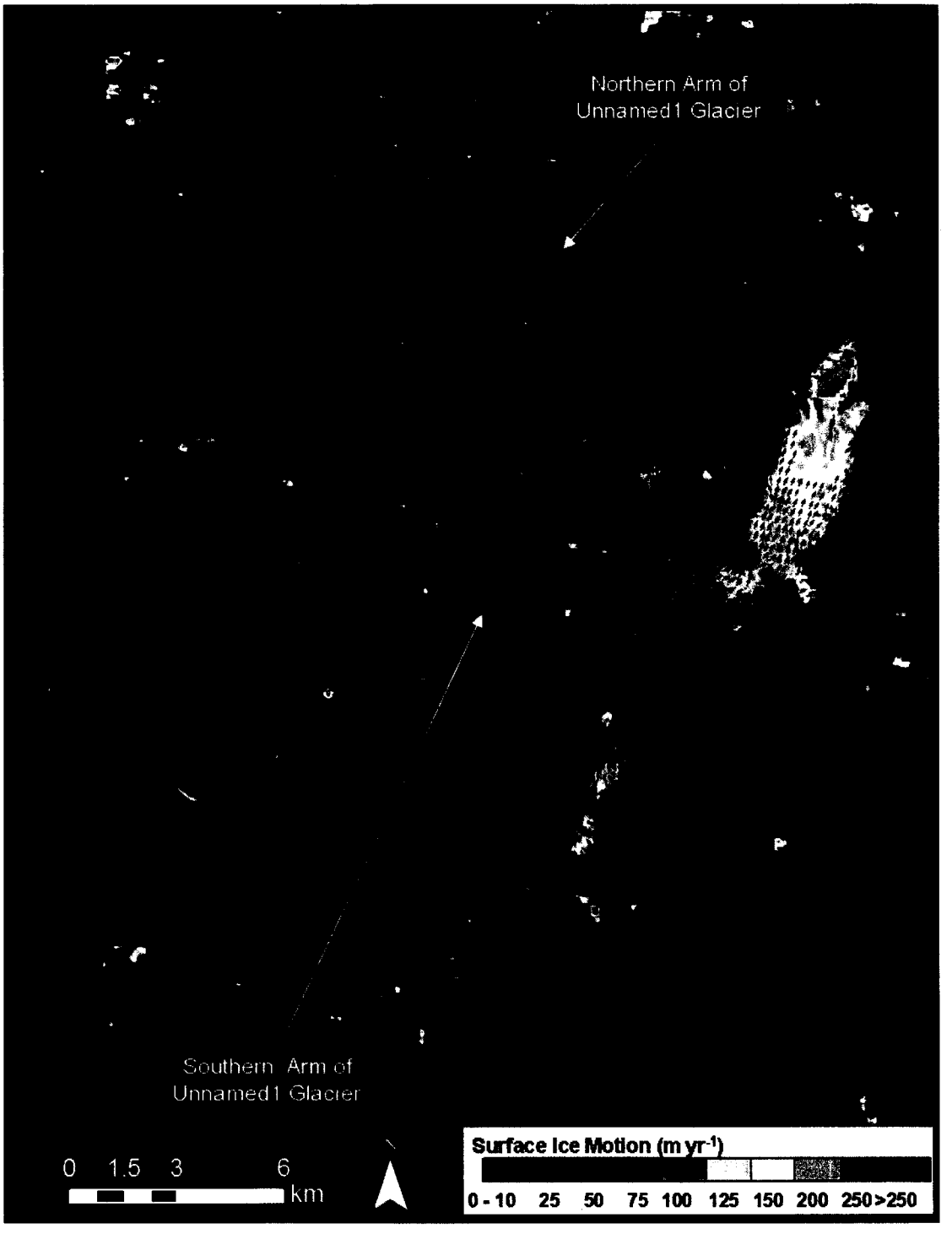

Figure 5.10: *Surface ice velocities along Unnamed1 Glacier.*

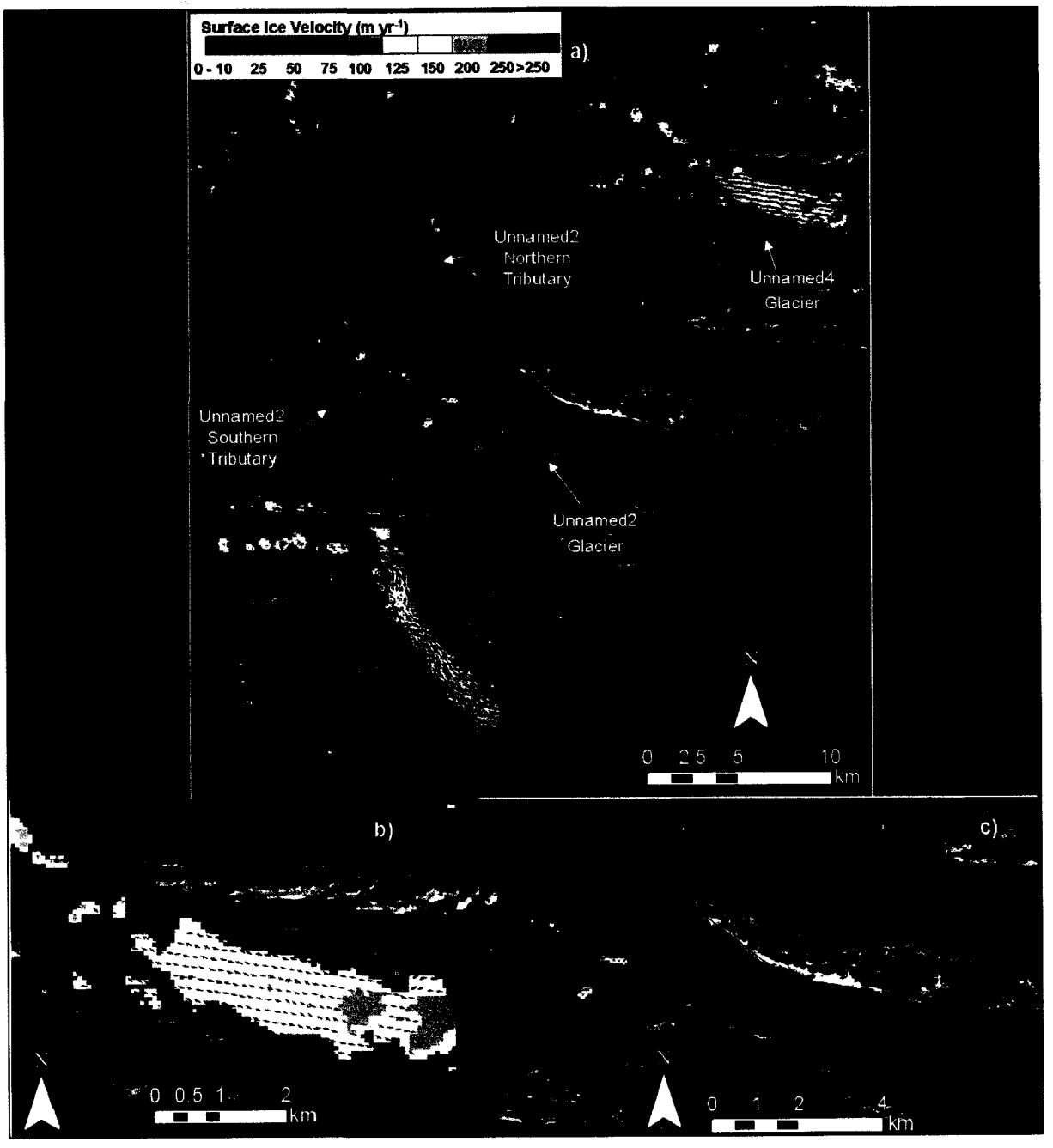

Figure 5.11: a) *Surface ice velocities along outlet glaciers of the Northeast Quadrant; b) Terminus of Unnamed3 Glacier; c) Terminus of Unnamed4 Glacier; d) Zoom in of Unnamed2 Glacier*

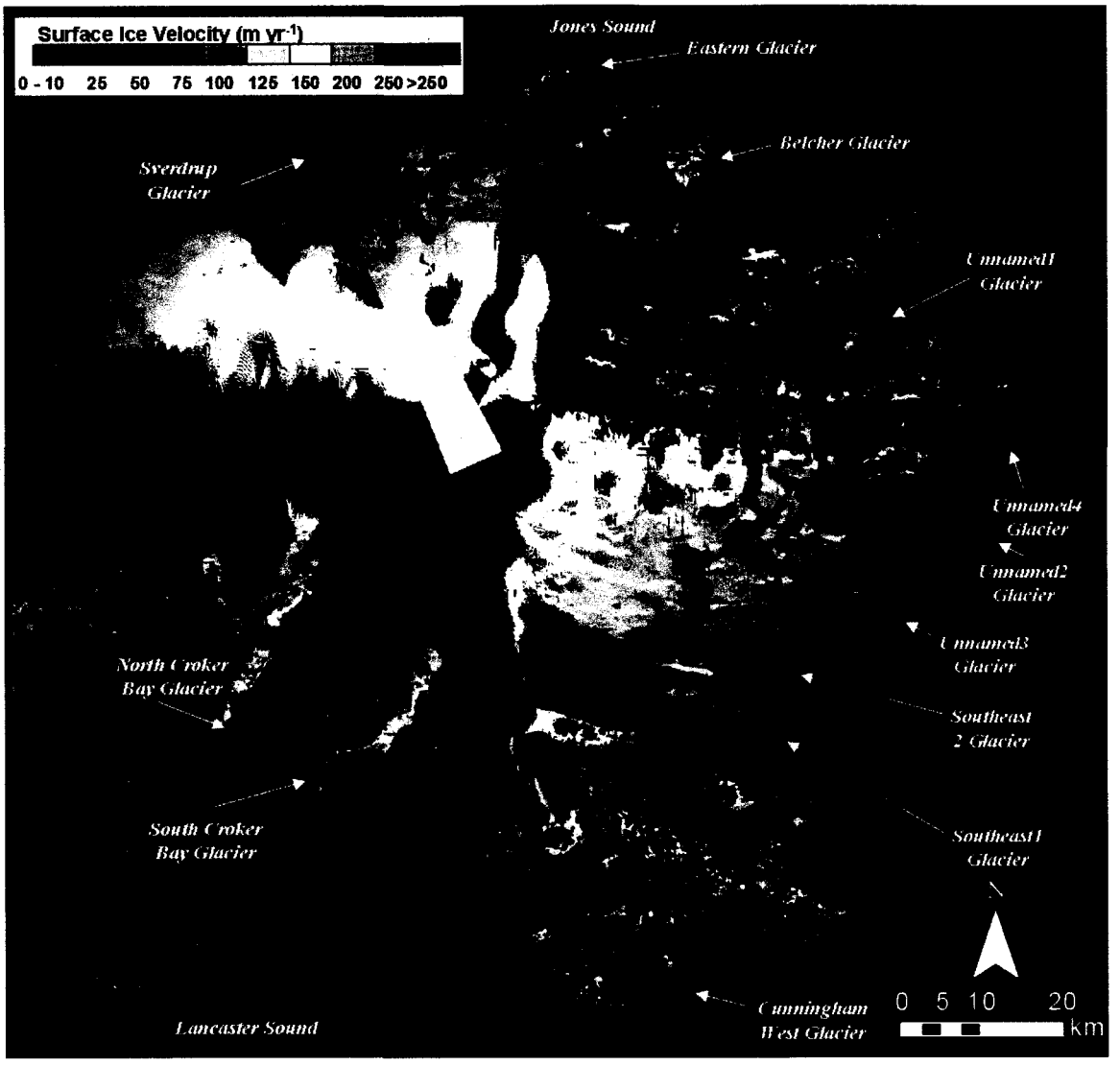

Figure 5.12: *Downslope surface ice velocity of the Devon Ice Cap (Burgess_2006).*

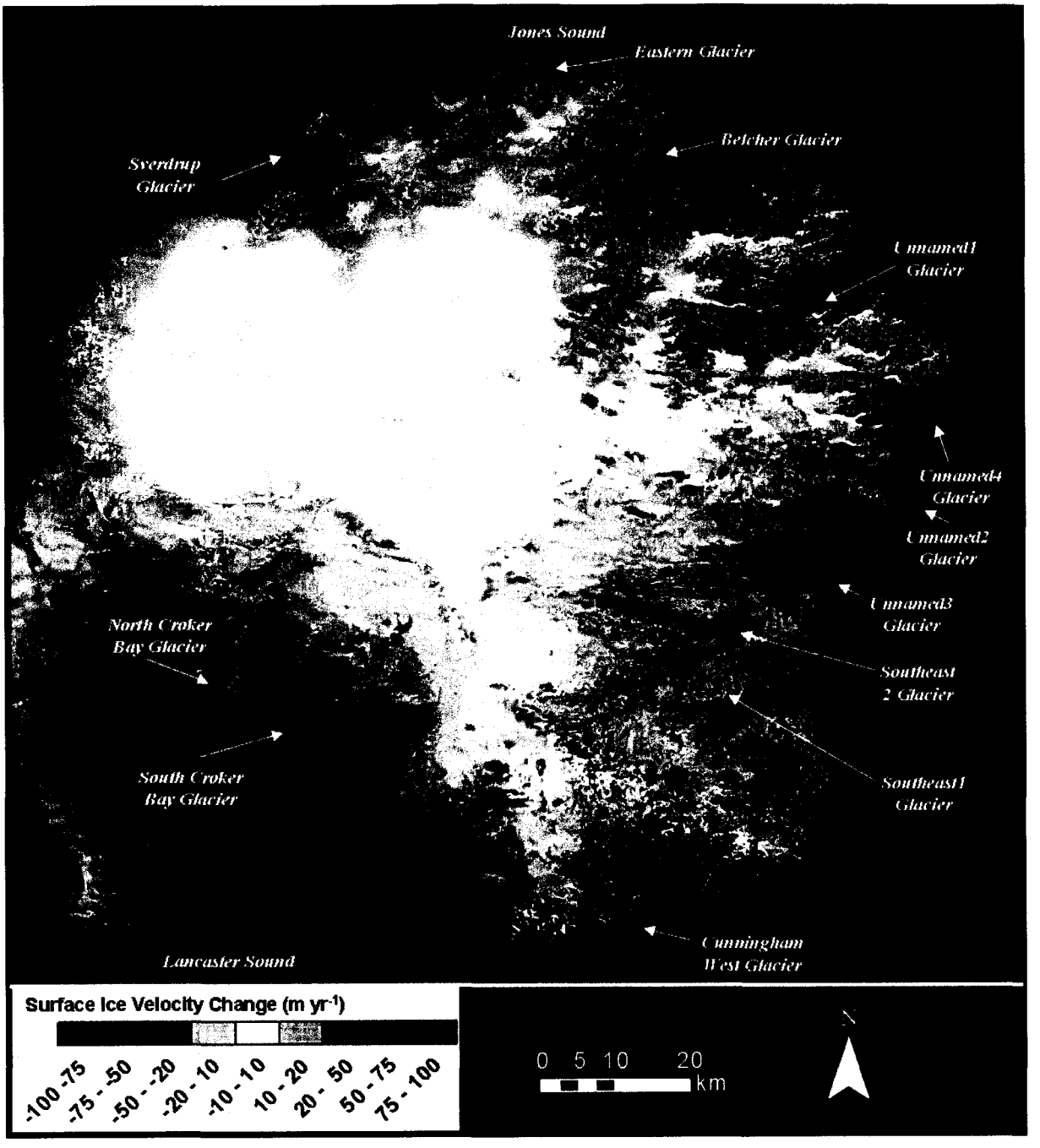

Figure 5.13: *Map of velocity differences between Burgess (2006) and the results of this thesis (Burgess 2006 – Present results).*

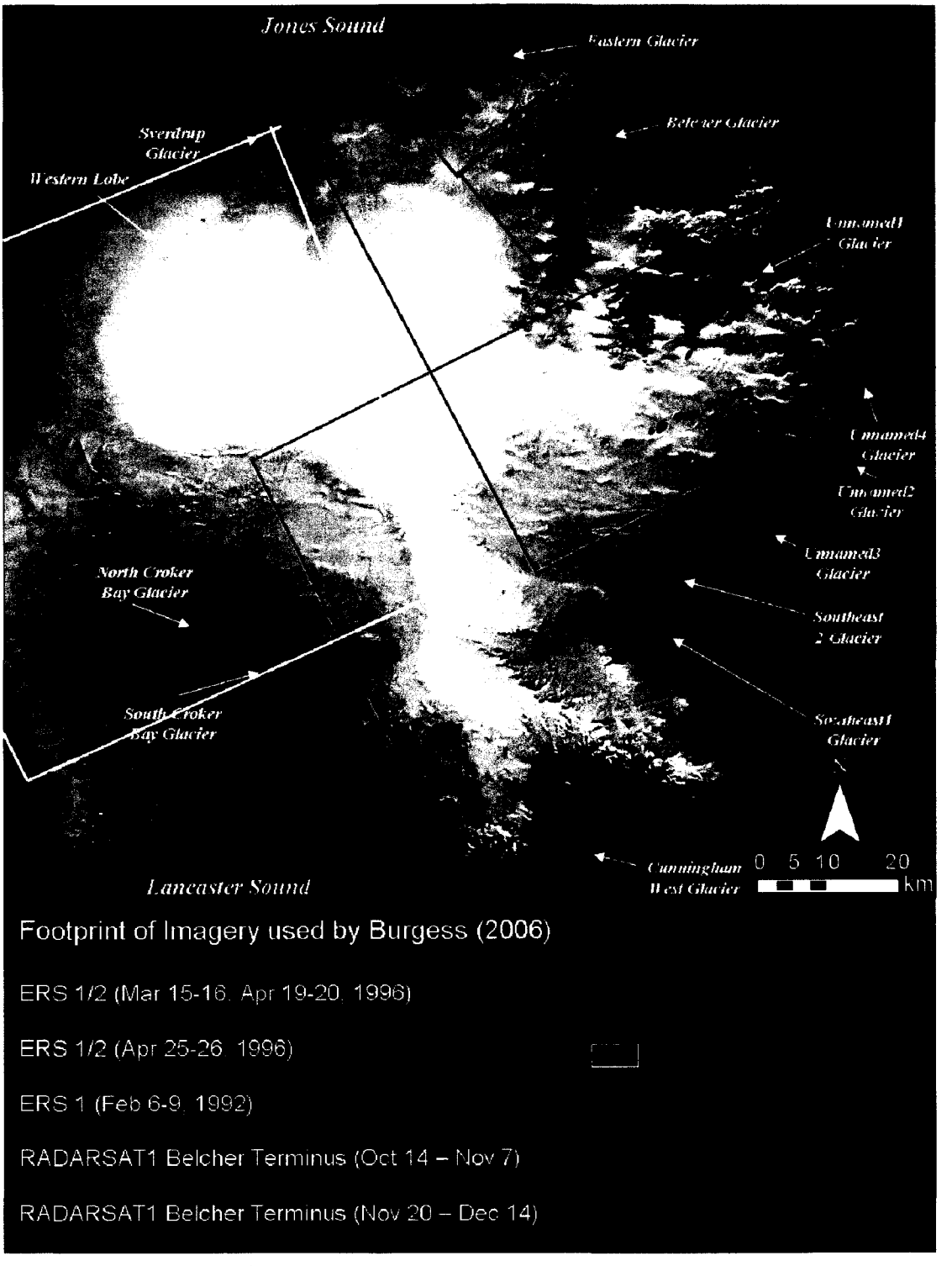

Figure 5.14: *Footprint of imagery used by Burgess (2006) to determine ice motion over the Devon Ice Cap.*

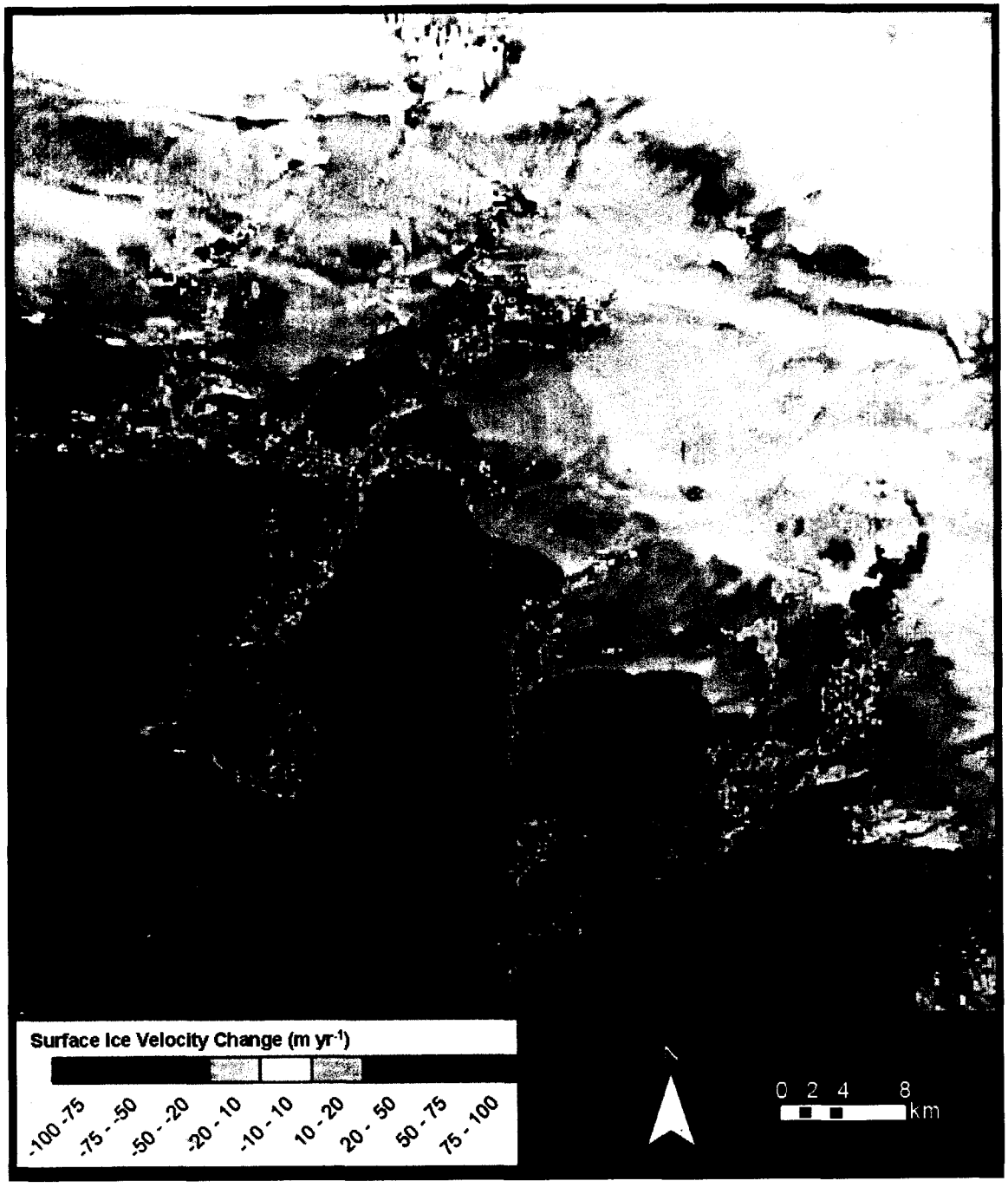

Figure 5.15: *Velocity difference map for the North and South Croker Bay Glaciers between results presented in this thesis and Burgess (2006) (Burgess 2006 – Present results).*

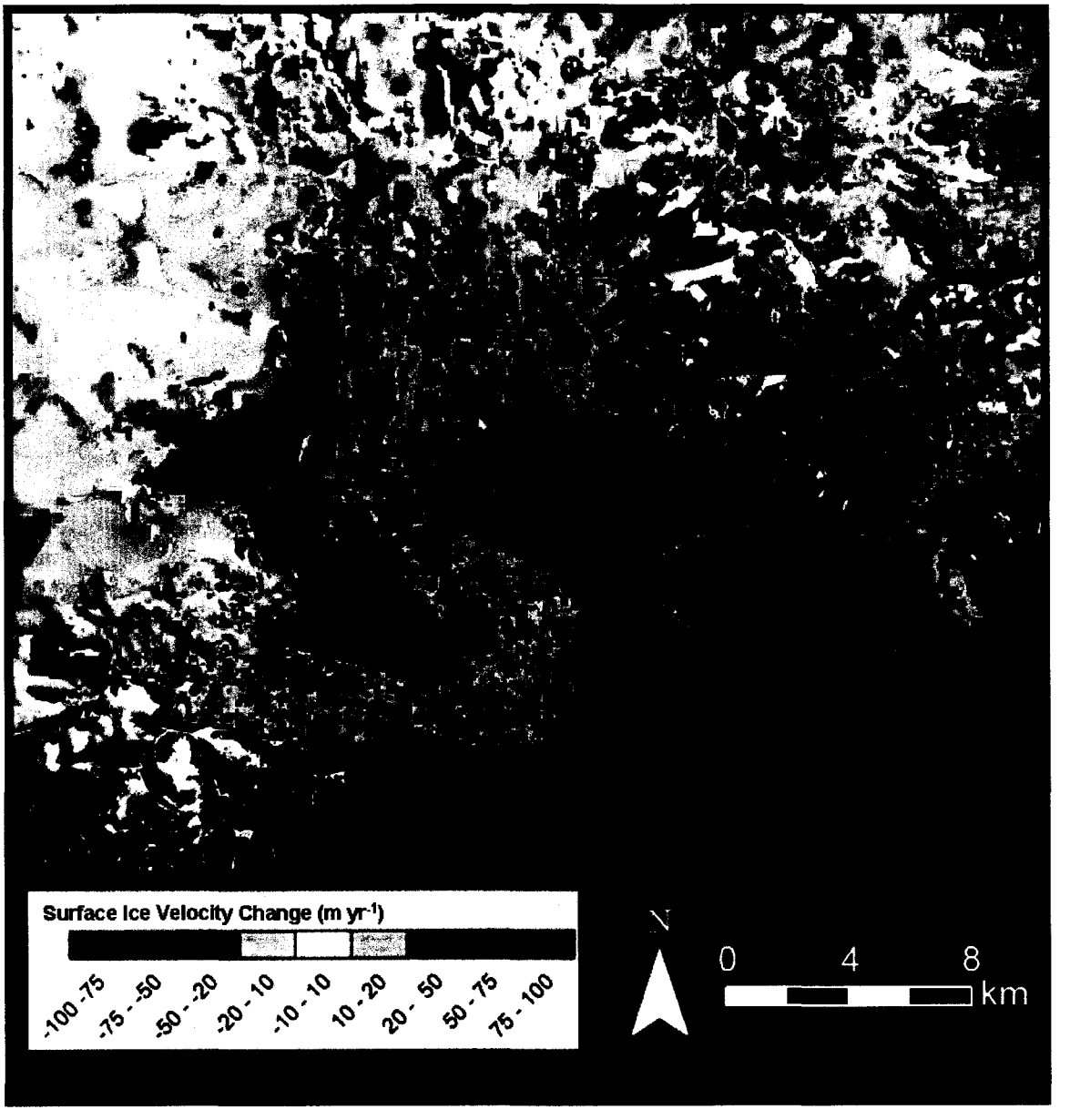

Figure 5.16: *Velocity difference map for southern terminating glaciers and Cunningham West Glacier between results presented in this thesis and Burgess (2006) (Burgess 2006 – Present results).*

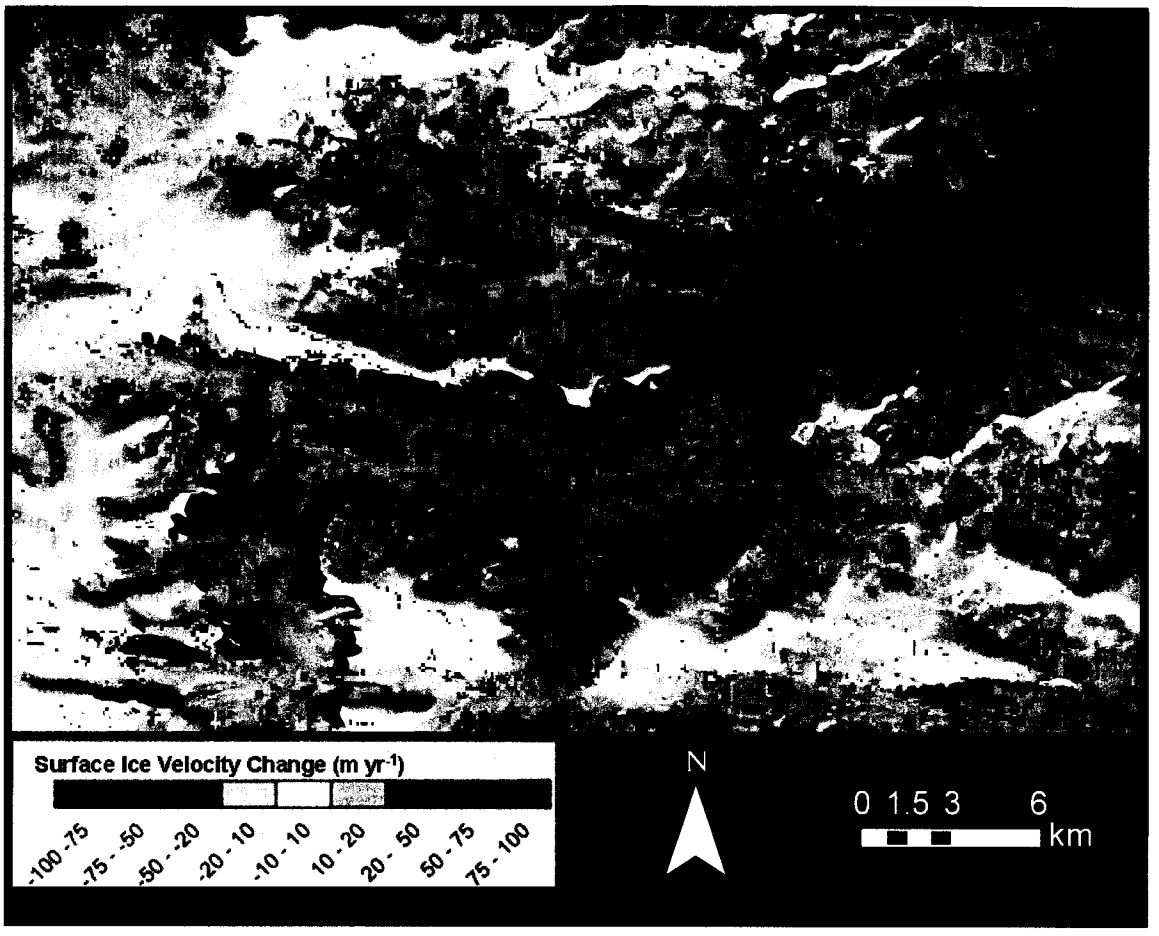

Figure 5.17: *Velocity difference map for Unnamed1 Glacier between results presented in this thesis and Burgess (2006) (Burgess 2006 – Present results).*

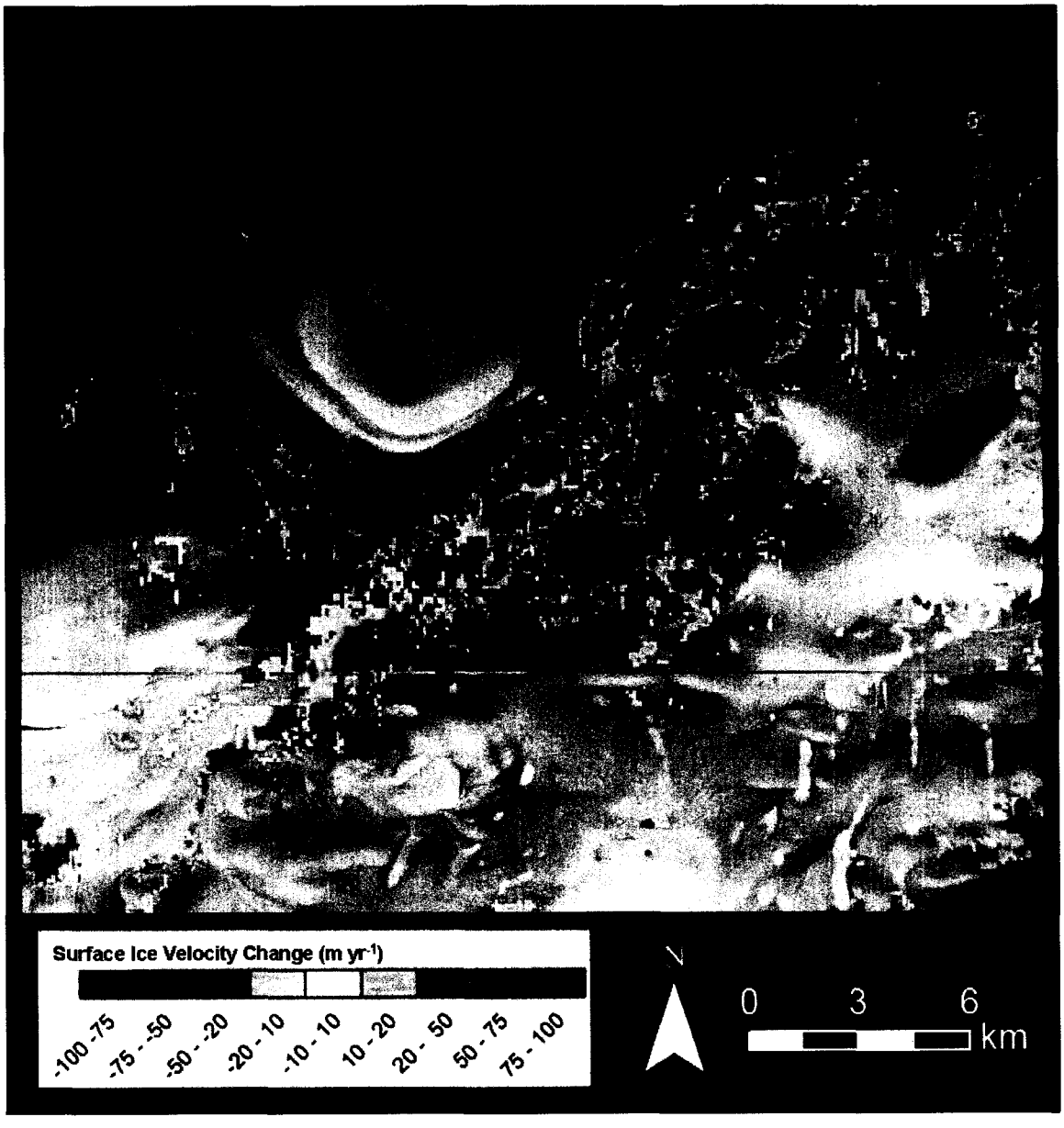

Figure 5.18: *Velocity difference map for Eastern Glacier between results presented in this thesis and Burgess (2006) (Burgess 2006 – Present results).*

Figure 5.19 *Velocity difference map for Belcher Glacier between results presented in this thesis and Burgess (2006) (Burgess 2006 – Present results).*

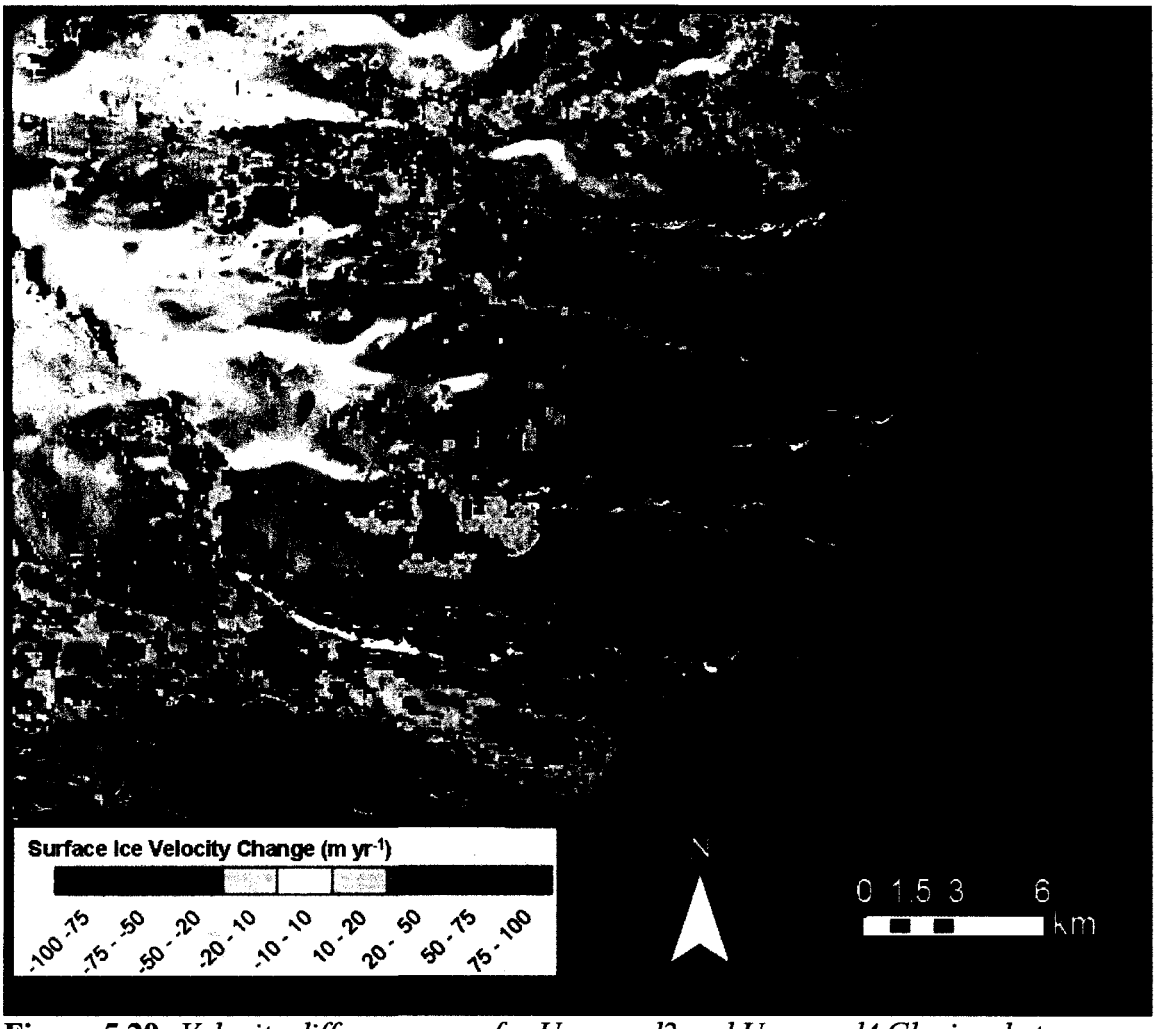

Figure 5.20: *Velocity difference map for Unnamed2 and Unnamed4 Glaciers between results presented in this thesis and Burgess (2006) (Burgess 2006 – Present results).*

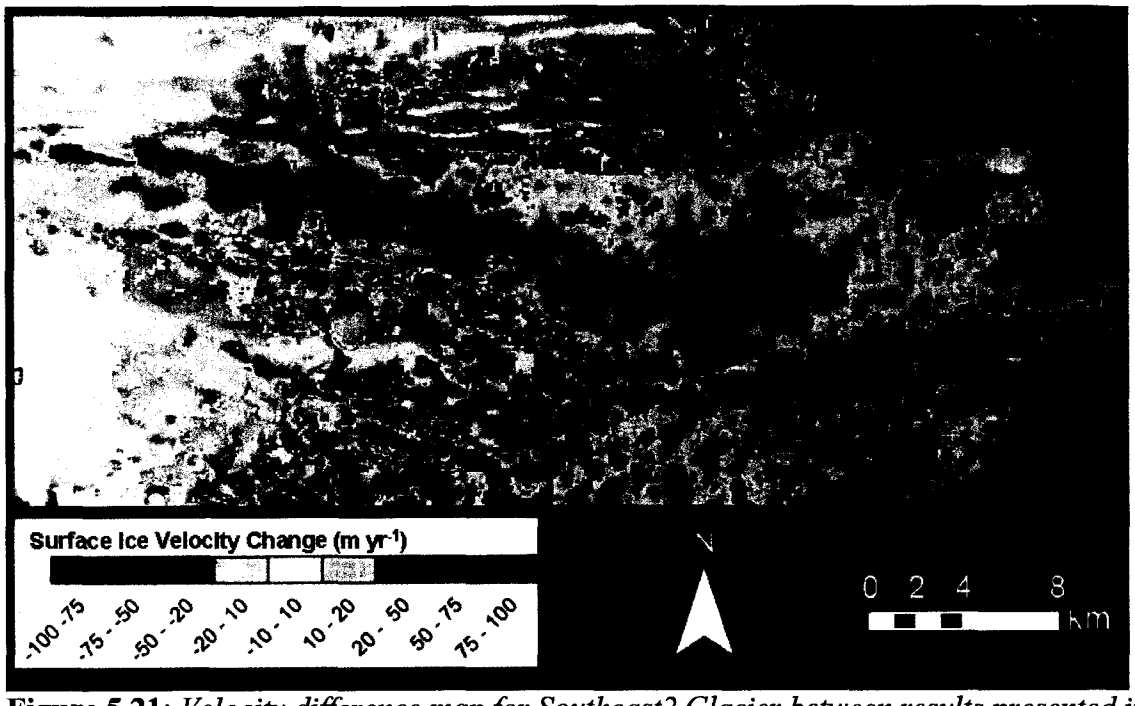

Figure 5.21: *Velocity difference map for Southeast2 Glacier between results presented in this thesis and Burgess (2006) (Burgess 2006 – Present results).*

Chapter 6: Conclusions

This study has presented the most comprehensive surface velocity maps to date for Devon Ice Cap and Belcher Glacier. These are the first ever velocity maps for the entire ice cap that avoid look-direction problems, and hence are believed to be the most accurate. The study utilized speckle tracking of fine beam Radarsat-2 imagery acquired in March 2009 to determine ice motion for the entire ice cap, and seasonally acquired fine and ultrafine beam Radarsat-2 imagery for seasonal velocity maps of the Belcher Glacier. All imagery had good coherence except for the summer imagery, which was only usable for determining ice motion at the Belcher Glacier terminus. Errors associated with the method were assessed based on ice situ dGPS observations and areas of known zero velocity (rock outcrops). Analysis of these results reveal an average error of ~9.5 m yr^{-1} for magnitude (or ~10% of average ice velocities for the Belcher Glacier) and average error of 4.81° for orientation (in areas with reliable velocity). Overall, there is high confidence that that the speckle tracking method provides results that can be used to reliably to determine surface ice motion. Areas of difficulty for determining ice motion were determined to be slow moving tributaries constrained within narrow valley walls. This is likely to be related to the optimal chip size used for the cross correlation method, and is in agreement with previously reported difficulties of the method for slower moving, narrow glaciers (Short and Gray 2004).

6.1 Belcher Glacier Velocity Structure

Seasonal velocity maps (Mar 5-29/09, July 3-27/09, Oct 3-27/09, Dec 21/09-Jan 14/10, Feb 8-Mar 3/010) generated by the speckle tracking method reveal that Belcher Glacier undergoes seasonal variations in surface ice motion (summer seasonal velocities were only determined at the terminus, as coherence was lost over the upper regions of the glacier due to surface melt). Specifically, minimum velocities in the autumn are followed by a gradual increase throughout the winter on the lower portion of the main trunk. In contrast, the terminus experiences its maximum velocity during the autumn and velocities decrease through the winter. Velocity variations along the lower portion of the main trunk are likely due to changes of basal lubrication (related to a change from a discrete to distributed subglacial drainage system) while changes at the terminus are likely linked to

changes in sea ice conditions at the snout. These findings are consistent with previous studies such as Nienow et al (1998), Bingham et al (2008), Bingham et al (2005) and Copland et al (2003b) in terms of velocity fluctuations in relation to changes in subglacial hydrology. In terms of terminus velocity fluctuations and sea ice interactions, the findings of this thesis agree well with previously measured patterns and are consistent with the findings of Reeh et al (2001), Masson et al (2006) and Copland et al (2007).

Calculated flux results reveal that ice discharge becomes greater further downglacier with the input of more tributaries. Burgess et al (2005) reported an ice flux of ~0.27 km^3 yr^{-1} at the Belcher Glacier terminus. A flux gate created at the terminus using the velocities generated by this study indicate that average annual ice flux at the Belcher terminus is ~0.091 km^3 yr^{-1}, about 33% of the flux reported previously. Reasons for this discrepancy may relate to differences in velocities measured at the terminus (due to differences in seasonal acquisition of used imagery) and the different ice thicknesses used for the flux gates (airborne 1 km resolution ice thickness data versus a finer detailed bedDEM). It is possible, however, that flux through the basin is less than previously reported and that the Belcher Glacier may not be as large of a contributor to mass discharge from DIC as previously thought. Results from this study illustrate the validity of using speckle tracking techniques to accurately monitor seasonal ice dynamics for a High Arctic ice cap.

6.2 Changes in the Velocity Structure of Devon Ice Cap

Descending fine beam mode Radarsat-2 imagery from March 2009 was used to determine ice motion for the entire Devon Ice Cap, and results revealed a distinct east to west difference in velocity structure. In the east, ice is generally faster flowing (enhanced basal sliding) through numerous, deep tidewater outlet glaciers, whereas in the west ice is generally slower moving and dominated internal ice creep. This east-west ice dynamic difference is attributed to regional changes in underlying topography, ice thickness and surface melt (Boon et al 2010, Burgess et al 2005, Dowdeswell et al 2004).

Comparisons of the velocity structure of Devon Ice Cap as determined by speckle tracking shows good agreement with previous ice dynamic studies (Shepherd et al 2007, Dowdeswell et al 2004, Burgess et al 2005). All studies agree on the general flow structure of the ice cap, although differences occur as to the magnitude of displacements at the terminus of outlet glaciers. Specifically, Shepherd et al (2007) determine maximum ice velocity as 150 m yr^{-1}, while the results of this study indicate that velocities at the terminus of tidewater outlet glaciers can reach ~275 m yr^{-1} (Belcher Glacier, Unnamed1 glacier). The flow structure closely matched the flow regimes described by Burgess et al (2005). Regions of slower flow were found in regions that Burgess et al (2005) determined as areas where the ice mass was frozen to its bed, while faster flow was found in regions identified as regions where motion was controlled by basal lubrication or bed deformation.

An in-depth comparison with the work of Burgess et al (2005) and Burgess (2006) was undertaken to determine whether velocity change has occurred over the last ~10-15 years (1996 – 2009 for western southeastern DIC, 1992 – 2009 for northeastern DIC, and 2000 – 2009 for the Belcher Glacier terminus). Previous studies have identified Southeast2 as a possible surge type glacier (Burgess et al 2005, Boon et al 2010), and the speckle tracking results determine support this as they show increases of ~20-100 m yr^{-1} over the past 13 years. This is consistent with Landsat 7 feature tracking over the last 5 years which has shown a velocity increase throughout this period (F, Wyatt. Personal Communication, 2010), and IceSAT data which shows a thickening of the stagnant ice which the glacier drains into (Boon et al 2010, M. Sharp, Personal Communication. 2010).

6.3 Future Work

In this study, it has been demonstrated that speckle tracking of Radarsat-2 data can provide a cheap and efficient method of monitoring ice motion across large glaciers and ice caps in the Canadian High Arctic. Continued acquisitions should enable improved assessment of the inter- and intra-annual variations in ice motion over a longer time period. A data acquisition plan for the Belcher Glacier throughout summer 2010 and into

2011 will allow for continued monitoring of the region. This will improve the understanding of the interplay between summer melt and winter dynamics, although it is only possible to determine velocity changes that occur over a period of 24 days or longer using technique. Long-term monitoring is relatively easy and cost-effective with the greatest challenge being continued access to Radarsat-2 data.

Additional long-term Radarsat-2 acquisitions for the entire ice cap would also be beneficial as it would allow for the determination of velocity structure change on an annual basis. This type of velocity mapping over the entire DIC would also allow for possible surging glaciers to be identified. Expanding the seasonal velocity mapping to other outlet glaciers of the DIC would also be beneficial, as it would be possible to determine the seasonal velocity structure and subglacial drainage evolution on other glaciers in the region. To strengthen this research, further fieldwork which helps determine the nature and seasonal evolution of the subglacial drainage system (e.g. GPR, dye tracing) would be beneficial.

Finally, future work should include the implementation of speckle tracking on more glaciers across the Arctic and sub-Arctic. Dynamic thinning has been demonstrated to be an important mass loss mechanism for Greenland (Bell 2008, Bartholomaus et al 2007, Zwally et al 2002, Holland et al 2008), but for large portions of the Canadian Arctic the importance of this mechanism is unknown due to lack of good velocity data. Results from this study show that velocities over an Arctic glacier can be determined with high accuracy using speckle tracking, and thus the method provides a good means of obtaining the velocity data which is currently lacking. Overall, further implementation of speckle tracking on more glaciers will provide insight as to how glacier motion will be affected in a warming climate.

Chapter 7: References

Allard, M., B. Wang, and J.A. Pilon. (1995). Recent cooling along the southern shore of Hudson Strait Quebec, Canada, documented from permafrost temperature measurements. *Arctic and Alpine Research.* (**27**): 157–166.

Alley, R.B., Dupont, T.K., Parizek, B.R., Anadakrishnan, S. (2005). Access of surface meltwater to beds of sub-freezing glaciers: preliminary insights. *Annals of Glaciology.* (**40**)1: 8-14.

Alt, B. (1978). Synoptic climate controls of mass-balance variations on Devon Island Ice Cap. *Arctic and Alpine Research*, (**10**)1: 61-80.

Alt, B. (1987). Developing synoptic analogs for extreme mass balance conditions on Queen Elizabeth Island Ice Caps. *Journal of Climate and Applied Meteorology.* (**26**)12: 1606-1623.

Annan, A. P. (2002). GPR—History, Trends, and Future Developments. *Subsurface Sensing Technologies and Applications*, (**3**)4: 253-270.

Arctic Climate Impact Assessment (ACIA). (2004). Chapter 4: Cryosphere and Hydrology. *Arctic Climate Impact Assessment.*

Bamber, J.L, Alley, R.B. Joughin, I. (2007). Rapid response of modern day ice sheets to external forcings. *Earth and Planetary Science Letters.* (**257**)1: 1-13.

Barber, D. G., Galley, R., Asplin, M. G., Abreu, R. D., Warner, K., Puc, M. (2009). Perennial pack ice in the southern Beaufort Sea was not as it appeared in the summer of 2009. *Geophysical Research Letters.* (**36**): 1-5.

Barholomaus, T.C., Anderson, R.S., Anderson, S.P. (2007). Response of glacier basal motion to transient water storage. *Nature Geosciences.* (**1**): 33-37.

Bell, R. (2008). The role of subglacial water in ice-sheet mass balance. Nature Geosciences. (**1**): 297-304.

Benn, D., & Evans, D. (1998). Glaciers and Glaciation (1st Edition., 734pp). London: Arnold.

Berthier, E., Vadon, H., Baratoux, D., Arnaud, Y., Vincent, C., Feigl, K. L., et al. (2005). Surface motion of mountain glaciers derived from satellite optical imagery. *Remote Sensing of Environment.* (**95**): 14 - 28.

Bindschadler, R. (1983). The importance of pressurized subglacier water in separation and sliding at the glacier bed. *Journal of Glaciology.* (**29**)101: 3-19.

Bingham, R. G., Nienow, P. W., Sharp, M. J., & Boon, S. (2005). Subglacial drainage processes at a High Arctic polythermal valley glacier. *Journal of Glaciology*. (**51**)172: 15-24.

Bingham, R. G., Nienow, P. W., Sharp, M. J., & Copland, L. (2006). Hydrology and dynamics of a polythermal (mostly cold) High Arctic glacier. *Earth Surface Processes and Landforms.* (**31**)12: 1463-1479.

Bingham, R. G., Hubbard, A. L., Nienow, P. W., & Sharp, M. J. (2008). An investigation into the mechanisms controlling seasonal speedup events at a High Arctic glacier. *Journal of Geophysical Research.* (**113**): 1-13.

Boon, S., and Sharp, M.J. (2003). The role of hydrologically driven ice fracture in drainage system evolution on an Arctic Glacier. *Geophysical Research Letters.* (**30**)18: 1916-1919.

Boon, S., Sharp, M.J., Nienow, P. (2003). Impact of an extreme melt event on the runoff and hydrology of a High Arctic Glacier. *Hydrological Processes.* (**17**):1051-1072.

Boon, S., Burgess, D., Koerner, R. M., & Sharp, M. J. (2010). Forty-seven years of research on the Devon Island Ice Cap , Arctic Canada. *Arctic.* (**63**)1: 13 - 29.

Boulton, G., and Hindmarsh, R. (1987). Sediment deformation beneath glaciers: rheology and geological consequences. *Journal of Geophysical Research.* (**92**)B9: 9059-9082.

Boulton, G.S., Dobbie, K. and Zatsepin, S. (2001). Sediment deformation beneath glaciers and its coupling to the subglacial hydraulic system. *Quaternary International.* (**86**)1: 3-28.

Box, J., Bromwich, D., Veenhuis, B., Le-Shieng, B., Stroeve, J., Rogers, J., et al. (2006). Greenland Ice Sheet surface mass balance variability (1988–2004) from calibrated polar MM5 output*. *Journal of Climate.* (**19**): 2783-2801.

Burgess, D. O. & Sharp, M. J. (2004). Recent changes in areal extent of the Devon Ice Cap, Nunavut, Canada. *Arctic, Antarctic and Alpine Research.* (**36**)2: 261-271.

Burgess, D. O., Sharp, M., Mair, D., Dowdeswell, J., & Benham, T. (2005). Flow dynamics and iceberg calving rates of Devon Ice Cap, Nunavut, Canada. *Journal of Glaciology.* (**51**)173: 219-230.

Burgess, D. (2006). Ice dynamics and recent geometric changes of the Devon Island Ice Cap. *PhD Thesis.* University of Alberta, Department of Earth and Atmospheric Science.

Burgess, D. & Sharp, M. J. (2008). Recent changes in thickness of the Devon Island Ice Cap, Canada. *Journal of Geophysical Research.* (**113**): 1-18.

Broll, G., C. Tarnocai, and J. Gould. (2003) Long-term high Arctic ecosystem monitoring in Quttinirpaaq National Park, Ellesmere Island, Canada. In: *Proceedings of the 8th International Conference on Permafrost, 21-25 July 2003, Zurich, Switzerland* [Phillips, M., S.M. Springman, and L.U. Arenson (eds.)]. A.A. Balkema, Lisse, the Netherlands, pp. 89—94.

Canadian Ice Service (CIS). (2010). Weekly regional ice charts. Online Archive: Available: http://ice-glace.ec.gc.ca.

Clarke, G. K. C. (1987). Subglacial till: A physical framework for its properties and processes. *Journal of Geophysical Research.* (**92**): 9023–9036.

Clarke, G.K.C. (1987b). Fast glacier flow: Ice streams, surging and tidewater glaciers. *Journal of Geophysical Research.* (**92**)B9: 8835-8841.

Comiso, J.C., (2003): Large scale characteristics and variability of the global sea ice cover. In: *Sea Ice - An Introduction to its Physics, Biology, Chemistry, and Geology.* Thomas, D. and G.S. Dieckmann (eds.). Blackwell Science, Oxford, UK, pp. 112—142.

Copland, L., & Sharp, M. (2001). Mapping thermal and hydrological conditions beneath a polythermal glacier with radio-echo sounding. *Journal of Glaciology.* (***47***)157: 232-242.

Copland, L., Sharp, M., & Nienow, P. (2003a). Links between short-term velocity variations and the subglacial hydrology of a predominantly cold polythermal glacier 1. *Journal of Glaciology.* (***49***)166: 337-348.

Copland, L., Sharp, M. and Dowdeswell, J. (2003b). The distribution and flow characteristics of surge-type glaciers in the Canadian High Arctic. *Annals of Glaciology,* (**36**): 73-81.

Copland, L., Sharp, M., Nienow, P. and Bingham, R. (2003c). The distribution of basal motion beneath a High Arctic polythermal glacier. *Journal of Glaciology,* (**49**)166: 407-414.

Copland, L., Mueller, D.R. and Weir, L. (2007). Rapid loss of the Ayles Ice Shelf, Ellesmere Island, Canada, *Geophysical Research Letters.* (**34**): 1-6.

Copland, L., Pope, S., Bishop, M. P., Shroder, J. F., Clendon, P., Bush, A. (2009). Glacier velocities across the central Karakoram. *Annals Of Glaciology,* (***50***)1: 1-9.

Cress, P., & Wyness, R. (1961). The Devon Island Expedition: Observations of glacial movements. *Arctic.* (**14**): 252-265.

DesJarlais, C. (2004). *S''adapter aux Changements Climatiques*. Ouranos, Montreal, 91pp.

Demuth, M.N. & Pietroniro, A. (2007). Climate Change Impacts on Canadian Glaciers: Why Worry? Workshop on Adapting to Water Supply Issues in a Changing Climate: Earth Science Contributions.

Dowdeswell, J. A., Ove Hagen, J., Bjornsson, H., Glazovsky, A., Harrison, W., Holmlund, P., et al. (1997). The mass balance of Circum-Arctic glaciers and recent climate change. *Quaternary Research.* (**14**)48: 1-14.

Dowdeswell, J. A., & Evans, S. (2004). Investigations of the form and flow of ice sheets and glaciers using radio-echo sounding. *Reports on Progress in Physics*, (**67**)10: 1821-1861.

Dowdeswell, J.A. and J.O. Hagen. (2004). Arctic ice masses. Chapter 15. In: J.L. Bamber and A.J. Payne (eds.). Mass Balance of the Cryosphere. Cambridge University Press, 712pp.

Dowdeswell, J. A., Benham, T., Gorman, M., Burgess, D., & Sharp, M. (2004). Form and flow of the Devon Island Ice Cap, Canadian Arctic. *Journal of Geophysical Research.* (**109**)F2: 1-14.

Duguay, C. R. (2006). Recent trends in Canadian lake ice cover. *Hydrological Processes.* (***20***): 781-801.

Dye, D. G. (2002). Variability and trends in the annual snow-cover cycle in Northern Hemisphere land areas, 1972 – 2000. *Hydrological Processes.* (**16**): 3065- 3077.

Fountain, A.G. and Walder, J.S. (1998). Water flow through temperate glaciers. *Reviews of Geophysics.*(**36**)3: 299–328.

Fudge, T.J., Harper, J.T., Humphrey, N.F. Pfeffer, T. (2005). Diurnal water-pressure fluctuations: timing and pattern of termination below Bench Glacier, Alaska, USA. *Annals of Glaciology.* (**40**)1: 102-106.

Fudge, T., Harper, J., Humphrey, N., & Pfeffer, W. (2009). Rapid glacier sliding, reverse ice motion and subglacial water pressure during an autumn rainstorm. *Annals of Glaciology.* (***50***)52: 101-108.

Gardner, A., & Sharp, M. (2007). Influence of the Arctic circumpolar vortex on the mass balance of Canadian High Arctic Glaciers. *Journal of Climate.* (**20**): 4586-4598.

Gray, A. L., Short, N., Mattar, K. E., and Jezek, K. C. (2001). Velocities and flux of the Filchner Ice Shelf and its tributaries determined from speckle tracking interferometry. *Canadian Journal of Remote Sensing,* (**27**)3: 193 206.

Gudmundsson, H., Raymond, C., & Bindschadler, R. (1998). The origin and longevity of flow stripes on Antarctic Ice Streams. *Annals Of Glaciology.* (**27**): 145-152.

Haeberli, W., and C.R. Burn. (2002). Natural hazards in forests: glacier and permafrost effects as related to climate change. In: *Environmental Change and Geomorphic Hazards in Forests* [Sidle, R.C. (ed.)]. IUFRO Research Series 9, CABI Publishing, Wallingford and New York, pp. 167—202.

Hanna, E., Huybrechts, P., Steffen, K., Cappelen, J., Huff, R., Shuman, C. (2008). Increased runoff from melt from the Greenland Ice Sheet: A response to global warming. *Journal of Climate.* (**21**): 331-341.

Hilmer, M., Lemke, P. (2000). On the decrease of Arctic sea ice volume, *Geophysical Research Letters.* (**27**): 3751 - 3754.

Hodgkins, R. (1997). Glacier hydrology in Svalbard, Norwegian High Arctic. *Quaternary. Science Review.* (**16**)9: 957-973.

Holland, D.M., Thomas, R.H., de Young, B., Ribergaard, M.H., Lyberth, B. (2008). Acceleratiion of Jakobshavn Isbrae triggered by warm subsurface ocean waters. *Nature Geoscience.* (**1**): 659-644.

Howat, I.M., Joughin, I., Scambos, T.A. (2007a). Rapid changes in ice discharge from Greenland outlet glaciers. *Science.* (**325**)5818: 1559-1561.

Howat, I., Joughin, I., Fahnestock, M., Smith, B. E., & Scambos, T. A. (2007b). Synchronous retreat and acceleration of southeast Greenland outlet glaciers 2000–06: ice dynamics and coupling to climate. *Journal of Glaciology.* (***54***)187: 646-660.

Hyndman, R.D. 1965. Gravity measurements on the Devon Island Ice Cap and an adjoining glacier. *Journal of Glaciology.* (**5**): 489 – 496.

Iken, A., & Truffer, M. (1997). The Relationship between subglacial water pressure and velocity of Findelengletscher, Switzerland, during its advance and retreat. *Journal of Glaciology.* (***43***)144: 328-338,

Irvine Fynn, T.D.L., Moorman, B.J., Williams, J.L.M., Walter, F.S.A. (2006). Seasonal changes in ground penetrating signature observed at a polythermal glacier, Bylot Island, Canada. *Earth Surface Process and Landforms.* (**31**)**:** 892 909.

Isaksen, K., P. Holmlund, J.L. Sollid, and C. Harris. (2001). Three deep alpine-permafrost boreholes in Svalbard and Scandinavia. *Permafrost and Periglacial Processes.* (**12**)1: 13–25.

Jeffers, S., Agnew, T. A., Alt, B. T., De Abreu, R., & McCourt, S. (2001). Investigating the anomalous sea-ice conditions in the Canadian High Arctic (Queen Elizabeth Islands) during summer 1998. *Annals of Glaciology.* (**33**)1: 507-512.

Johannessen, O., Khorostovsky, K., Miles, M., & Bobylev, L. (2005). Recent ice-sheet growth in the interior of Greenland. *Science.* (**310**): 1013-1015.

Joughin, I., Kwok, R., and Fahnestock, M. (1998). Interferometric estimation of three dimensional ice flow using ascending and descending passes. *IEEE Transactions on Geoscience and Remote Sensing.* (**36**)1: 25-37.

Joughin, I. (2002). Ice-sheet velocity mapping: a combined interferometric and speckle-tracking approach. *Annals Of Glaciology.* (**34**)1: 195-201.

Joughin, I., Das., S., King, M., Smith, B., Howat, I., Moon, T. (2008). Seasonal speedup along the western flank of the Greenland Ice Sheet. *Science.* (**320**)5877: 781-783.

Kaab, A. (2005a). Remote sensing of mountain glaciers and permaforst creep. Schriftenreihe Physische Geographie No. 48. University of Zurich, Department of Geography. (466 pp).

Kaab, A. (2005b). Remote sensing of glacier- and permafrost-related hazards in high mountains: an overview. *Natural hazards and Earth System Sciences.* (**5**): 527-554.

Kamb, B. (1987). Glacier surge mechanism based on linked cavity configuration of the basal water conduit system. *Journal of Geophysical Research.* (**92**)B9: 9083-9100.

Kamb, B., Engelhardt, H., Fahnestock, M.A, Humphrey, N., Meier, M and Stone, D. (1994). Mechanical and hydrological basis for the rapid motion of a large tidewater glacier. *Journal of Geophysical Research.* (**99**)B9:231-244.

King, M., Edward., S., & Clarke, P. (2002). Precise Point Positioning: Breaking the Monopoly of Relative GPS Processing. *GPS Techniques, Engineering Surveying Showcase.*

Knight, P. (1999). Glaciers. Stanley Thornes. (261 pp).

Koerner, R. M. (1966). Accumulation on the Devon Island Ice Cap, Northwest Territories, Canada. *Journal of Glaciology.* (**6**)45: 383-392.

Koerner, R.M. (1970): The mass balance of Devon Island ice cap Northwest Territories, Canada, 1961–1966. *Journal of Glaciology.* (**9**)57: 325 – 336.

Koerner, R. M. (1977). Ice thickness measurements and their implications with respect to past and present ice volumes in the Canadian High Arctic ice caps. *Canadian Journal of Earth Science.* (**14**): 2697-2705.

Koerner, RM. (1979). Accumulation, ablation, and oxygen isotope variations on the Queen Elizabeth Islands Ice Caps, Canada. *Journal of Glaciology.* (**22**)86: 25-41.

Koerner, R. M. (2005). Mass balance of glaciers in the Queen Elizabeth Islands, Nunavut, Canada. *Annals of Glaciology.* (**42**)1: 417-423.

Krabill, W., Hanna, E., Huybrechts, P., Abdalati, W., Cappelen, J., Csatho, B. (2004). Greenland Ice Sheet: Increased coastal thinning. *Geophysical Research Letters.* (**31**): 1-4.

Kwok, R. (2007). Near zero replenishment of the Arctic multiyear sea ice cover at the end of 2005 summer. *Arctic. (**34**):* 1-6.

Kwok, R. and M.A. Fahnestock. (1996). Ice sheet motion and topography from radar interferometry. *IEEE Trans. Geosci. Remote Sens.* (**34**)1: 189–200.

Lachenbruch, A.H., and B.V. Marshall. (1986). Changing climate: geothermal evidence from permafrost in the Alaskan Arctic. *Science.* (**234**)4777: 689—696.

Lappegard, G., and Kohler, J. (2005). Determination of basal hydraulic systems based on subglacial high-pressure pump experiments. *Annals of Glaciology.* (**40**)1: 37-42.

Lemke, P., J. Ren, R.B. Alley, I. Allison, J. Carrasco, G. Flato, Y. Fujii, G. Kaser, P. Mote, R.H. Thomas and T. Zhang, 2007: Observations: Changes in Snow, Ice and Frozen Ground. In: *Climate Change 2007: The Physical Science Basis. Contribution of Working Group I to the Fourth Assessment Report of the Intergovernmental Panel on Climate Change* [Solomon, S., D. Qin, M. Manning, Z. Chen, M. Marquis, K.B. Averyt, M. Tignor and H.L. Miller (eds.)]. Cambridge University Press, Cambridge, United Kingdom and New York, NY, USA.

Lewkowicz, A. G. (2007). Dynamics of Active-layer Detachment Failures , Fosheim Peninsula , Ellesmere Island , Nunavut , Canada. *Permafrost and Periglacial Processes, (103),* 89-103.

Lüthi, M., Funk, M., Iken, A., Gogineni, S, and Truffer, M. (2002). Mechanisms of fast flow in Jakobshavn Isbræ, West Greenland: Part III. *Journal of Glaciology.* (**48**)162: 369-385.

Magnuson, J. J., Robertson, D. M., Benson, B. J., Wynne, R. H., Livingstone, D. M., Arai, T., et al. (2000). Historical trends in lake and river ice cover in the Northern Hemisphere. *Advancement of Science.* (***289***)5485: 1743-1746.

Mair, D., Nienow, P., Willis, I., & Sharp, M. (2001). Spatial patterns of glacier motion during a high-velocity event : Haut Glacier d ' Arolla, Switzerland. *Journal of Glaciology.* (**47**)156: 9-20.

Mair, D., Burgess, D., & Sharp, M. (2005). Thirty-seven year mass balance of Devon Ice Cap, Nunavut, Canada, determined by shallow ice coring and melt modeling. *Journal of Geophysical Research.* (**110**): 1-13.

Macheret, Yu. Ya., Moskalevsky, M. Yu., Vasilenko, E.V. (1993). Velocity of radio waves in glaciers as an indicator of their thermal state, structure and regime. *Journal of Glaciology*. **39**(132): 373 384.

Maslanik, J. A., Fowler, C., Stroeve, J., Drobot, S., Zwally, J., Yi, D., et al. (2007). A younger, thinner Arctic ice cover : Increased potential for rapid, extensive sea-ice loss. *Geophysical Research Letters.* (**34**): 2004-2008.

Masson, R.A., Scambos, T., Squire, V., Williams, T., MacAyeal, D., Stammerjohn, S., Aster, R., Sponsler, M., Simmonds, I., Pook, M., Turner, J. (2006). The contribution of extreme events in the austral sping-summer of 2001/2 to the disintegration of the Larsen-B ice shelf. *Abstract of Research presented at the International Symposium on Cryospheric Indicators of Global Climate Change.* Cambridge, UK. August 21-25, 2006.

Meier, M.F., Dyurgerov, M.B., Rick, U.K., O'Neel, S., Pfeffer, T.W., Anderson, R.S., Nderson, S.P., Glazovsky, A.F. (2007). Glaciers dominate eustatic sea-level rise in the 21st century. *Science.* (**317**): 1064-1067.

Meier, M.F., and Post, A. (1987). Fast tidewater glaciers. *Journal of Geophysical Research.* (**92**)B9: 9051-9058.

Mote, T. (2007). Greenland surface melt trends 1973–2007: Evidence of a large increase in 2007. *Geophysical Research Letters.* (***34***): 1-5.

Muller, F., and Iken, A. (1973), Velocity fluctuations and water regime of Arctic valley glaciers. *International Association of Scientific Hydrology Publication.* (**95**): 165–182.

Nelson, F. (2003). (Un)frozen in Time. *Science.* (**299**)5613: 1673-1675.

Nghiem, S. V., Chao, Y., Neumann, G., Li, P., Perovich, D. K., Street, T. (2006). Depletion of perennial sea ice in the East Arctic Ocean. *Geophysical Research Letters.* (**33**): 1-6.

NASA. (2007). "Greenland's Ice Island Alarm." *NASA Earth Observatory* . 28 Aug 2007. NASA, Web. 15 Sep 2009. <http://earthobservatory.nasa.gov/Features/Greenland/>.

Nienow, P., Sharp, M., & Willis, I. A. (1998). Seasonal changes in the morphology of the subglacial drainage system, Haut Glacier D'Arolla, Switzerland. *Earth Surface Process and Landforms.* (**23**)9: 825-843.

Nye, F. (1969). Water at the bed of a glacier. *Proceedings of symposium on the hydrology of glaciers, International Association of Scientific Hydrology Publication.* (**95**):189-194.

Oberman, N.G., and G.G. Mazhitova. (2001). Permafrost dynamics in the northeast of European Russia at the end of the 20th century. *Norwegian J. Geography.* **(55):** 241–244.

Osterkamp, T.E. (2005). The recent warming of permafrost in Alaska. *Global Planetary. Change.* **(49)**3: 187—202.

Parizek, B., & Alley, R. (2004). Implications of increased Greenland surface melt under global-warming scenarios: ice-sheet simulations. *Quaternary Science Reviews.* **(23)**9, 1013-1027.

Parkinson, C. L., & Cavalieri, D. J. (2008). Arctic sea ice variability and trends, 1979–2006. *Journal of Geophysical Research.* **(113)**, 1-28.

Paterson, W.S.B.(1976). Temperatures in the Devon Island ice cap, Arctic Canada. *Journal of Glaciology.* **(16)**74: 277-278

Paterson, W.S.B., & Koerner, R. (1974). Radio echo sounding on four ice caps in Arctic Canada. *Arctic.* **(27)**: 225-233.

Paterson, W.S.B., and Waddington, E.D. 1984. Past accumulation rates at camp century and Devon Island deduced from ice core measurements. *Annals of Glaciology.* **(5)**: 222 – 223.

Paterson, W.S.B. (1994). The Physics of Glaciers, Third Edition. Elsevier Science. (481 pp).

Pavlov, A.V. (1996). Permafrost-climate monitoring of Russia: analysis of field data and forecast. *Polar Geography.* **20**(1): 44–64.

PulseEKKO Pro User Guide. (2006). Techinical User Guide. *Sensor's and Software: Subsurface Imaging Solutions.* (260pp).

Qiu, G., Y. Zhou, D. Guo, and Y. Wang, (2000). The map of geocryological regionalization and classification in China. In: *Geocryology in China* [Zhou, Y., D. Guo, G. Qiu, G. Cheng, and S. Li (eds.)]. Science Press, Beijing (in Chinese). The digital version of the map is available at the National Snow and Ice Data Center, University of Colorado at Boulder, Boulder, CO.

Quincey, D.J., Copland, L., Mayer, C., Bishop, M., Lackman, Belo, M. (2009). Ice Velocity and climate variations for Baltoro Glacier, Pakistan. *Journal of Glaciology.* **(55)**194: 1061-1671.

Radarsat-2 Brochure. (2009). Radarsat-2: A New Era in Synthetic Aperture Radar. MDA Promotional Material. Available online: http://www.radarsat2.info/about/r2brochure.pdf.

Rabus, B.T. and Echelmeyer, K.A. (1997). The flow of a polythermal glacier: McCall Glacier, Alaska, U.S.A. *Journal of Glaciology.* (**43**)145: 522-536.

Reeh, N., Thomsen, H.H., Higgins, A.K., and Weidick, A. (2001). Sea ice and the stability of north and northeast Greenland floating glaciers. *Annals of Glaciology.* (**33**): 474-480.

Rignot, E., & Kanagaratnam, P. (2006). Changes in the velocity structure of the Greenland Ice Sheet. *Science.* (***311***)*5763*: 986-990.

Rigor, I. G., & Wallace, J. M. (2004). Variations in the age of Arctic sea ice and summer sea-ice extent, *Geophysical Research Letters.* (***31***)*: 1-4.*

Rignot, E. and R.H. Thomas. (2002). Mass balance of the polar ice sheets. *Science.* (**297**)5568: 1502–1506.

Rothlisberger, H. (1972). Water pressure in intra- and subglacier channels. *Journal of Glaciology.* (**11**): 177-203.

Rothrock, D. A., Yu, Y., & Maykut, G. A. (1999). Thinning of the Arctic Sea-Ice Cover. *Geophysical Research Letters.* (**26**)23: 3469-3472.

Serreze, M. C., Serreze, M. C., Holland, M. M., & Stroeve, J. (2007). Perspectives on the Arctic's shrinking sea ice cover. *Science.* (**315**)5818: 1533-1536.

Sharp, M.J., Campbell, G., Tison, J.L. (1989). Structure and stability of the former subglacial drainage system of the glacier de Transfleuron, Switzerland. *Earth Surface Processes.* (**14**): 119-134.

Shepherd, A., Du., Z, Benham, T.J., Dowdeswell, J.A., Morris., E. (2007). Mass balance of Devon Ice Cap, Canadian Arctic. *Annals of Glaciology.* (**46**)1: 249-254.

Short, N. H., & Gray, A. L. (2004). Potential for RADARSAT-2 interferometry: glacier monitoring using speckle tracking. *Canadian Journal for Remote Sensing.* (**30**)3: 504-509.

Short, N. H., & Gray, A. L. (2005). Glacier dynamics in the Canadian High Arctic from RADARSAT-1 speckle tracking. *Canadian Journal for Remote Sensing.* (**31**)3: 225-239.

Smith, S. L., & Burgess, M. M., Taylor, A.E. (2003). High Arctic permafrost observatory at Alert , Nunavut – analysis of a 23 year data set. In *Permafrost.* Phillips, Springman and Arenson (eds), pp 1-6.

Smith, S. L., Burgess, M. M., Riseborough, D., & Nixon, F. M. (2005). Recent Trends from Canadian Permafrost Thermal Monitoring Network Sites. *Permafrost and Periglacial Processes.* (**16**)1: 19-30.

Steffen, K., Nghiem, S. V., Huff, R., & Neumann, G. (2004). The melt anomaly of 2002 on the Greenland Ice Sheet from active and passive microwave satellite observations. *Geophysical Research Letters.* (**31**): 1-5.

Strozzi,T., Luckman, A., Murray, T., Wegmüller, U., Werner, CL. (2002). Glacier motion estimation using SAR offset tracking procedures. *IEEE Transaction Geosciences and Remote Sensing.* (40)11: 2384 2391.

Swift, D.A., Nienow, P.W., Spedding, N., Hoey, T.B. (2002). Geomorphic implications of subglacial drainage configuration: rates of basal sediment evacuation controlled by seasonal drainage system evolution. *Sedimentary Geology.* (149)1: 5-19.

Thomas, R., Frederick, E., Krabill, W., Manizade, S., & Martin, C. (2006). Progressive increase in ice loss from Greenland. *Geophysical Research Letters.* (**33**)10: 2-5.

van De Wal, R., Boot, W., Van Den Broeke, M., Smeets, C., Reijmer, C., Donker, J. (2008). Large and rapid melt-induced velocity changes in the ablation zone of the Greenland Ice Sheet. *Science.* (**321**)5885: 111-113.

Vogtli, K. (1967). D.C. resistivity soundings on Devon Island, N.W.T., Canada. *Journal of Glaciology.* (**6**):635 – 642.

Vonder Mühll, D., J. Nötzli, K. Makowski, and R. Delaloye, (2004): Permafrost in Switzerland 2000/2001 and 2001/2002. *Glaciological Report (Permafrost) No. 2/3, Glaciological Commission of the Swiss Academy of Sciences.* Zurich, (86 pp).

Walder, J. S. (1982). Stability of sheet flow of water beneath temperate glaciers and implications for glacier surging. *Journal of Glaciology.* (**28**)99: 273-293.

Walsh, J. (2005). Cryosphere and hydrology. In: *Arctic Climate Impact Assessment.* Cambridge University Press, Cambridge and New York, pp. 183–242.

Weertman, J. (1964). The theory of glacier sliding. *Journal of Glaciology.* (**5**)39: 287-303.

Weertman, J. (1969). Water lubrication mechanism of glacier surges. *Canadian Journal of Earth Sciences.*

Willis, I.C. (1995). Intra-annual variations in glacier motion: a review. *Progress in Physical Geography.* (**19**)1: 61-106.

Woodward, J., and Burke, M. J. (1995). Applications of Ground-Penetrating Radar to Glacial and Frozen Materials. *Journal of Environmental and Engineering Geophysics.* (**12**)1: 69-85.

Wu, Q. & Y. Liu, 2003: Ground temperature monitoring and its recent change in Qinghai—Tibet Plateau. *Cold Regions Science Technology.* (**38**)2: 85–92.

Zhao, L., et al. (2004). Changes of climate and seasonally frozen ground over the past 30 years in Qinghai-Xizang (Tibetan) Plateau, China. *Global Planetary Change.* (**43**)1: 19—31.

Zhao, L., G. Cheng, and Li, S. (2003): Changes of plateau frozen-ground and environmental engineering effects. In: *The Formation Environment and Development of Qinghai-Tibet Plateau* [Zheng, D., et al. (eds)]. Heibei Science and Technology Press, Shijiazhang, pp. 143—150.

Zumberge, J. F., Heftin, M. B., Jefferson, D. C., & Watkins, M. M. (1997). Precise point positioning for the efficient and robust analysis of GPS data from large networks. *Journal of Geophysical Research.* (**102**)B3: 5005-5017.

Zwally, J., Abdalati, W., Herring, T., Larson, K., Saba, J., Steffen, K. (2002). Surface melt-induced acceleration of Greenland ice-sheet flow. *Science.* (***297***)5579: 218-222.